การตรวจติดตามการผันแปรของปริมาณอิเล็กตรอนรวมในชั้นบรรยากาศไอโอโนสเฟียร์เนื่องจาก
แผ่นดินไหวในช่วงปี พ.ศ. 2552-2554

นายรัชกฤช ศุภกุลโอภาส

วิทยานิพนธ์นี้เป็นส่วนหนึ่งของการศึกษาตามหลักสูตรปริญญาวิทยาศาสตรมหาบัณฑิต
สาขาวิชาโลกศาสตร์ ภาควิชาธรณีวิทยา
คณะวิทยาศาสตร์ จุฬาลงกรณ์มหาวิทยาลัย
ปีการศึกษา 2555

MONITORING OF TOTAL ELECTRON CONTENT
VARIATION IN IONOSPHERIC REGION CAUSED BY
EARTHQUAKES DURING 2009-2011

Mr. Radchagrit Supakulopas

A Thesis Submitted in Partial Fulfillment of the Requirements

for the Degree of Master of Science Program in Earth Sciences

Department of Geology

Faculty of Science

Chulalongkorn University

Academic Year 2012

Thesis Title MONITORING OF TOTAL ELECTRON CONTENT VARIATION IN IONOSPHERIC REGION CAUSED BY EARTHQUAKES DURING 2009-2011

By Mr. Radchagrit Supakulopas

Field of Study Earth Sciences

Thesis Advisor Sathon Vijarnwannaluk, Ph.D.

Thesis Co-advisor Nithiwatthn Choosakul, Ph.D.

Accepted by the Faculty of Science, Chulalongkorn University in Partial Fulfillment of the Requirements for the Master's Degree

……………………………………………….. Dean of the Faculty of Science
(Professor Supot Hannongbua, Dr. rer. nat.)

THESIS COMMITTEE

……………………………………………….. Chairman
(Assistant Professor Sombat Yumuang, Ph.D.)

……………………………………………….……. Thesis Advisor
(Sathon Vijarnwannaluk, Ph.D.)

……………………………………………….. Thesis Co-advisor
(Nithiwatthn Choosakul, Ph.D.)

……………………………………………….. Examiner
(Assistant Professor Srilert Chotpantarat, Ph.D.)

……………………………………………….. External Examiner
(Associate Professor Pornchai Supnithi, Ph.D.)

iv

รัชกฤช ศุภกุลโอภาส : การตรวจติดตามการผันแปรของปริมาณอิเล็กตรอนรวมในชั้น
บรรยากาศไอโอโนสเฟียร์เนื่องจากแผ่นดินไหวในช่วงปี   พ.ศ.   2552-2554.
(MONITORING OF TOTAL ELECTRON CONTENT VARIATION IN
IONOSPHERIC REGION CAUSED BY EARTHQUAKES DURING 2009-2011)
อ. ที่ปรึกษาวิทยานิพนธ์หลัก : ดร. สธน วิจารณ์วรรณลักษณ์, อ. ที่ปรึกษาวิทยานิพนธ์
ร่วม : ดร. นิธิวัฒน์ ชูสกุล 130 หน้า.

งานวิจัยนี้มีจุดประสงค์เพื่อติดตามการผันแปรของปริมาณอิเล็กตรอนรวมในชั้น
บรรยากาศไอโอโนสเฟียร์หลังเหตุการณ์แผ่นดินไหวที่มีขนาดความรุนแรงมากกว่า 7.5 และ
ความลึกของจุดกำเนิดแผ่นดินไหวน้อยกว่า 30 กิโลเมตรจากผิวดินในช่วงปี พ.ศ. 2552-2554
โดยใช้ข้อมูลจากดาวเทียมจีพีเอส โดยเหตุการณ์แผ่นดินไหวมีทั้งหมด 6 เหตุการณ์ซึ่ง
สอดคล้องกับขอบเขตของการศึกษานี้ แต่มีเพียง 4 เหตุการณ์แผ่นดินไหวที่สามารถตรวจจับ
การผันแปรของปริมาณอิเล็กตรอนรวมได้ ได้แก่ เหตุการณ์แผ่นดินไหวบริเวณใกล้กับชายฝั่ง
ตะวันตกใกล้กับเกาะใต้ของประเทศนิวซีแลนด์ เหตุการณ์แผ่นดินไหวบริเวณหมู่เกาะซามัว
เหตุการณ์แผ่นดินไหวบริเวณนอกชายฝั่งตะวันออกของเกาะฮอนชู ประเทศญี่ปุ่น และ
เหตุการณ์แผ่นดินไหวบริเวณหมู่เกาะเคอร์มาเดก โดยข้อมูลจากดาวเทียมจีพีเอสได้จากตัวรับ
สัญญาณจีพีเอสบริเวณรอบจุดศูนย์กำเนิดแผ่นดินไหว ข้อมูลจีพีเอสได้บันทึกข้อมูลปริมาณ
อิเล็กตรอนรวมในชั้นบรรยากาศไอโอสเฟียร์ซึ่งจะถูกกรองสัญญาณโดยวงจรกรองความถี่สูง
จากนั้นข้อมูลได้ถูกปรับให้เรียบโดยวิธีซาวิตสกี-โกเลย์ ขั้นตอนสุดท้ายข้อมูลได้ถูกนำไป
วิเคราะห์โดยวิธีฟาสฟูเรียร์ทรานส์ฟอร์มเพื่อหาคาบการผันแปรของปริมาณอิเล็กตรอนรวมใน
ชั้นบรรยากาศไอโอโนสเฟียร์

จากการศึกษาพบว่าปริมาณอิเล็กตรอนรวมจะเกิดการผันแปรหลังเกิดแผ่นดินไหวเป็น
เวลา 6 นาทีเป็นต้นไป สืบเนื่องมาจากแผ่นดินไหวก่อให้เกิดคลื่นบรรยากาศเรียกว่าคลื่นอะ-
คูสติก ซึ่งเดินทางจากผิวดินไปยังชั้นบรรยากาศไอโอโนสเฟียร์ในเวลาประมาณ 6 นาที และ
คาบการผันแปรของปริมาณอิเล็กตรอนรวมในชั้นบรรยากาศไอโอโนสเฟียร์อยู่ในช่วง 3.5
นาที ถึง 9.2 นาที ซึ่งสอดคล้องกับคาบของคลื่นอะคูสติกซึ่งอยู่ในช่วง 2 นาที ถึง 10 นาที

ภาควิชา........ธรณีวิทยา...........................ลายมือชื่อนิสิต...
สาขาวิชา......โลกศาสตร์........................ ลายมือชื่อ อ.ที่ปรึกษาวิทยานิพนธ์หลัก....................
ปีการศึกษา...2555................................ ลายมือชื่อ อ.ที่ปรึกษาวิทยานิพนธ์ร่วม.....................

5372313023 : EARTH SCIENCES

KEYWORDS : TOTAL ELECTRON CONTENT / GPS / EARTHQUAKE

RADCHAGRIT SUPAKULOPAS : MONITORING OF TOTAL ELECTRON CONTENT VARIATION IN IONOSPHERIC REGION CAUSED BY EARTHQUAKE DURING 2009-2011. ADVISOR : SATHON VIJARNWANNALUK, Ph.D., CO-ADVISOR : NITHIWATTHN CHOOSAKUL, Ph.D., 130 pp.

This research aims to observe the total electron content (TEC) variations after the earthquakes that magnitudes are greater than 7.5 and the depths of focus are less than 30 km beneath the ground surface during 2009-2011 using GPS data. There are six earthquake events which correspond to this research target. There are four out of six events that caused the TEC variations. Four earthquakes include the earthquake near the west coast of South Island in New Zealand, the earthquake in Samoa islands region, the earthquake near the east coast of Honshu in Japan and the earthquake in Kermadec Islands Region. The TEC variations were recorded by the GPS receivers near the epicenter zones. The GPS data provide the TEC data which was applied high pass filter in order to remove high frequencies. Then, the TEC data was smoothed using Savitzky-Golay method. Finally, the TEC data was analyzed power spectrum using fast fourier transform method in order to find the periods of the TEC variations.

The results of this research show the time lags of the TEC variations are six minutes after the earthquakes origin times. The earthquakes generated the atmospheric wave called direct acoustic wave. The direct acoustic wave took six minutes from the ground surface to the ionosphere. The periods of TEC variations found in this study are 3.5 to 9.2 minutes which correspond to the periods of acoustic wave (2-10 minutes).

Department :	Geology	Student's Signature:	
Field of Study :	Earth Sciences	Advisor's Signature:	
Academic Year :	2012	Co-advisor's Signature:	

ACKNOWLEDGEMENTS

CONTENTS

LIST OF TABLES

LIST OF FIGURES

Figure

Figure

CHAPTER I

INTRODUCTION

1.1 Introduction

Ionosphere is composed by the charge particles such as electron and positive ion. It covers the Earth at height about 75-1,000 km. Ionosphere can disturb the radio waves which pass through the Ionosphere. This phenomenon is called ionospheric scintillation. At different height, the Ionosphere has different density. The density of the ionosphere is used to classify the layers. There are four layers of the ionosphere in the daytime including D, E, F_1 and F_2, while there are 2 layers at night (E and F). Though, there is low electron density in the E layer at night. In practical purpose, the E layer is assumed to be zero.

Nowadays, the telecommunication system links the communication networks all over the World (Theerapatpaiboon *et al.*, 2005). Global Positioning System (GPS), which was developed by the U.S. Department of Defense, is one of the ways of the telecommunication system. There are 24 GPS satellites in six orbital planes at height about 20,200 km. The GPS satellites propagate two dual frequencies of radio waves at L1 (1575.42 MHz) and L2 (1227.60 MHz) to ground-based GPS receivers (Norsuzila *et al.*, 2010). When the GPS radio waves travel to the ionosphere, they are delayed by the charged particles in the Ionosphere. The time delay between two radio waves can be used to calculate the total electron content (TEC) which is the integration number of electrons along the path between the satellites and the GPS receivers.

The research on ionospheric disturbance due to the acoustic and gravity waves induced by the earthquake, tsunami and volcanic eruption has been investigated since 1960s (e.g. Bolt, 1964; Davies and Baker, 1965; Yuen *et al.*, 1969; Kanamori *et al.*, 1994; Artru *et al.*, 2005; Otsuka *et al.*, 2006; Choosakul *et al.*, 2009: Hasbi *et al.*, 2009; Saito *et al.*, 2011; Matsumura *et al.*, 2011; Tsugawa *et al.*, 2011). It has been reported that the earthquakes generate acoustic wave from the focal area which is called direct acoustic wave (e.g. Heki *et al.*, 2005; Otsuka *et al.*, 2006). The direct acoustic wave is one of the sources of the ionospheric variations after the earthquakes. Gravity wave and secondary acoustic wave are also the source of the ionospheric

variations. It was reported that gravity wave would be the result of tsunami wave (Artru *et al.*, 2005) and secondary acoustic wave is due to Rayleigh wave (Ducic *et al.*, 2003). The acoustic wave propagates vertically to the ionosphere at height about 100 km with the speed of sound wave of about 343 m/s (Yuen *et al*., 1969). Artru *et al.* (2005) proposed that the velocity of the gravity wave in the vertical direction is about 50 m/s.

The GPS can be applied to measure the ionospheric variations in term of TEC. The TEC was measured in TEC unit (TECU) and 1 TECU is 10^{16} electrons/m^2. Artru *et al.* (2005) applied GPS data from GPS network (GEONET) in Japan to measure the TEC perturbations which were the result of the gravity wave induced by Tsunami wave from Peru earthquake with Mw 8.2 on 23 June 2001. The periods range from 10-20 minutes of the TEC oscillations were generated by the Peru earthquake. Choosakul *et al.* (2009) observed the TEC variations caused by acoustic resonance between the ground surface and the lower thermosphere in 2004 Sumatra-Andaman earthquake with Mw 9.2 on 26 December 2004. The period of four minutes of the TEC oscillation was detected by a GPS receiver in Thailand. Saito *et al.* (2011) detected the acoustic resonance and the plasma depletion by TEC using GEONET in Japan in Tohoku earthquake on 11 March 2011 and found that the periods of TEC perturbation were 3-4.5 minutes. Chen *et al.* (2011) observed the propagation of ionospheric disturbances and found that the wave front propagated southward from Japan to Taiwan with speed of about 1,000 and 1,700 m/s.

1.2 Objectives

1. To observe the TEC variations after the earthquakes between 2009 and 2011.

2. To study the relationship between the origin time of the TEC variations and the onset time of the earthquakes.

3. To identify the sources of the TEC variations including the solar activity, geomagnetic activity and earthquake.

1.3 Scope of Research

This work aimed to monitor the TEC variations caused by the earthquakes with magnitude above 7.5. Some previous reports (e.g. Heki, 2007; Choosakul, 2009) suggested that the shallow earthquakes with magnitude higher than 7.5 can disturb the ionosphere. The focuses of the earthquakes are less than 30 km beneath the ground surface. The parameter that will be studied in this research is the TEC in the vertical direction during 2009 to 2011.

1.4 Study Area

There are six areas of study in this research during 2009-2011. Most of listed earthquakes as shown in Figure 1-1 have magnitude higher than 7.5 and the depth of focuses from the ground surface is less than 30 km. The locations of the earthquake epicenter are shown in Figure 1-1.
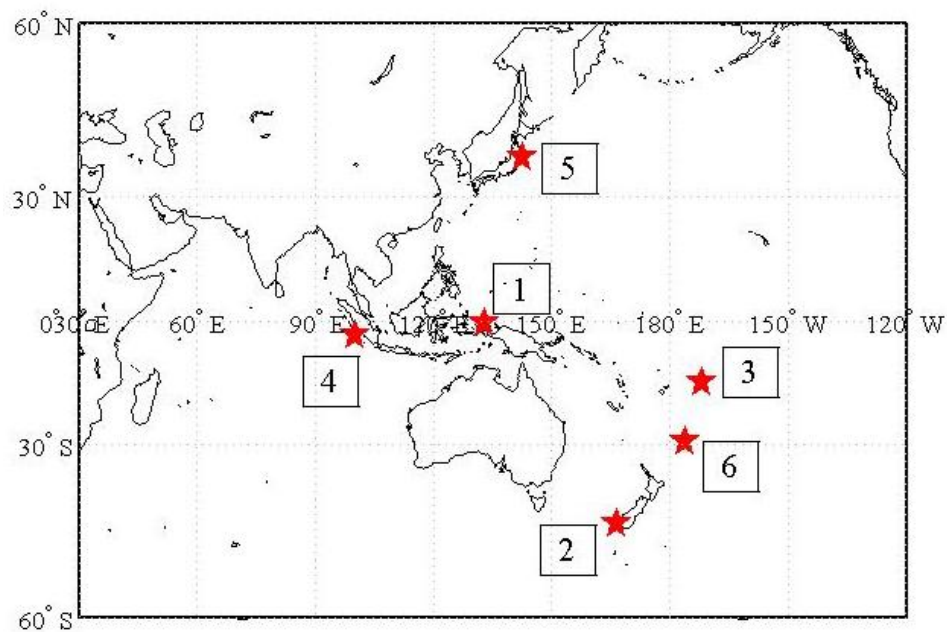
Figure 1-1 Study Area of this research

1. Near the north coast of Papua, Indonesia
2. Off west coast of the south island, N.Z.
3. Samoa islands region
4. Kepulauan mentawai region, Indonesia
5. Near the east coast of Honshu, Japan
6. Kermadec islands region

CHAPTER II
THEORY

2.1 The Earth's Upper Atmosphere

2.1.1 Ionosphere

The earth's ionosphere is an upper atmosphere which consists of neutral and charged particles. The charged particles are electrons and ions. Nowadays, the thickness of the ionosphere is not clearly identified yet. It is considered to extend from about 60 to 1,000 km from the earth's surface. The charged particles of the ionosphere come from ionization of neutral gases by extreme ultraviolet (EUV) and X-ray waves. The variations of these particles depend on altitude because of different pervasive influence of the earth's gravity at different altitudes. The particles' densities vary over space and time. The ionosphere also has the different aspects in accordance with latitude (Tsugawa, 2004). The vertical structure of the ionosphere will be mentioned first and the characteristics of the ionosphere depending on latitudes will be mentioned later.

The vertical structure of the ionosphere is categorized as D, E, F_1 and F_2 layers from low altitude to high altitude as shown in Figure 2-1 (right). The D layer extends from 60 km to 90 km altitude. This region is generated by hard X-ray wave which has the wave length smaller than 1 nm. The chemical process is the important process of the D region. This region is formed by molecular ions such as NO^+ and O_2^+, water cluster ions, negative ions generated via hydration and chemical reaction with neutral particles such as N_2, O_2, and O. The D region can absorb high frequency band of the radio wave. There is the small absorption at night and there is the strong absorption at the midday (Tsugawa, 2004).

The E region extends between 90 km and 150 km. The chemical processes are still important for this region. However, photo-ionization becomes more effective to form the E layer. The photo-ionization by soft X-ray and ultraviolet (UV) generates NO^+, O_2^+ and N_2^+ which are the dominant gases of this region (Tsugawa, 2004).

The F$_1$ layer extends between 150 km and 250 km altitude. Ion-neutral charge exchange and transportation processes become more important in this region. The F$_2$ layer from 250 km to 1,000 km altitude is above the F$_1$ layer. At the F$_2$ region, the electron density reaches the maximum peak called F$_2$ peak. The F$_2$ peak is the result of a balance between plasma transport and chemical loss process. The major atom in the F$_2$ region is O atom. Therefore, the O^+ is the main ionized ion near the F$_2$ peak. The O^+ can survive in the nighttime because there is low recombination rate in the F$_2$ region (Tsugawa, 2004).

The ionosphere also varies depending on latitude because the components of the earth's magnetic field are difference. At high latitude, the geomagnetic field lines play as an important role to connect ionosphere and magnetosphere. The open field lines let the electrons and ions escape from the ionosphere to the magnetosphere. There is also precipitation of energetic particles from the magnetosphere to the ionosphere. This can produce the ionized particles in the auroral zone (Tsugawa, 2004).

At mid-latitude, the magnetic field lines does not influence on the ionosphere directly. The collision between charged particles and neutral particles become more important process because of without restriction of the earth's magnetic field. The neutral wind blows from subpolar point to the nightside. This bring the plasma down on the dayside and uplift the plasma on the nightside along the field line. (Tsugawa, 2004).

At low latitude, the geomagnetic field line is nearly horizontal. This causes the unique transport process of the ionospheric plasma. The plasma flow direction is perpendicular to the geomagnetic field line (Tsugawa, 2004).

2.1.2 Neutral Atmosphere

The neutral atmosphere extends from the earth's surface to 1,000 km. The density of the neutral atmosphere decreases exponentially with altitude. The temperature profile varies depending on the atmospheric layers as shown in Figure 2-1 (left).

Troposphere is the atmospheric layer which is closest the earth's surface. It extends from the earth surface beyond 13 km. This layer deals with the atmospheric weather. The temperature profile decreases according to altitude. The cap of this layer is called tropopause which the temperature is constant. The next layer above the troposphere is stratosphere. The layer extends from 10 km to 45 km. The main gas of this layer is Ozone which causes the increase of the temperature profile with altitude because the Ozone absorbs solar UV radiation. Above the stratosphere is mesosphere. The mesosphere extends from 45 km to 95 km altitude. The temperature begins to decrease with altitudes again and reaches the local minimum at the mesopause. Mesosphere is the coldest layer of the terrestrial atmosphere. Above the mesosphere is thermosphere. Thermosphere is the hottest layer of the earth's atmosphere because the absorption of UV and EUV via photo-dissociation of O_2 molecule and ionization of N_2 molecule and O atom. The temperature reaches 1,000 K (Tsugawa, 2004).
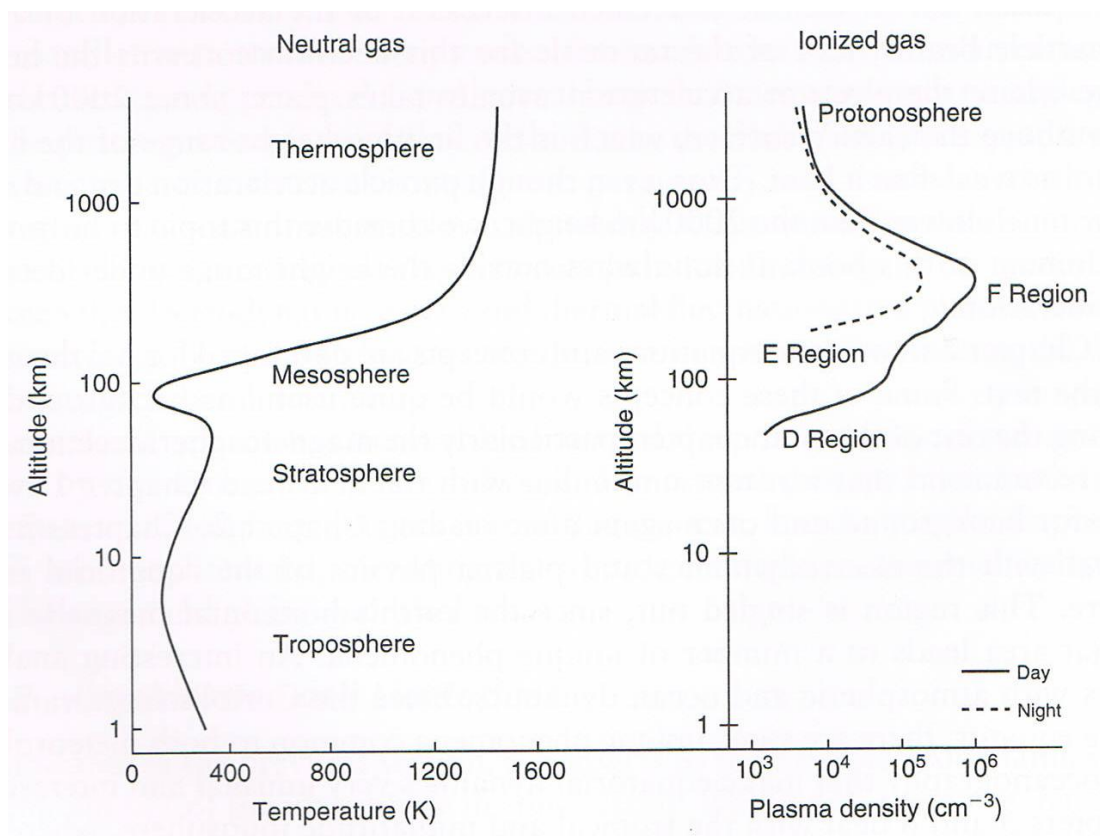
Figure 2-1 The neutral atmosphere (left) and the ionosphere (right) (Kelley, 2009).

2.2   Total Electron Content

Total electron content (TEC) is an integration number of electrons along satellite-receiver path of GPS. The TEC can be derived by measuring two radio waves of GPS signal through the free electrons. The TEC is a parameter which is used to describe the ionosphere. It is measured in TEC unit (TECU) which 1 TECU is equal to 10^{16} electrons per square meter (e/m^2). The maximum value of the TEC appears in the daytime approximately at mid-afternoon while the minimum value of the TEC occurs in the nighttime at around midnight. The number of TEC decreases in the nighttime because of the recombination of electrons and ions.

2.3   Atmospheric Waves

Several wave phenomena of the earth's atmosphere are categorized into three kinds according to their temporal and spatial scales. Planetary waves and tides are the largest scales which are global and shows pattern in both latitude and longitude. The smaller group is classified as atmospheric gravity waves (AGWs). Their horizontal wavelengths are approximately 100 to 3,000 km and their periods are about 30 to 800 minutes. AGWs are classified as medium scale AGWs and large scale AGWs in accordance with their velocity and period (Schunk and Nagy, 2000). The horizontal wavelength of large scale AGWs is greater than 1,000 km and its periods are about 30 minutes to several hours. The horizontal wavelength of medium scale AGWs is several hundred kilometers and its periods are about 15 to 60 minutes. The smallest scale is acoustic wave (AcW). The periods of AcW are several minutes. Usually, the AGWs can travel in the upper atmosphere. However, the AcW does not play as an important role in the upper atmosphere. It is reported in the past related research that some earth's phenomena such as volcanic eruptions and earthquakes are the source of the AcW (e.g. Ducic *et al.*, 1951; Leonard and Barnes, 1965; Yuan *et al.*, 1969; Kanamori and Mori, 1992; Kanamori *et al.*, 1994; Iyemori *et al.*, 2005; Otsuka *et al.*, 2006; Mikumo *et al.*, 2008; Choosakul *et al.*, 2009; Hasbi *et al.*, 2009).

Hines (1960) developed the basic theory of acoustic-gravity wave that can explain most of ionosperic disturbance phenomena. In the theoretical model, the

atmosphere is supposed to be stationary and uniform. Under these conditions, the atmosphere is governed by continuity equation, equation of motion and adiabatic state equation, i.e.,

Continuity   : $$\frac{\partial \rho}{\partial t} + V \cdot \nabla \rho = -\rho \nabla \cdot V \qquad (2.1)$$

Momentum   : $$\frac{\partial \rho}{\partial t} + V \cdot \nabla V = g - \frac{1}{\rho} \nabla \cdot P \qquad (2.2)$$

Adiabaticity   : $$\frac{\partial P}{\partial t} + V \cdot \nabla P = C_S^2 \left(\frac{\partial \rho}{\partial t} + V \cdot \nabla P \right) \qquad (2.3)$$

where ρ is the density of the atmosphere, V is the velocity of the neutral gas, g is the gravitational acceleration, P is the atmospheric pressure and C_S is the sound speed. In Cartesian coordinate, x refers eastward direction, y refers northward direction and z refers upward direction. In the equilibrium state, V_0 is set to be zero, and ρ_0 and P_0 are proportional to $e^{z/2H}$, where $H = C_S^2 / \gamma g$ is the density scale height and γ is the specific heat ratio.

Assuming ρ_1, P_1 and V are small fluctuations with no dependency along y-axis, the harmonic solutions that ρ_1 / ρ_0, P_1 / P_0 and V are proportional to $\exp\left[i\left(\omega t - k_x x - k_z z\right) \right]$ can be obtained by solving linearized equations. If k_z' is assumed as $k_z' = k_z + i/2H$, the dispersion relation below can be obtained:

$$\omega^4 - \omega^2 C_S^2 \left(k_x^2 + k_z'^2 \right) + (\gamma - 1) g^2 k_x^2 / C_S^2 - \gamma^2 g^2 \omega^2 / 4 C_S^2 = 0 \qquad (2.4)$$

From equation (2.4), if k_z' is real, two frequency modes are exist: acoustic mode ($\omega_a = \gamma g / 2 C_S$) and gravity mode ($\omega_g = (\gamma - 1)^{1/2} g / C_S$). The acoustic mode is controlled primarily by compression while the gravity mode is controlled primarily by bouncy. ω_a is the cut off frequency and ω_g is the Brunt-Väisälä frequency. Normally

in the lower atmosphere, $\omega_a/2\pi = 3.3mHz$ and $\omega_g/2\pi = 2.9mHz$. The scale height forces the exponential increase of amplitude with altitude.

2.4 Global Positioning System

Before the global positioning system (GPS) era, the first navigation system called TRANSIT was developed by the United States Navy in 1960. This system was very important for military use in that age. However, the system was not stable and there were some problems. This system also gave low navigation accuracy. These problems lead to the development of GPS.

GPS is a satellite system developed by the United State Department of Defense using for navigation purpose. This system has been improved in order to solve the problems found on TRANSIT system. The GPS gives higher accuracy compared to TRANSIT system and it has been operating until now (Wellenhof *et al.*, 2001). There are three major segments including space segment, control segment and user segment. The details of each segment will be mentioned in this section.

2.4.1 Space Segment

The space segment consists of 24 satellites being operated and 4 satellites being spared. There are six orbital planes of the GPS satellites at 20,200 km altitude from the earth's surface or $4.8R_E$ from the earth's center as shown in Figure 2-2. Each orbit contains four GPS satellites which make sure that 5-10 GPS satellites will appear over the single points on the earth's surface. Each satellite has its own orbital period of approximately 12 hours. The GPS satellites emit dual-frequency of radio waves including L1=1,575.42 MHz and L2=1,227.60 MHz (Wellenhof *et al.*, 2001). The dual-frequency of GPS which passes through the earth's ionosphere and troposphere can be applied to study some ionospheric and tropospheric phenomena such as plasma bubble and water vapor.

Peter H. Dana 9/22/98
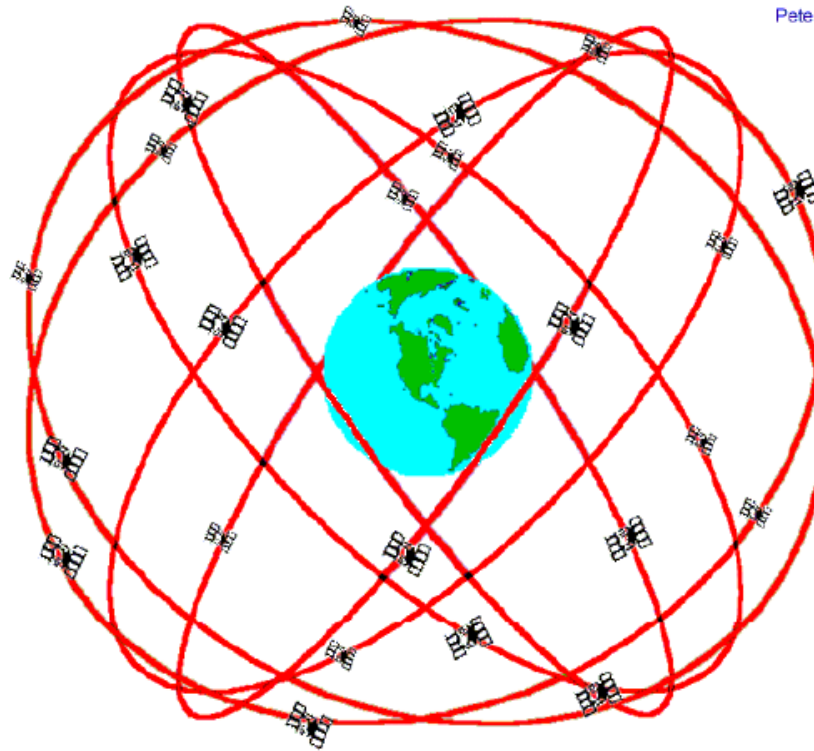
GPS Nominal Constellation
24 Satellites in 6 Orbital Planes
4 Satellites in each Plane
20,200 km Altitudes, 55 Degree Inclination

Figure 2-2 Six orbital planes of GPS satellites (Dana 2013).

2.4.2   Control Segment

The GPS control segment consists of one master control station located in Consolidation Space Operation Center (CSOC), Colorado Spring, Colorado and five monitor stations located in Diego Garcia, Ascension Island, Kwajalein, Hawaii and Colorado Spring. The responsibility of the master control station is to compute the satellite orbits and clock parameters and upload these data to the GPS satellites. The monitor stations will provide all necessary data of the GPS satellite and send it to master control station. Then, all parameters will be computed by master control station using all data provided by minor stations. Another responsibility of monitor stations is to communicate with GPS satellites in order to update the data (Wellenhof *et al.*, 2001).

2.4.3 User Segment

The user segment means GPS receivers and users. There are two types of GPS receiver, C/A-code (Coarse/Acquisition-code) receiver can detect C/A-code and P-code (Precision-code) receiver can receive P-code. There are two groups of users. The first group is the U.S. military and the second group is noncombatants. The U.S. military can use both C/A-code and P-code while civilian group are limited to use only some signals. Today, there are widespread uses of GPS data by noncombatant users. The accuracy of the GPS data relies on the purpose of usage. For example, the standard GPS data is enough for navigation in cars. However, the study of crustal deformation requires high accuracy of GPS data (Michel *et al.*, 2000).

To provide high accuracy GPS data, the biases must be taken into account. There are three types of bias including satellite bias, signal bias and receiver bias. The sources of satellite error come from clock bias and orbit errors. The GPS signal error can be caused by tropospheric delay and ionospheric delay. The sources of receiver error are from clock bias and variation of antenna phase (Wellenhof *et al.*, 2001).

When two radio waves of GPS propagate from a satellite to a ground-based receiver, the radio waves are delayed by neutral particles, electrons and ions in the ionosphere and by water vapor in the troposphere. These cause propagation errors to the GPS signal. The ionospheric delay can be removed by comparing time difference between dual-frequency. Also the tropospheric delay can be solved by some models and mathematical methods.

2.5 GPS Network Around the World

Several GPS networks around the world such as International GPS Service (IGS), GPS Earth Observation Network (GEONET) in Japan and Continuously Operating Reference Stations (CORS) in the United States have been running and developing. The GPS receiver distributions of IGS, GEONET and CORS as of November 2003 are shown in Figure 2-3.

IGS was formally planned in 1993 and founded in 1994 by the International Association of Geodesy (IAG) in order to provide GPS data, tracking data and other

data to support geodesy and geophysical research via the IGS site (http://igscb.jpl.nasa.gov). There are up to 1,000 IGS stations around the world as shown in Figure 2-3(a). The global TEC map can be provided by GPS data from the IGS network all over the world.

GEONET, Japan is the continuous GPS network over Japan operated by the Geographical Survey Institute (GSI), Japan. In April 2004, 110 GPS receivers were first installed. Today, about 1,000 receivers have been installed with 25 km spacing interval as shown in Figure 2-3(b). These receivers provide GPS data with 30 seconds of sampling rate. The GPS RINEX format can be retrieved from GSI homepage. However, there are some limitations of retrieving data and viewing site. For example, only last three months data can be downloaded from GSI space. The users who need old data must contact GSI by email. Also the GSI space was provided in Japanese version.

The U.S. National Geodetic Survey (NGS) operated CORS which provides GPS data from approximately 400 stations around the United States as shown in Figure 2-3(c). Since May 2010, Global Navigation Satellite System (GNSS) data has been provided by CORS in order to support three dimensional positioning, meteorological study, space weather study and geophysical applications. The GNSS data consist of carrier phase and code range. The data is derived from around 1,450 stations today. The users can retrieve the data from the CORS homepage, http://www.ngs.noaa.gov/CORS/.

The GPS data from other networks such as European Reference Frame (RUREF) and Southern California Integrated GPS Network (SCIGN) can be downloaded from the SOPAC site (http://sopac.ucsd.edu/sites/).

The lists of GPS network around the world that the users can retrieve the data from SOPAC space are summarized in Table 2-1.
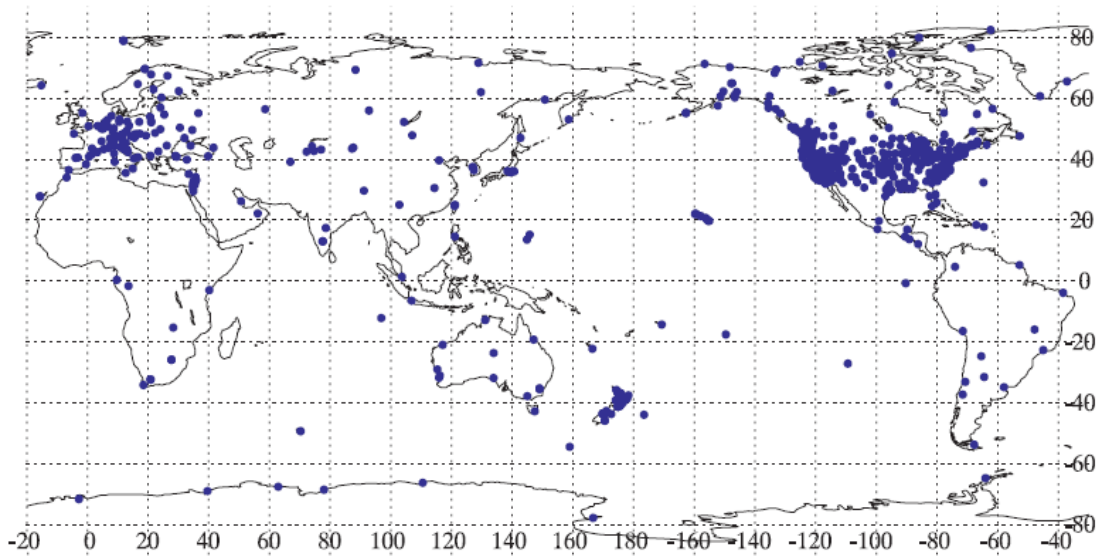
(a) IGS GPS Stations
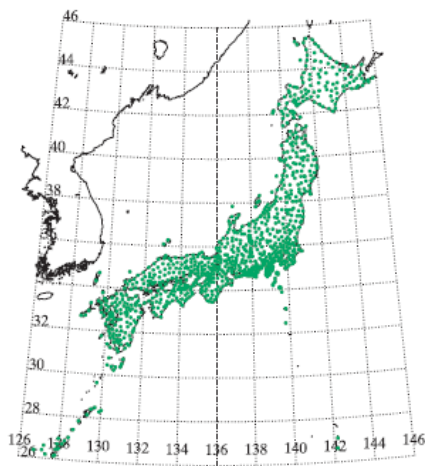
(b) GEONET GPS Stations
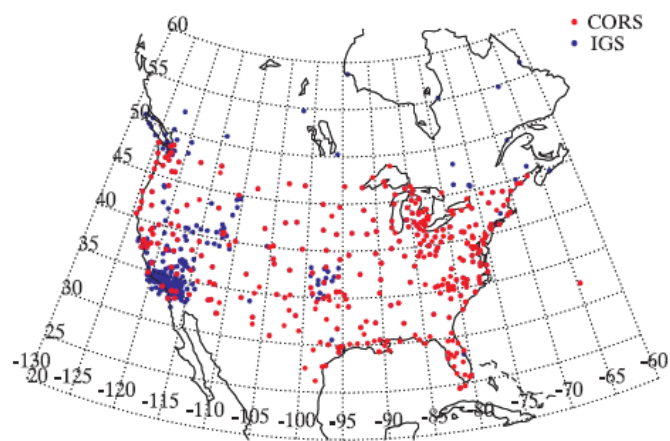
(c) CORS GPS Stations

Figure 2-3 GPS stations of (a) International GPS Service (IGS), (b) GPS Earth Observation Network (GEONET) in Japan and (c) Continuously Operating Reference Stations (CORS) in the United States (Tsugawa, 2004).

Table 2-1 The list of GPS networks around the world.

Network Name	Website	E-mail
Australian Regional GPS Network (ARGN)	http://www.ga.gov.au/earth-monitoring/geodesy/gnss-networks/gnss/ARGN.html	geodesy@ga.gov.au
Bay Area Regional Deformation GPS Network (BARD)	http://seismo.berkeley.edu/bard/	bard@seismo.berkeley.edu
Basin and Range GPS Network (BARGN)	http://cfa-www.harvard.edu/space_geodesy/BARGEN/	jnormandeau@cfa.harvard.edu
Canadian Active Control System (CACS)	http://www.geod.nrcan.gc.ca/	information@geod.nrcan.gc.ca
California Passive Network (CALPAN)	http://csrc.ucsd.edu	ybock@ucsd.edu
Canary GNSS Center Network (CGCN)	N/A	nacho@canaryadvancedsolutions.com
Continuously Operating Reference Stations (CORS)	http://www.ngs.noaa.gov/CORS/cors-data.html	richard.snay@noaa.gov
Central Valley Spatial Reference Network (CVSRN)	N/A	giana_cardoza@dot.ca.gov
Eastern Basin Range Yellowstone (EBRY)	http://www.uusatrg.utah.edu/RBSMITH/public_html/RESEARCH/UUGPS.html	rbsmith@mines.utah.edu
Estaciones de Referencia GPS/GNSS de Valencia (ERVA)	http://www.gva.es/icv	Capilla_raq@gva.es
European Reference Frame (EUREF)	http://www.euref-iag.net	C.Bruyninx@oma.be
Friuli Regional Deformation Network (FREDNET)	N/A	dzuliani@inogs.it
Earth System Research Laboratory (FSL)	http://gpsmet.noaa.gov/	Seth.I.Gutman@noaa.gov

Table 2-1 (continue)

Network Name	Website	E-mail
Galileo Sensor Stations Network (GALILEO)	N/A	Tim.Springer@esa.int
GPS Array for Mid-America (GAMA)	N/A	rsmalley@memphis.edu
GeoNet New Zealand (GEONET)	http://www.geonet.org.nz	info@geonet.org.nz
GEOSPATIAL INFORMATION AUTHORITY OF JAPAN (GSI)	http://www.gsi.go.jp/ENGLISH/	N/A
International GNSS Service (IGS)	http://igscb.jpl.nasa.gov	igscb@igscb.jpl.nasa.gov
West Java / Bali GPS Network (INATEWS)	N/A	csubarya@bakosurtanal.go.id
Institute for High Temperatures (IVTAN)	http://www.jiht.ru/	bragin@tiger.gdirc.ru
Mediterranean GPS Network (MGN)	N/A	N/A
nearnet (NEARNET)	http://geodesy.unr.edu/networks/index.html	gblewitt@unr.edu
Northeast Eurasia Deformation Array (NEDA)	N/A	steblov@gps.gsras.ru
National Geospatial-Intelligence Agency (NGA)	http://earth-info.nga.mil/GandG/satht ml/	gps@nga.mil
Nepal Geodetic Monitoring Network (NGMN)	N/A	John Galetzka
Geodetic Survey Division, Natural Resources Canada (NRCAN)	http://www.geod.nrcan.gc.ca/	Michael.Craymer@NRCan-RNCan.gc.ca
CORSnet-NSW (NSW)	http://www.corsnet.com.au	CORSnetCustomerSupport@lpi.nsw.gov.au
Oregon Real Time GPS Network (ORGN)	N/A	minera@Geology.cwu.EDU

Table 2-1 (continue)

Network Name	Website	E-mail
Ohio State University (OSU)	N/A	kendrick.42@osu.edu
Pacific Northwest Geodetic Array (PANGA)	http://www.geodesy.cwu.edu	panga@geology.cwu.edu
PBO GPS Network (PBO)	http://pbo.unavco.org	anderson@unavco.org
Pierce County Survey (PC3N)	http://spider.co.pierce.wa.us/	mholden@co.pierce.wa.us
Pacific GPS Facility (PGF)	N/A	jfoster@leka.soest.hawaii.edu
Permanent GPS network of the Canary Islands (PGPSNCI)	N/A	nacho@canaryadvancedsolutions.com
renag (RENAG)	http://webrenag.unice.fr	Gilbert.Ferhat@insa-strasbourg.fr
Azores REPRAA network (REPRAA)	N/A	nacho@canaryadvancedsolutions.com
Red Geodesica Nacional Activa (RGNA)	N/A	evazquez@dgg.inegi.gob.mx
Kuker-Ranken (RGPS)	N/A	minera@Geology.cwu.EDU
SuomiNet Geodetic (SNG)	http://www.suominet.ucar.edu/	bjorn@unavco.ucar.edu
Southern Baja Network (SOBNET)	http://www.geodesy.cwu.edu	panga@geology.cwu.edu
Survey of Israel (SOI)	N/A	sade_mapi@int.gov.il
South Pacific Sea Level Climate Monitoring Program (SPSLCMP)	http://www.ga.gov.au/geodesy/slm/spslcmp/network.jsp	geodesy@ga.gov.au
Sumatran GPS Array (SUGAR)	N/A	sieh@gps.caltech.edu
Tibet GPS Initiatives, Chinese Academy of Sciences (TIGICAS)	N/A	N/A

Table 2-1 (continue)

Network Name	Website	E-mail
Tribhuvan University GNSS Network (TRIBHUGNET)	N/A	bnupreti@wlink.com.np
Universidad Nacional Autonoma de Mexico (UNAM)	http://usuarios.geofisica.unam.mx/vladimir/gpsred/gpsred.html	vladi@servidor.unam.mx
Unknown Affiliation (UNKNOWN)	N/A	N/A
USGS Southern California GPS Network (USGS-SC)	http://www.scign.org	dollar@iron.gps.caltech.edu
Venezia Consorzio Nuova (VENICE)	N/A	viviana.ardone@consorziovenezianuova.com
Western Canada Deformation Array (WCDA)	http://www.nrcan.gc.ca/earth-sciences/energy-mineral/geology/geodynamics/western-canada-deformation-array/8825	mschmidt@nrcan.gc.ca
Washington State Reference Network (WSRN)	http://wsrn.org	gavin.schrock@seattle.gov

Scripps Orbit and Permanent Array Center (SOPAC), 1990.

CHAPTER III

METHODOLOGY OF RESEARCH

3.1 Earthquake Events

The earthquake data was retrieved from the United States Geological Survey (USGS) database via http://earthquake.usgs.gov/. The USGS provides real time earthquake monitor. They also provide the earthquake data since 2002. This research focuses on the earthquake with magnitude higher than 7.5 and the depth of the earthquake's focus is not over 30 km beneath the ground surface. It is assumed that the large earthquakes may provide high energy to disturb plasma on the Ionosphere. Moreover, small depths of focuses were selected because the Rayleigh wave was supposed to have a small attenuation while it travels to the ground surface. The earthquake data including the date of earthquake, geographical latitude and longitude, origin time of earthquakes: universal time (UT) and local time (LT), magnitude, and depth of focus are shown in Table 3-1.

Table 3-1 The geographic and geomagnetic coordinates, earthquake onset times, magnitude and depth.

No.	Event	Date	Onset Time (UT)	Onset Time (LT)	Mag.	Depth (km)
1	Near the north coast of Papua, Indonesia	03 01 2009	19:43:50	04:43:50	7.7	17
2	Off west coast of the south island, N.Z.	15 07 2009	09:22:29	20:22:29	7.8	12
3	Samoa islands region	29 09 2009	17:48:10	06:48:10	8.1	18
4	Kepulauan mentawai region, Indonesia	25 10 2010	14:42:22	21:42:22	7.7	20.6
5	Near the east coast of Honshu, Japan	11 03 2011	05:46:24	12:46:24	9.0	30
6	Kermadec islands region	06 07 2011	19:03:16	07:03:16	7.6	20

U.S. Geological Survey (USGS), 1998.

3.2 Geomagnetic and Solar Indices

Three indices including disturbance storm time (Dst), Kp, and solar flares were used in this research. The Dst index is used to indicate the strength of the ring current which flows around the globe from east to west in the equatorial plane. The causes of ring current are solar protons and electrons. The ring current generates the magnetic field which has opposite direction to the earth's magnetic field. The negative Dst index means that the magnetic storm is in progress. The more negative value of Dst index means that there is intense magnetic storm and the earth's magnetic field becomes weaker. The Dst index can be viewed from the homepage of world data center (WDC) for geomagnetism (http://wdc.kugi.kyoto-u.ac.jp/). Figure 3-1 shows WDC homepage which provides the Dst data from 1957 to present. The Kp index is a three-hour intervals of geomagnetic activity relative to an assumed quiet day curve for the recording site. The Kp index values range from zero, which indicates very quiet condition, to nine, which indicates extremely disturbed condition. The Kp index data can be retrieved from the National Oceanic and Atmospheric Administration (NOAA) website: http://www.swpc.noaa.gov/ftpmenu/indices/old_indices.html. Figure 3-2 shows the homepage which provides Kp index and flare indices from 1994 to present. Both Dst and Kp indices are used to classify the geomagnetic activity on the earthquake day in this research. In the case of solar activity, the solar flare indices will be taken into account. Solar activity means any change in the Sun's appearance or behaviour. The Sun's activity is classified as being very low, low, moderate, high or very high. The terms below refer to the strength and the number of x-ray solar flares (Ionospheric Prediction Service (IPS), 2009).

Very Low:	x-ray events less than C-class
Low:	C-class x-ray events
Moderate:	isolated (1 to 4) M-class x-ray events
High:	several (5 or more) M-class x-ray events, or isolated (1 to 4) M5 or greater x-ray events
Very High:	several (5 or more) M5 or greater x-ray events
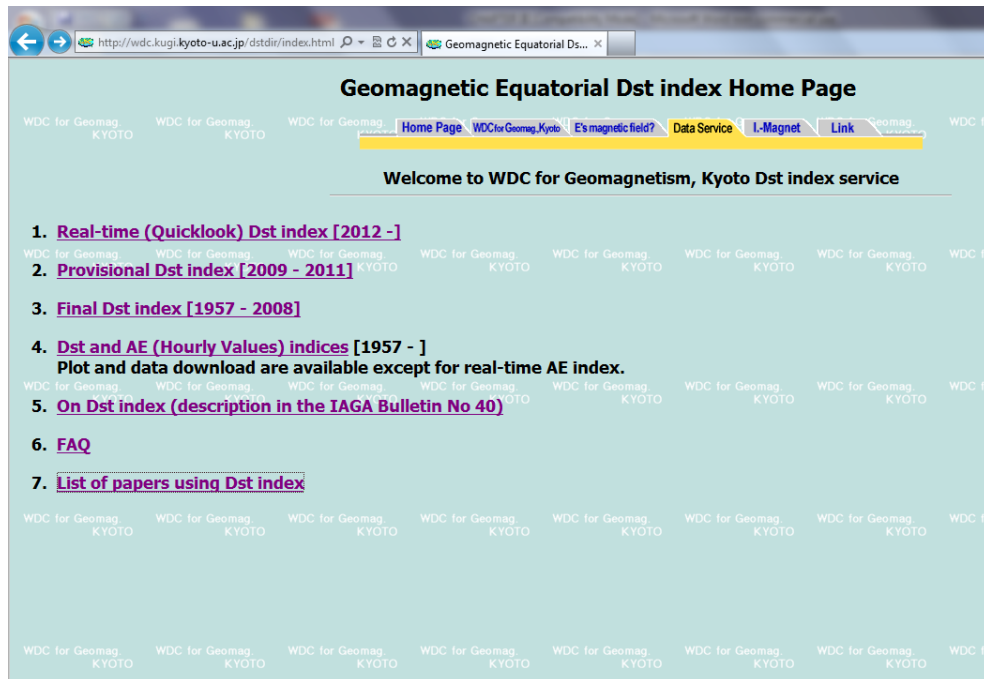
Figure 3-1 The Dst index homepage from World Data Center (WDC) for Geomagnetism, Kyoto University (World Data Center (WDC) for Geomagnetism, 1995).
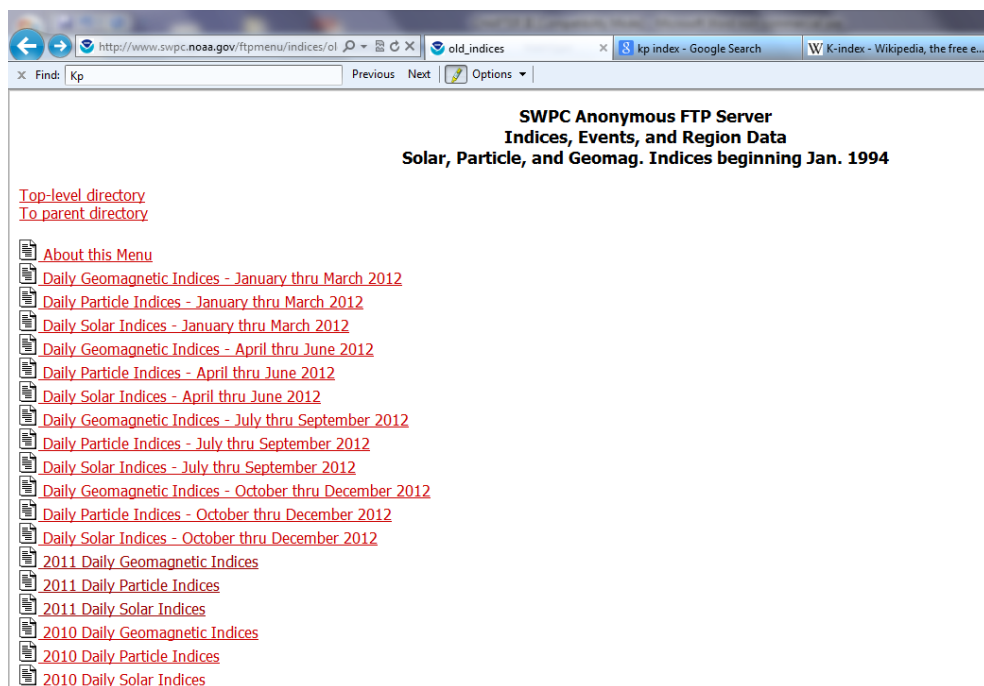
Figure 3-2 The Kp and flare indices site homepage from NOAA (National Oceanic and Atmospheric Administration (NOAA), 2009).

3.3 GPS-derived TEC

The major program which is used to calculate total electron content (TEC) in this project is RINEX GPS-TEC program version 2.1 developed by Dr. Gopi Seemala. This section will explain briefly how to derive the GPS TEC. The slant TEC along the satellite and receiver path, $T^j(t)$, at epoch time t and measured by satellite j is expressed in equation (3.1)

$$T^j(t) = \beta^j(t) - B^j, \tag{3.1}$$

where $\beta^j(t)$ is an observable TEC and B^j is the instrumental bias which is set to be constant for each satellite-receiver pair. The slant TEC is mapped to the vertical direction called vertical TEC, $V^j(t)$, using the assumption of ionospheric thin shell model as shown in Figure 3-3, i.e.,

$$T^j(t) = V^j(t) \cdot S(\theta), \tag{3.2}$$

where $S(\theta)$ is the single model mapping function as shown in equation (3.3) and θ is the elevation angle at the receiver site, i.e.,

$$S(\theta) = \frac{1}{\cos(\theta')}, \tag{3.3}$$

where θ' is the elevation angle at the ionospheric pierce point (IPP). To determine θ', it is necessary to use the geometry in Figure 3-3 in order to find the relationship between θ and θ'. Equation (3.4) shows the relationship between between θ and θ'. Then, θ' can be expressed in equation (3.4). Finally, the single model mapping function can be expressed as (3.6)

$$\sin \theta' = \left(\frac{R_E}{R_E + h_m} \right) \sin \theta \tag{3.4}$$

$$\theta' = \sin^{-1} \left\{ \left(\frac{R_E}{R_E + h_m} \right) \sin \theta \right\} \tag{3.5}$$

$$\therefore S(\theta) = \frac{1}{\cos \left\{ \sin^{-1} \left[\left(\frac{R_E}{R_E + h_m} \right) \sin \theta \right] \right\}} \tag{3.6}$$

h_m is set to be 350 km. From equation (3.1) and (3.2), the vertical TEC can be gained at every sampling interval of 30 seconds as equation (3.7)

$$V^j(t) = \left(\beta^j(t) - B^j \right) / S(\theta) \tag{3.7}$$
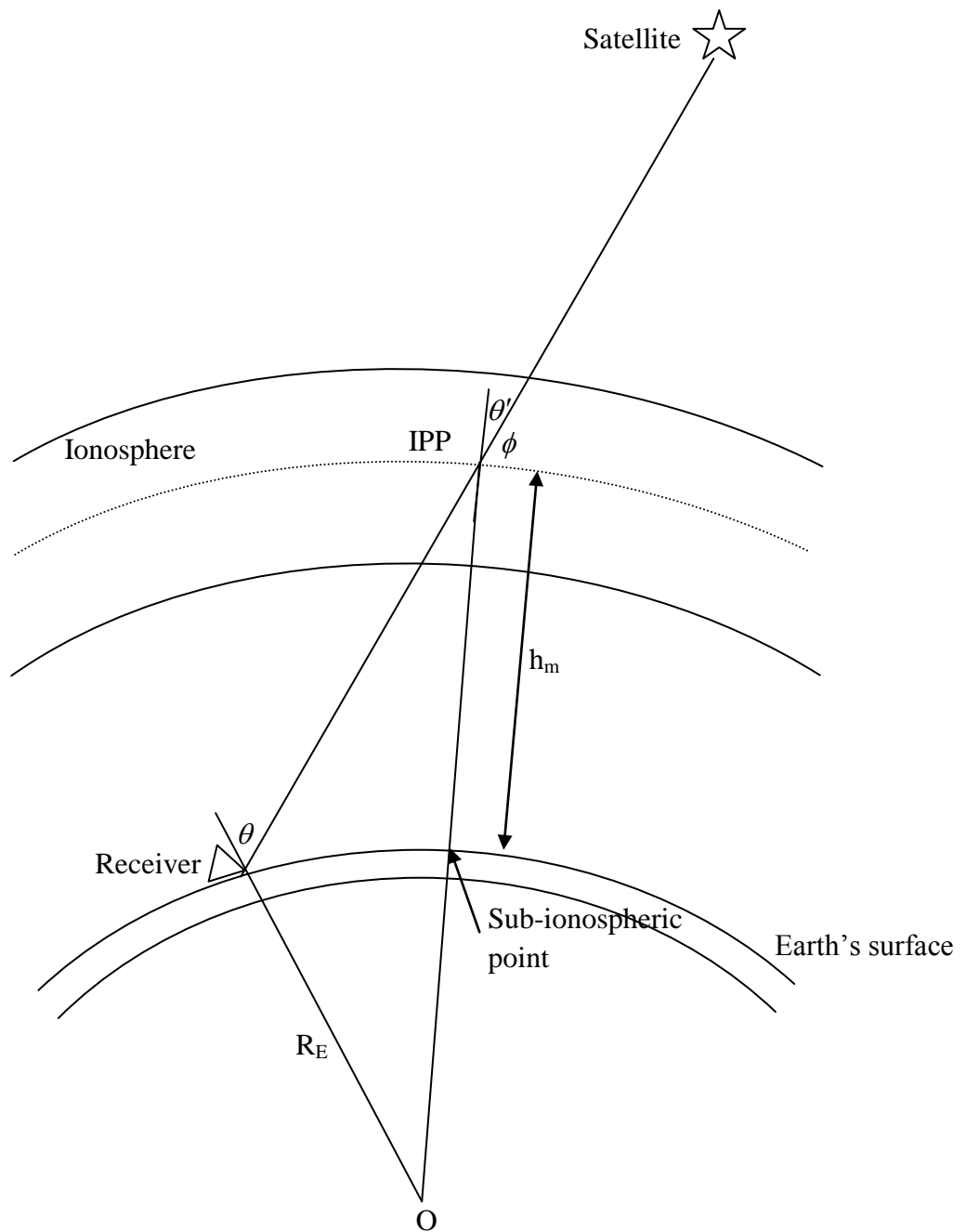
Figure 3-3 The ionospheric single model.

CHAPTER IV

DATA PROCESSING

The GPS dataset with 30 minutes of sampling rate was obtained from the International GPS Service (IGS) database via the website http://sopac.ucsd.edu/ for the first event and the third event to the fifth event. For the second event, the data was retrieved from GeoNet, New Zealand from the space http://www.geonet.org.nz. There are around 143 GPS stations of GeoNet as of July 2009 being used in the study area. Then, the GPS data was input to the RINEX GPS-TEC program version 2.1. There are 10 columns of the output data as shown in Figure 4-1.

Figure 4-1 Output data from Rinex GPS-TEC program version 2.1

At this stage, the program was developed by MATLAB in order to analyze the TEC data. There are four columns of raw data including Time, Lat, Lon and VTEC being loaded to this program. The flow chart of the program was shown in Figure 4-2.
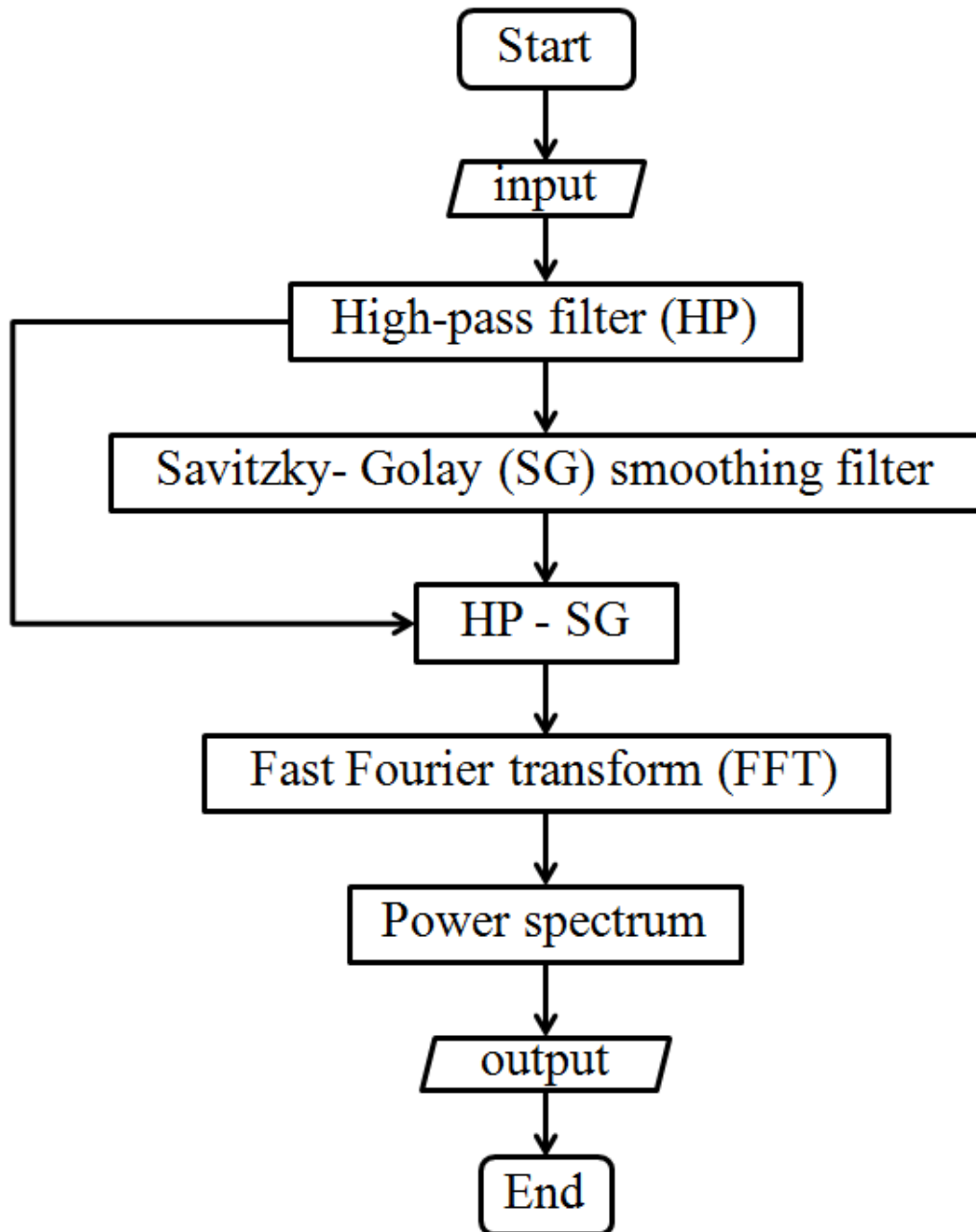
Figure 4-2 The flow chart of the program which was developed by MATLAB.

The program code for analyzing the TEC data was shown below:

Source Code 1

```
%------------------------The program is for calculating filtered data
%------------------------------------------By Radchagrit SUPAKULOPAS
%-----------Head of the data---------Time(1), Lat(2), Lon(3), VTEC(4)
%-----------Modified by Radchagrit on 08 March 2013------------------
data = xlsread('phkt13.xls');
T   = data(:,1);
V   = data(:,4);
lat = data(:,2);
lon = data(:,3);
%-----------------applied high-pass filter and Savitzky-Golay method
[b,a]= butter(2,.00167,'high');
HP  = filter(b,a,V);
SG  = sgolayfilt(HP,5,33);
TEC = HP - SG;
%--------------------------------------------------------------plot
figure(1), plot(T, V, 'k');
figure(2), plot(T, HP, 'k');
figure(3), plot(T, SG, 'k');
figure(4), plot(T, TEC, 'k');
%------apply fast fourier transform (FFT) for power spectral analysis
Ts = 30;
Fs = 1/Ts;
n = length(T);
fourier = fft(TEC,n);
f = (0:n-1)*(Fs/n);
power = fourier.*conj(fourier)/n;
figure(5),plot(f(1:floor(n/2)),power(1:floor(n/2)),'k');
%--------------------------------------------------------------End
```

The source code 1 above will be tested by analyzing the GPS data from Phuket station on 26 December 2004. This is to compare the outputs of this program with the results of Choosakul *et al.* (2009). Figure 4-3 expresses the original data of TEC after the Sumatra-Andaman earthquake on 26 December 2004. The earthquake occurred at 00:58:53 UT. The source code 1 plays the role to apply high-pass filter to the TEC data in order to remove high frequencies. The 10-minute cut off period was chosen to remove the periods of the TEC variations which come from the gravity wave and planetary waves and tides. The atmospheric gravity wave has the periods of about 15 minutes to several hours. The acoustic wave's period will be selected from the TEC data.
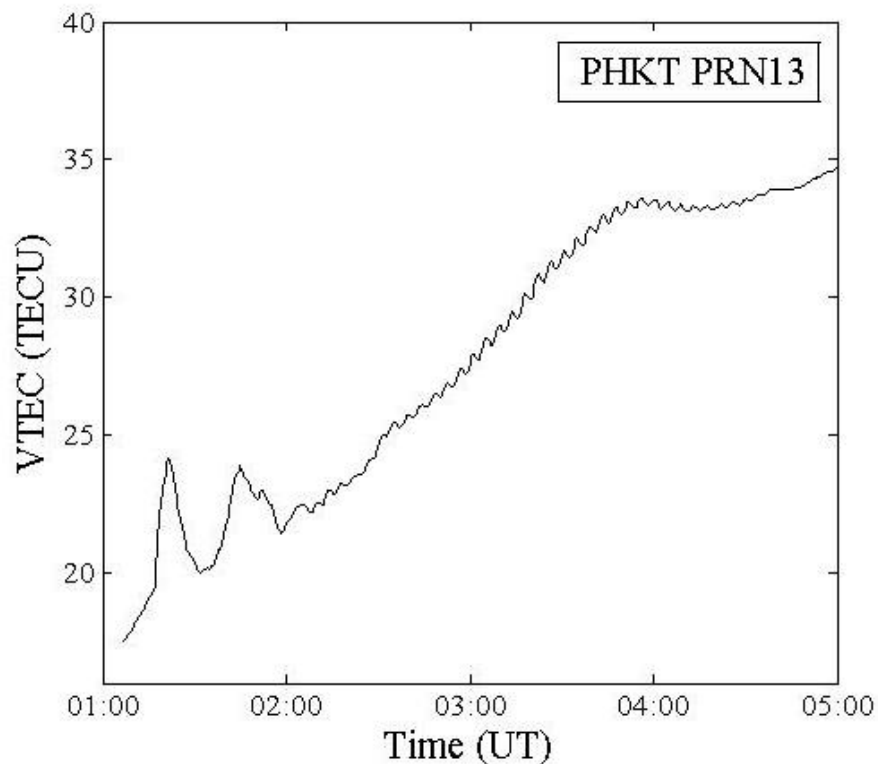
Figure 4-3 The original data of TEC variation observed by Phuket station on 26 December 2004.

After that, the TEC data was smoothed using the Savitzky-Golay method. The Savitzky-Golay method will smooth the TEC data but this method still maintains the shape and height of waveform peaks. Then, the smoothed high-pass filtered TEC data was subtracted by the high-pass filtered TEC data in order to extract the variation pulses. Figure 4-4(a) and 4-4(b) illustrates the high-pass filtered TEC data and smoothed high-pass filtered TEC data between 01:00 UT and 05:00 UT on 26 December 2004, respectively. After finishing this stage, the TEC variations on 26 December 2005 between 01:00 UT and 05:00 UT can be obtained as shown in Figure 4-5(a). The TEC variations from the same earthquake event observed by Phuket station from Choosakul *et al.* (2009) study are shown in Figure 4-5(b).
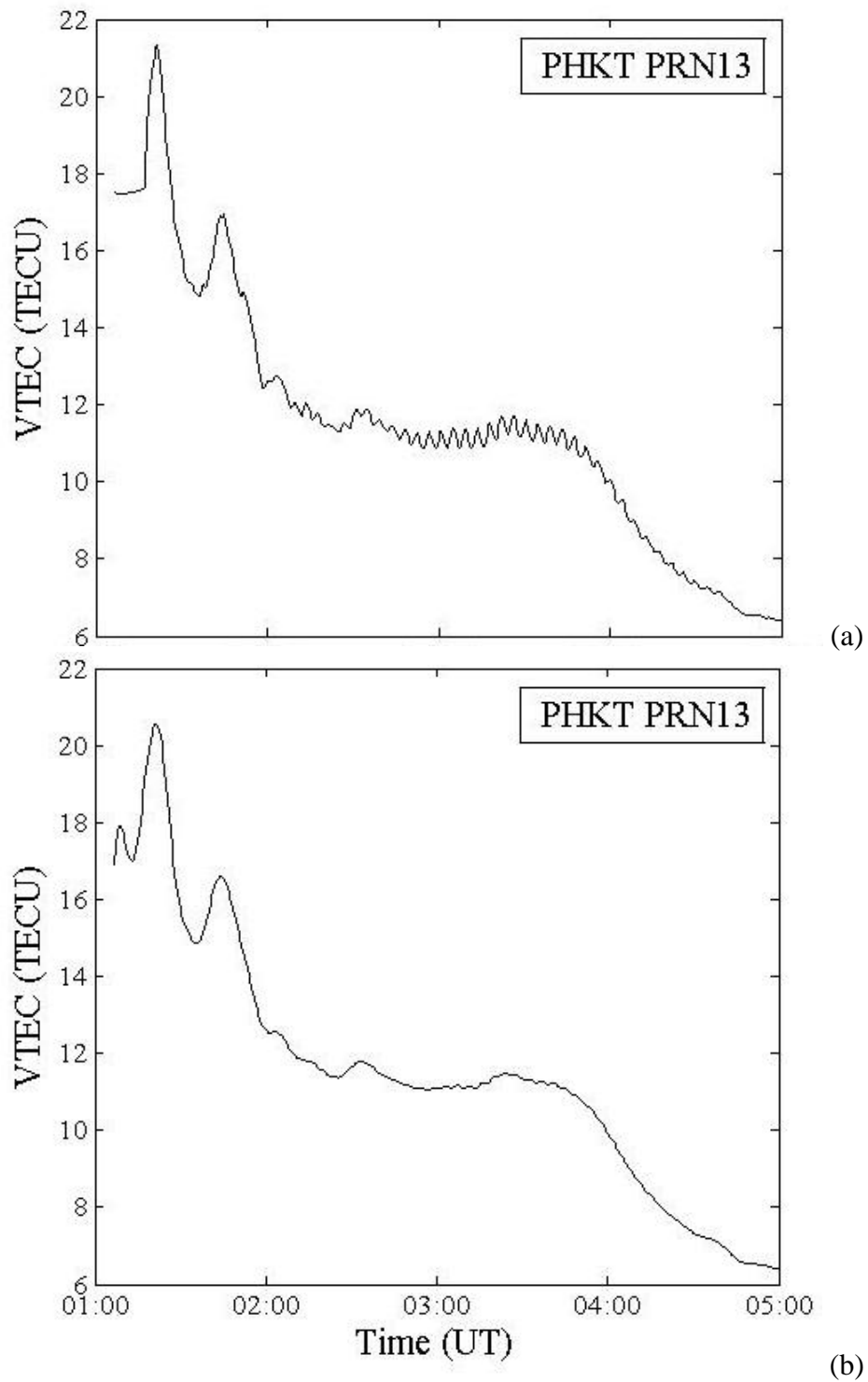
Figure 4-4 (a) The high-pass filtered TEC data with 10-minute cut off period and (b) the smoothed high-pass filtered TEC data.
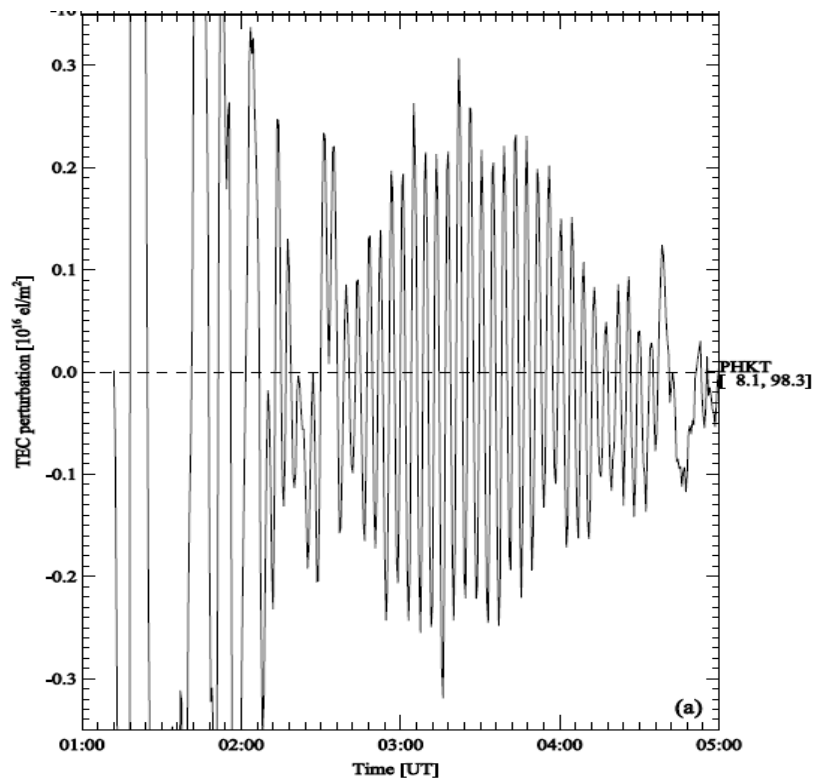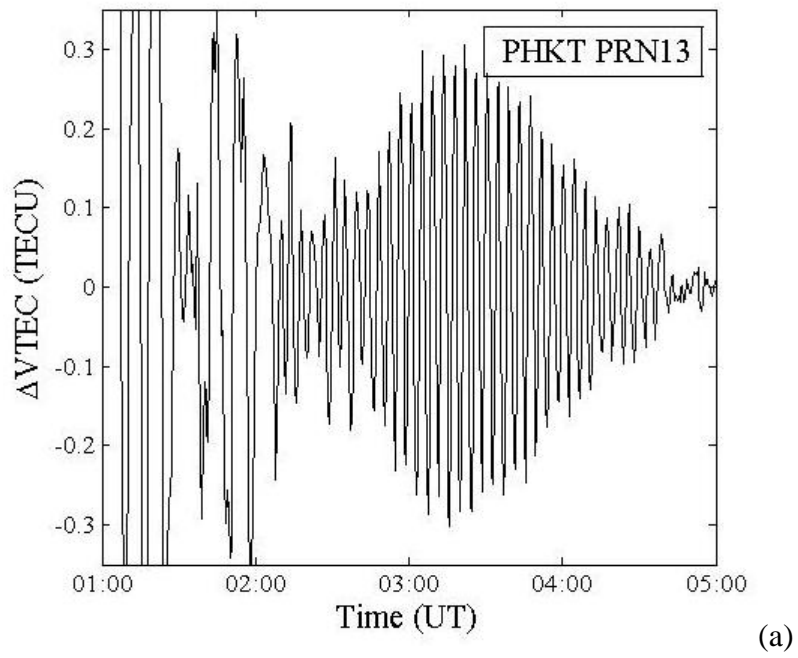
Figure 4-5 The TEC variation on 26 December 2004 from 01:00 UT to 05:00 UT (a) from source code 1 and (b) from Choosakul *et al.* (2009) report.

Next step of the process is analyzing the power spectrum of the TEC data using fast fourier transform (FFT) method. The FFT converts time domain of the data to frequency domain. The power spectrum will show the dominant frequencies of TEC data and the frequencies will be converted to the periods of the TEC variations. Before analyzing the power spectrum, the program must be tested. The synthetic sine wave during the time domain 0 to 3,600 seconds was input to the source code 1. The sine wave equation was expressed as equation (4.1).

$$A = \sin\left(\frac{2\pi t}{120}\right) + \sin\left(\frac{2\pi t}{300}\right) + \sin\left(\frac{2\pi t}{600}\right) + \sin\left(\frac{2\pi t}{1200}\right) \qquad (4.1)$$

Time domain is $t = 0 : 3,600;$. The periods of sine wave are 120, 300, 600 and 1200 seconds. That means the frequencies of sine wave are 8.33, 3.33, 1.67 and 0.83 mHz. Figure 4-6 shows the power spectrum of sine wave which the dominant frequencies are 8.33, 3.33, 1.67 and 0.83 mHz. It can confirm that the source code 1 has enough accuracy to analyze the TEC data.

The last step of this research is the comparison of the dominant frequencies of the TEC variations between 01:00 UT to 05:00 UT on 24 December 2004 obtained by source code 1 with Choosakul *et al.* (2009) study. The dominant frequency obtained from source code 1 is 3.9 mHz as shown in Figure 4-7(a). The source code 1 provides the dominant frequency of the TEC data which is equal to Choosakul *et al.* (2009) report. Figure 4-7 (b) shows the dominant frequency of 3.9 mHz from Choosakul *et al.* (2009) study. The period of the TEC variations is approximately 4 minutes.

The source code 1 developed by MATLAB provides the results which is equal to the results of Choosakul *et al.* (2009). The GPS-Derived TEC method of Choosakul *et al.* (2009) was developed by Associate Professor Dr. Akinori Saito at the Department of Geophysics, Kyoto University. The TEC data of Choosakul *et al.* (2009) were processed the signal processing by the interactive data language (IDL). There are no researchers who develop the program for data processing of the TEC on MATLAB. Therefore, MATLAB is the target for our laboratory. Next chapter, the source code 1 is going to be applied to study the Earth Science field.
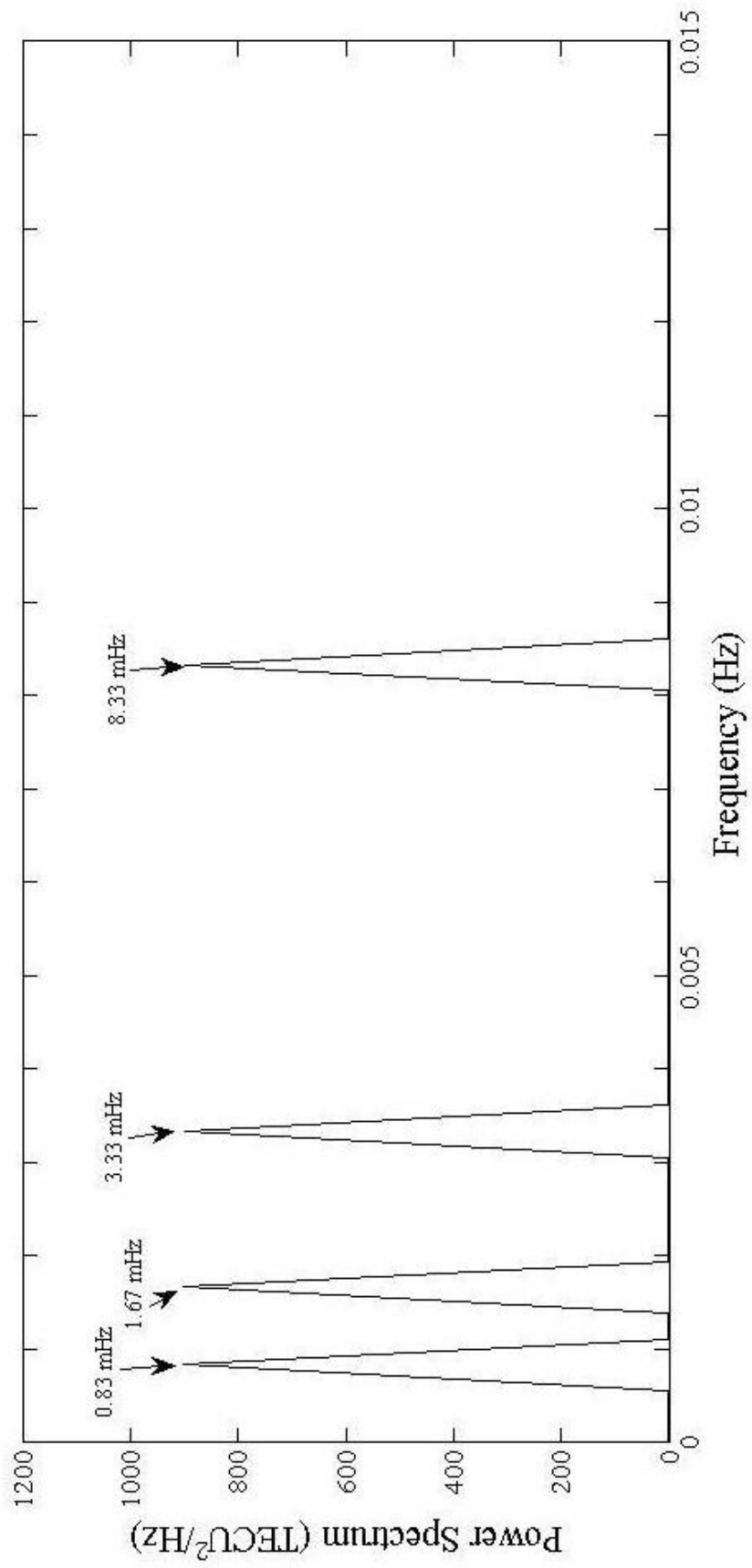
Figure 4-6 The power spectrum of sine waves.
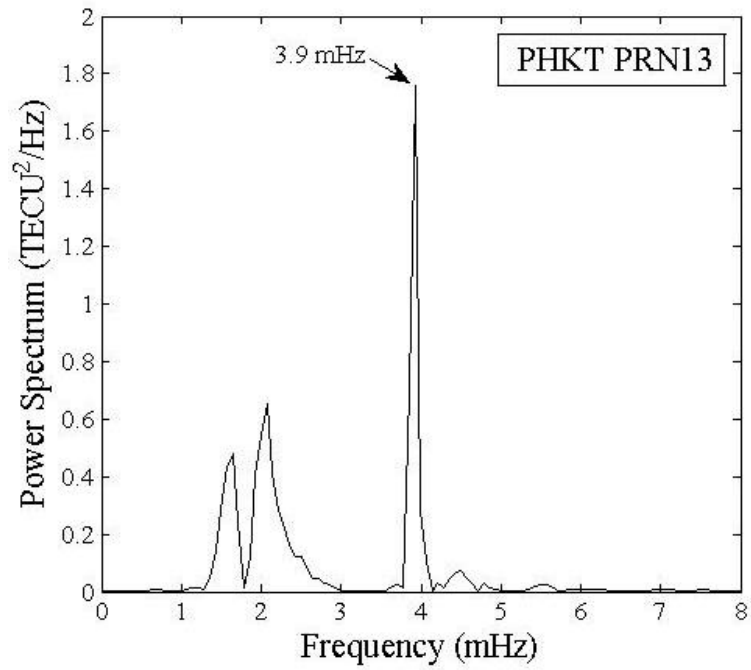
(a)
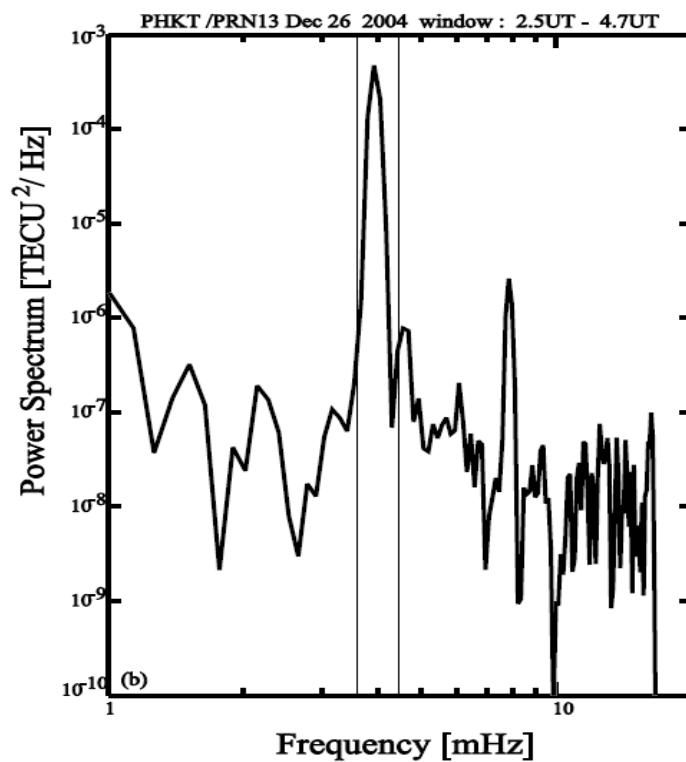
(b)

Figure 4-7 The power spectrum of TEC variations on 26 December 2004 (a) from 01:00 UT to 05:00 UT obtained from source code 1 and (b) from 02:30 UT to 04:42 UT from Choosakul *et al.* (2009) report.

CHAPTER V
RESULTS AND DISCUSSIONS

The previous chapter, the program was developed by using MATLAB and was tested its accuracy. This chapter, the program will be applied to study Earth Science phenomena. The data processing for the TEC data in the previous chapter could determine the result of the ionospheric variations in this chapter. Four out of 6 earthquakes could affect the TEC variations after the earthquake origin time as shown in Table 5-1.

Table 5-1 The lists of 6 earthquakes and their TEC variations.

No.	Event	Date	Onset Time (UT)	Mag.	Depth (km)	TEC variations
1	Near the north coast of Papua, Indonesia	03 01 2009	19:43:50	7.7	17	No
2	Off west coast of the south island, N.Z.	15 07 2009	09:22:29	7.8	12	Yes
3	Samoa islands region	29 09 2009	17:48:10	8.1	18	Yes
4	Kepulauan mentawai region, Indonesia	25 10 2010	14:42:22	7.7	20.6	No
5	Near the east coast of Honshu, Japan	11 03 2011	05:46:24	9.0	30	Yes
6	Kermadec islands region	06 07 2011	19:03:16	7.6	20	Yes

5.1 Near the north coast of Papua, Indonesia

The earthquake near the north coast of Papua in Indonesia occurred on 3 March 2009 at 19:43:50 UT (Universal Time) or 04:43:50 LT (Local Time). The magnitude of the earthquake is 7.7 and the focus's depth is 17 km beneath the ground surface. There are six GPS stations being used in this study area. The earthquake epicenter and GPS locations are shown in Figure 5-1.
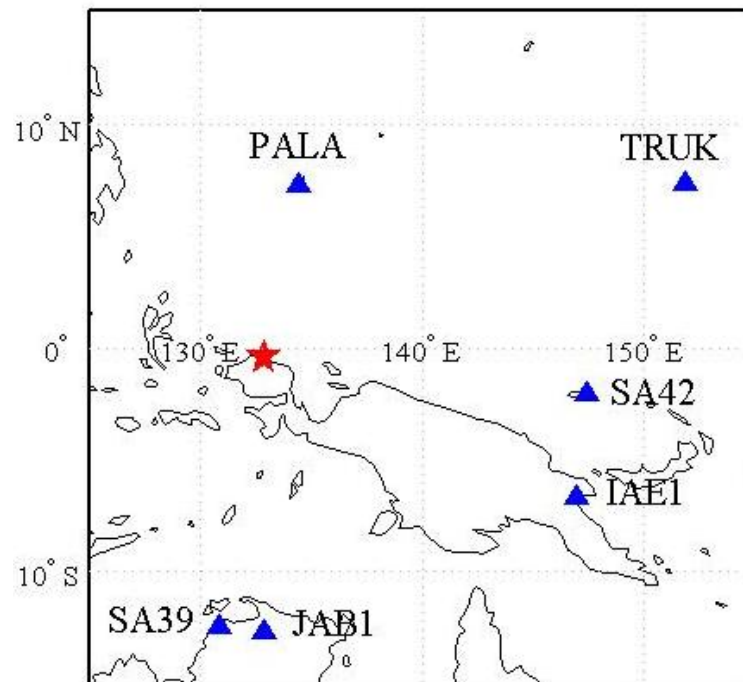
Figure 5-1 The locations of earthquake epicenter (red star) near the north coast of
Papua in Indonesia on 3 January 2009 and GPS stations (triangle).

However, several GPS receivers around the earthquake's epicenter didn't
provide GPS data for several years and also at the earthquake time. Thus, the TEC
variations cannot be studied in this event. The other GPS stations were also chosen.
However, they also didn't provide the GPS data for several years and their distances
from the epicenter are too far (>2,000 km).

5.2 Off West Coast of the South Island, New Zealand

Geomagnetic and solar indices

It is known that geomagnetic and solar activities could disturb TEC on the
Ionosphere (e.g. Zhang and Xiao, 2005; Tsugawa *et al.*, 2007). This study, the solar
activity level was classified by C, M and X class. No solar flare that is larger than C
class was reported on 15 July 2009. The flare indices indicated that the solar activity
level was very low. The Kp and Dst indices between 14 and 16 July 2009 are shown
in Figure 5-2(a) and 5-2(b). Kp was one at the earthquake origin time, while the Dst
index was higher than -15 nT during the earthquake day.

(a)

(b)
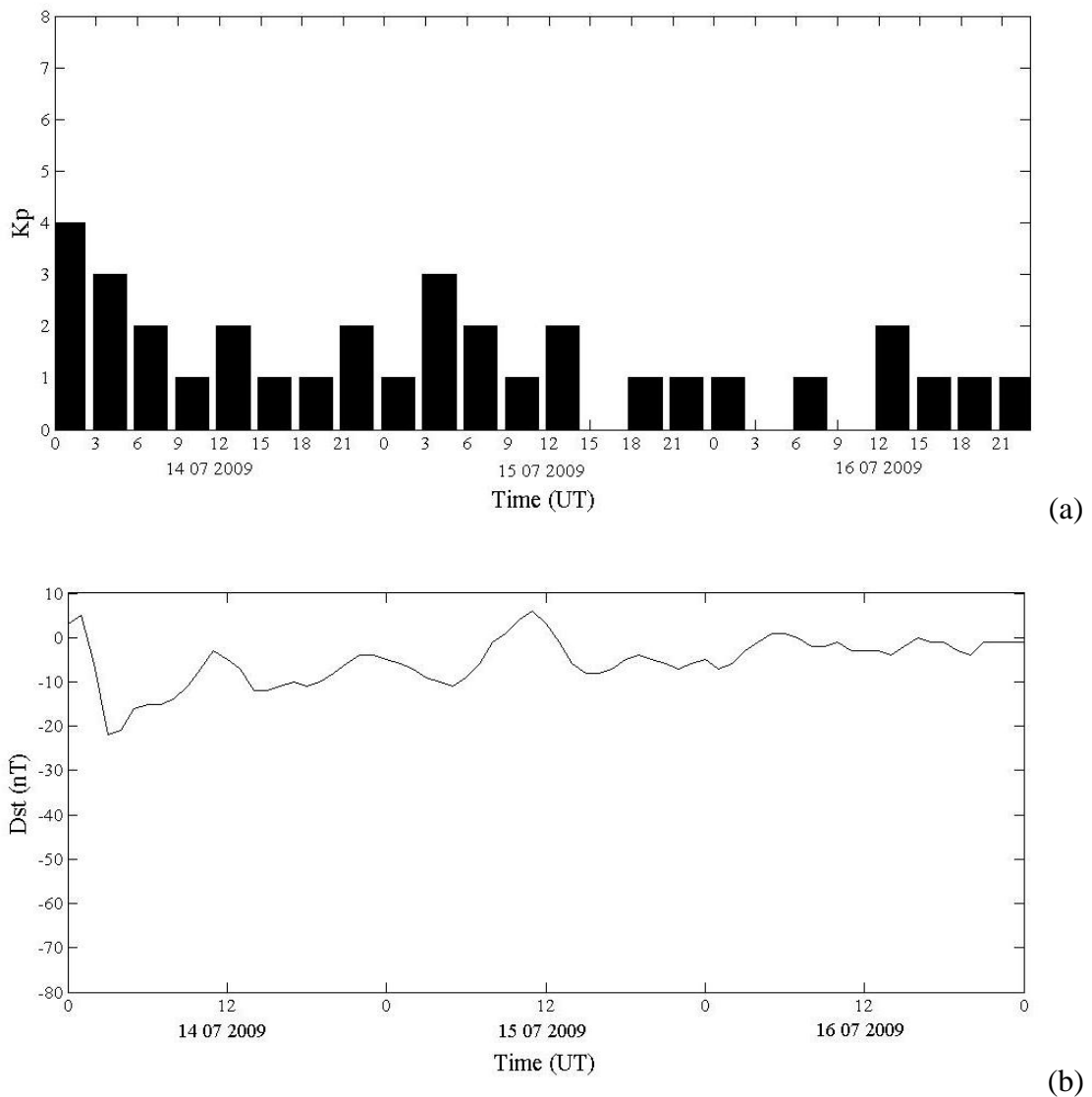
Figure 5-2 (a) Kp and (b) Dst indices from 14 to 16 July 2009.

TEC variations

The earthquake with magnitude 8.1 near west coast of South Island, New Zealand occurred on 15 July 2009 at 09:22:29 UT or 20:22:29 LT. New Zealand straddles the boundary between Pacific and Australian plates. The Australian plate moves to northeast direction at a rate of about 3.5-4.5 cm/yr relative to Pacific plate. Near the southwestern of the South Island, the Australian plate subducts beneath the Pacific plate at Puysegur Trench as shown in Figure 5-3. The movement of the Australian and the Pacific plates along the west of South Island causes a strike-slip fault called Alpine fault. The Alpine fault drives the uplift of the Southern Alps. Many

earthquakes occurred near the southwest of South Island in the area called Fiordland as shown in Figure 5-3. Fiordland is the complex area which is the result of subduction of Puysegur to the Alpine fault. This earthquake occurred from slip on the subduction thrust interface between the Pacific and Australian plates (U.S. Geological Survey (USGS), 2010).

GPS is a satellite system for navigation. Each GPS satellite emits two frequency radio waves. The two radio waves are delayed by ionospheric plasma when they pass through the ionosphere. This delay is called the ionospheric delay. The ionospheric delay can be used to calculate the integrated number of electrons along the path between satellites and receivers. This integrated number is called total electron content (TEC). The TEC is an important parameter to study the variations on the ionosphere. In this study, the slant TEC (STEC) was derived from pseudorange data and differential carrier phase data of GPS. This STEC data was converted to the vertical TEC (TEC) using the assumption of the single ionospheric layer. The GPS data in New Zealand with sampling period of 30 seconds was provided by GeoNet, New Zealand. There are 143 GPS stations of GeoNet used in this research. The locations of GPS stations of GeoNet and the earthquake epicenter on 15 July 2009 are shown in Figure 5-4.
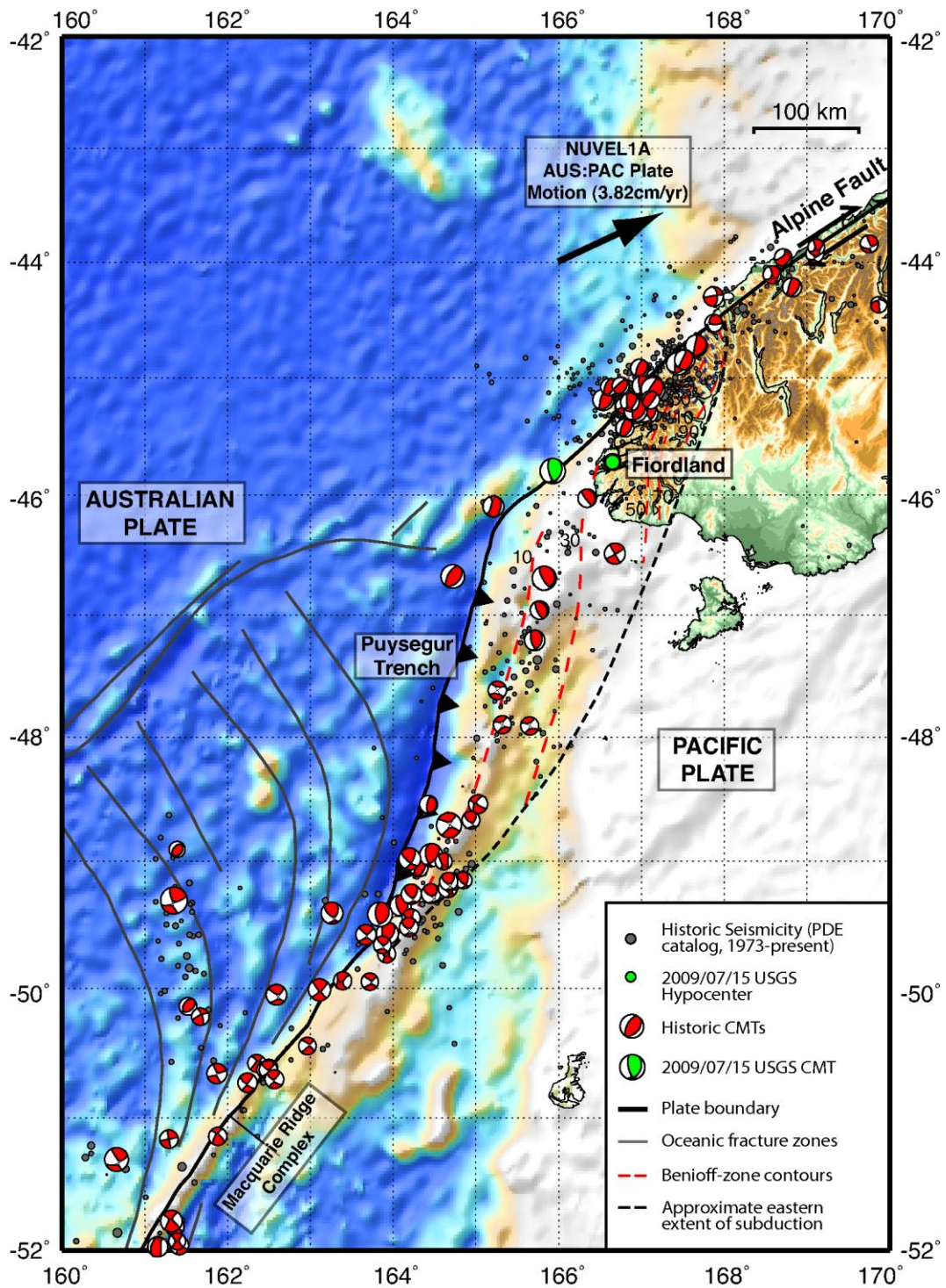
Figure 5-3 The boundary between Australian and Pacific Plates near the South Island in New Zealand (U.S. Geological Survey (USGS), 2009).
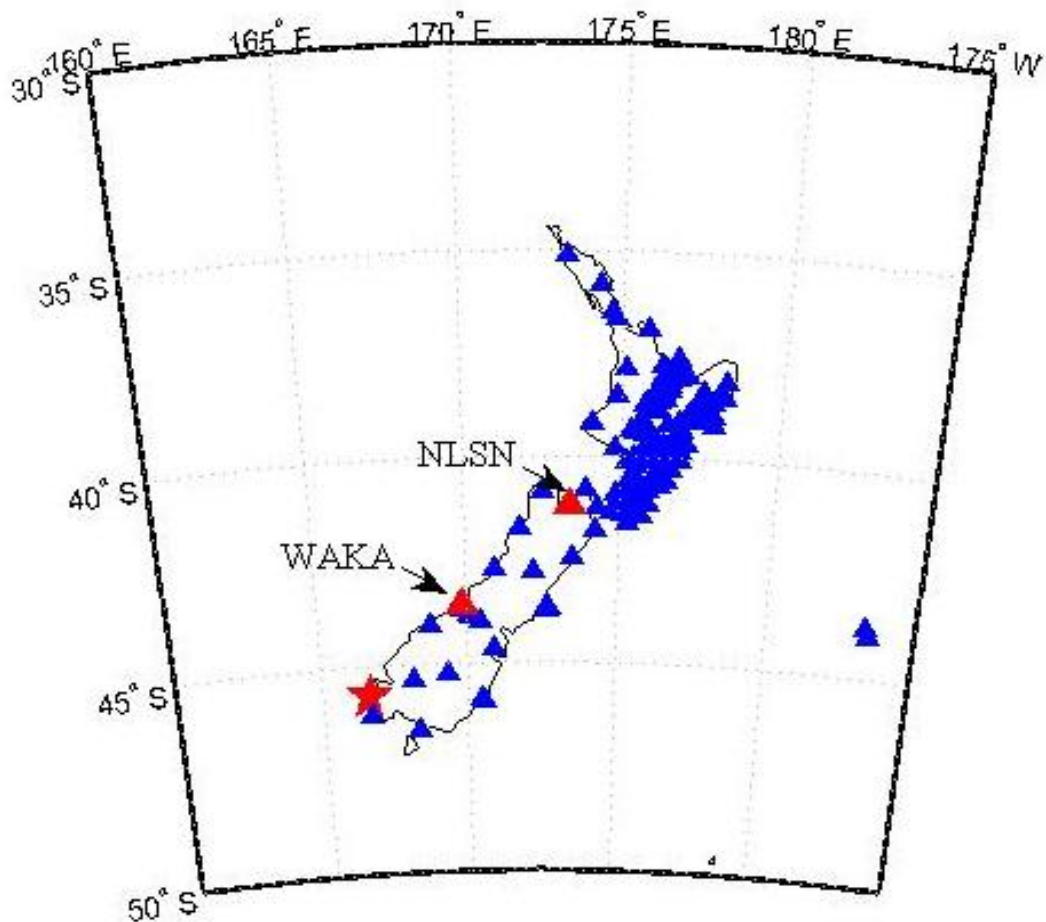
Figure 5-4 The locations of earthquake epicenter (red star) of the west coast of South Island in New Zealand on 15 July 2009 and GPS stations (triangle).

The TEC from 09:00:00 UT to 11:00:00 UT of NLSN station observed by PRN20 and WAKA station observed by PRN32 are shown in Figure 5-5(a) and 5-5(b), respectively. The geographic coordinates of NLSN and WAKA station are at (41.18°S, 173.43°E) and (43.58°S, 169.89°E), respectively. The geomagnetic coordinates of NLSN and WAKA station are at (44.45°S, 105.70°W) and (47.38°S, 108.60°W), respectively. The TEC perturbations are clearly seen after the earthquake origin time as shown in Figure 5-5. The vertical dot line indicates the time of the earthquake, 09:22:29 UT. The locations on the ionospheric pierce point (IPP) where the paths between satellites and receivers crossed were (46.83°S, 163.16°E) at 09:00:00 UT and (41.57°S, 170.78°E) at 11:00:00 UT for NLSN station, and (45.58°S, 166.08°E) at 09:00:00 UT and (42.53°S, 169.15°E) at 11:00:00 UT for

WAKA station. The points of observation moved to northeast and the elevation angles increased during the observation time. At NLSN station, there was a sudden increase of TEC value. The amplitude of the TEC variations was larger than 0.20 TECU at about 09:35:00 UT. Then, there was a rapid decrease and its amplitude was about 0.38 TECU at 09:37:00 UT. In the case of WAKA station, the TEC increased suddenly whose amplitude was approximately 0.2 TECU at around 09:34:00 UT. After that, it decreased rapidly which its amplitude was about 0.12 TECU at around 09:36 TECU.

The TEC data was applied high-pass filter that cut off period is 10 minutes. Then, it was smoothed using Savitzky-Golay method with 5 order polynomial and the window size of 33 points. As can be seen from Figure 5-6(a), the TEC started to fluctuate at 09:28:30 UT. The time lag of variations was 6.01 minutes. The maximum peak of variations was 0.23 TECU at 09:35:00 UT and The minimum peak of variations was -0.12 TECU at 09:37:00 UT. Figure 5-6(b) showed that the TEC started to oscillate at 09:29:30 UT at WAKA station. The time lag of the TEC variations was 7.01 minutes. It reached the maximum peak of 0.13 TECU at 09:34:00 UT, and reached the minimum peak of -0.08 TECU at 09:38:00 UT. As can be seen from Figure 5-6, there is an increasing number of the TEC value to the first peak of the TEC variations at 09:28:30 UT at NLSN station and at 09:28:00 UT at WAKA station before the TEC depletion occurred. This is the result of reverse fault which caused the increasing number of the TEC value after the earthquake origin time.
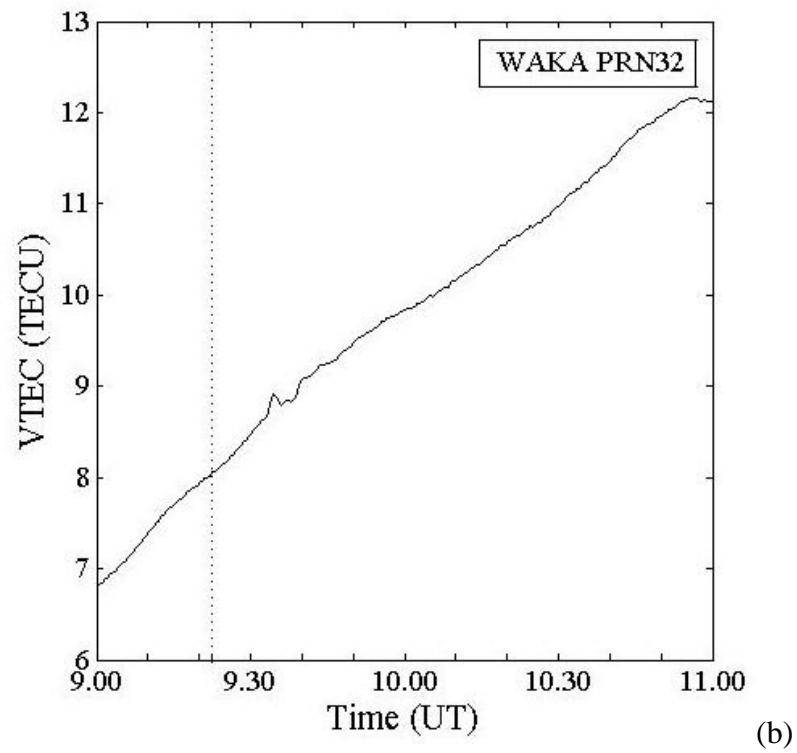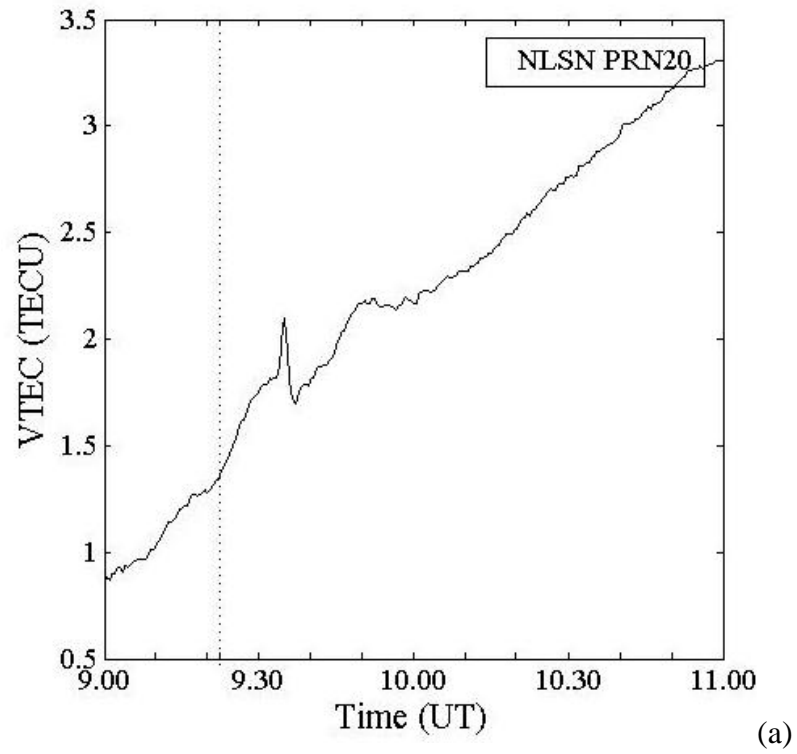
Figure 5-5 The TEC variations between 09:00:00 and 11:00:00 UT on 15 July 2009
(a) NLSN station and (b) WAKA station.

(a)

(b)
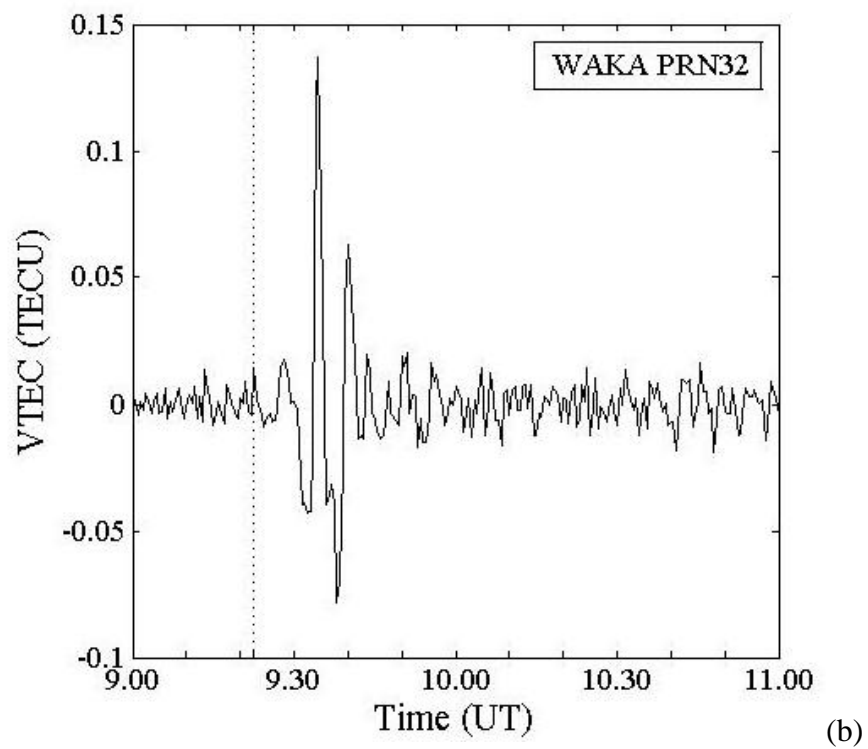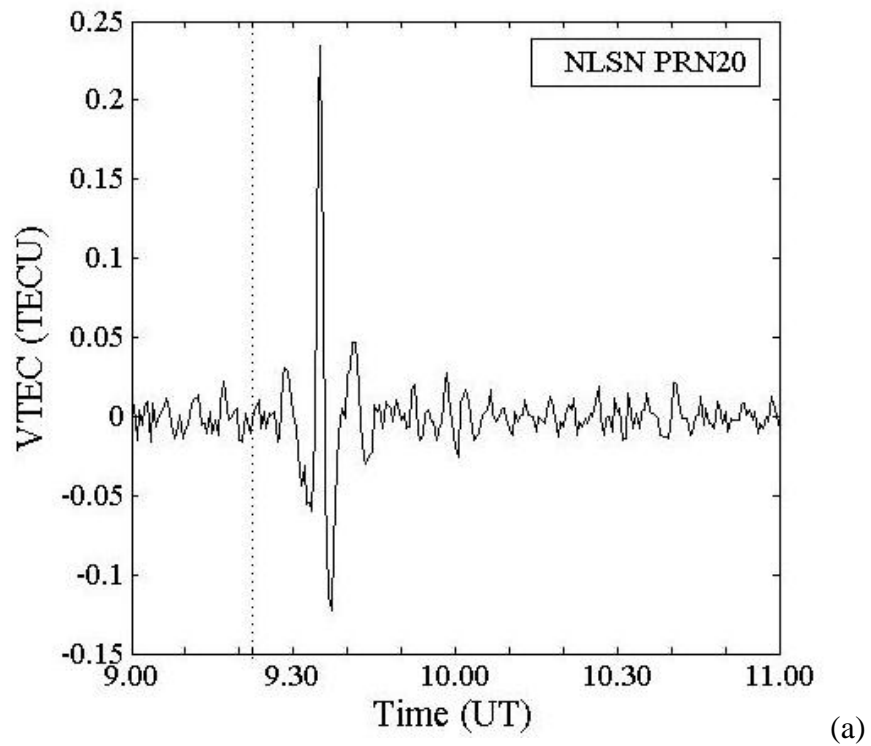
Figure 5-6 The vertical TEC variations on 15 July 2009 (a) NLSN station and (b) WAKA station.

The power spectrum of the TEC data was analyzed using fast fourier transform (FFT) method to obtain the period of the TEC oscillation. Figure 5-7 shows the power spectrum of the TEC data between 09:00:00 UT and 11:00:00 UT at NLSN and WAKA stations. The vertical dot lines indicate the cut off frequency of 1.67 mHz. The dominant frequency of the TEC variations observed by NLSN station is 2.8 mHz as shown in Figure 5-7(a). The dominant frequency was converted to a period of variations of 5.57 minutes. With regards to WAKA station as shown in Figure 5-7(b), the dominant frequency is 3.2 mHz. The periods of the TEC variations was 5.12 minutes.

The TEC data and its latitude and longitude at the IPP obtained from each GPS receiver were plotted in Figure 5-8 to Figure 5-11. There are 196 data being plotted in the maps. The TEC variations were found six minutes after the earthquake origin time. It can be seen from Figure 5-8(a) to 5-8(f) that there were no TEC variations between 09:22:30 UT and 09:27:30 UT. The TEC started to oscillate and showed the first peak at around 09:28:30 UT as indicated by green color in Figure 5-9(a). As can be seen from Figure 5-9(b) to 5-9(c), the first peak moves northeastward along New Zealand islands. After that, there was a sudden decrease of the TEC value to below -0.012 TECU as shown in Figure 5-9(d) to 5-9(f). Figure 5-10(a) shows the maximum peak of variation which is larger than 0.045 TECU at 09:34:30 UT and the peak of variations propagated northeastward along the South Island. It also can be seen from Figure 5-10(c) that the minimum peak of variations which is lower than -0.050 TEC occurred at 09:36:30 UT and also propagated to the northeast of New Zealand. Figure 5-11 illustrates a small peak-to-peak of the TEC variations (-0.031-0.026 TECU) after the maximum peak-to-peak. After that, the TEC turned to the normal state at around 09:50:00 UT.
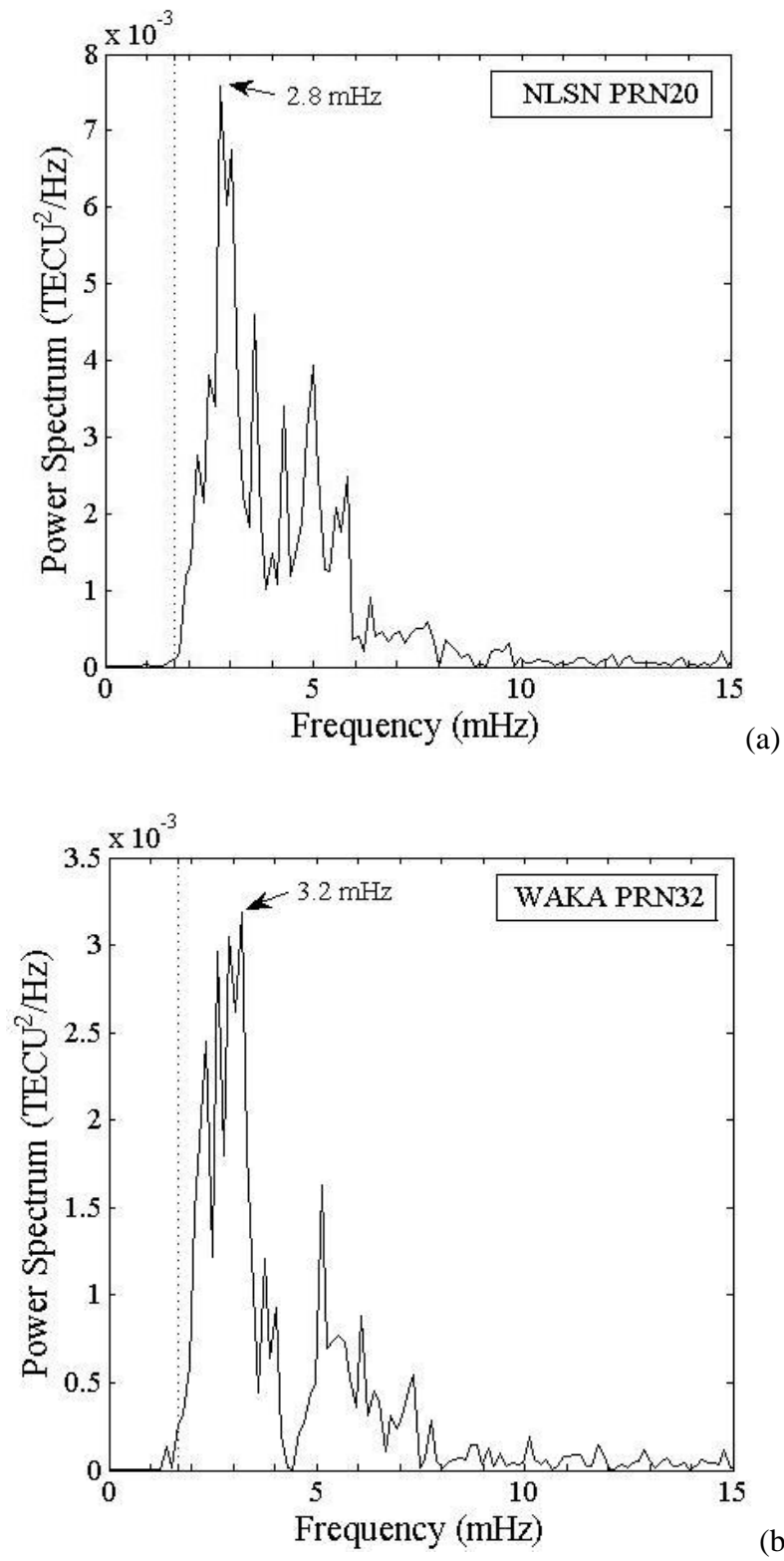
Figure 5-7 The power spectrum of TEC data on 15 July 2009 (a) NLSN station and (b) WAKA station.
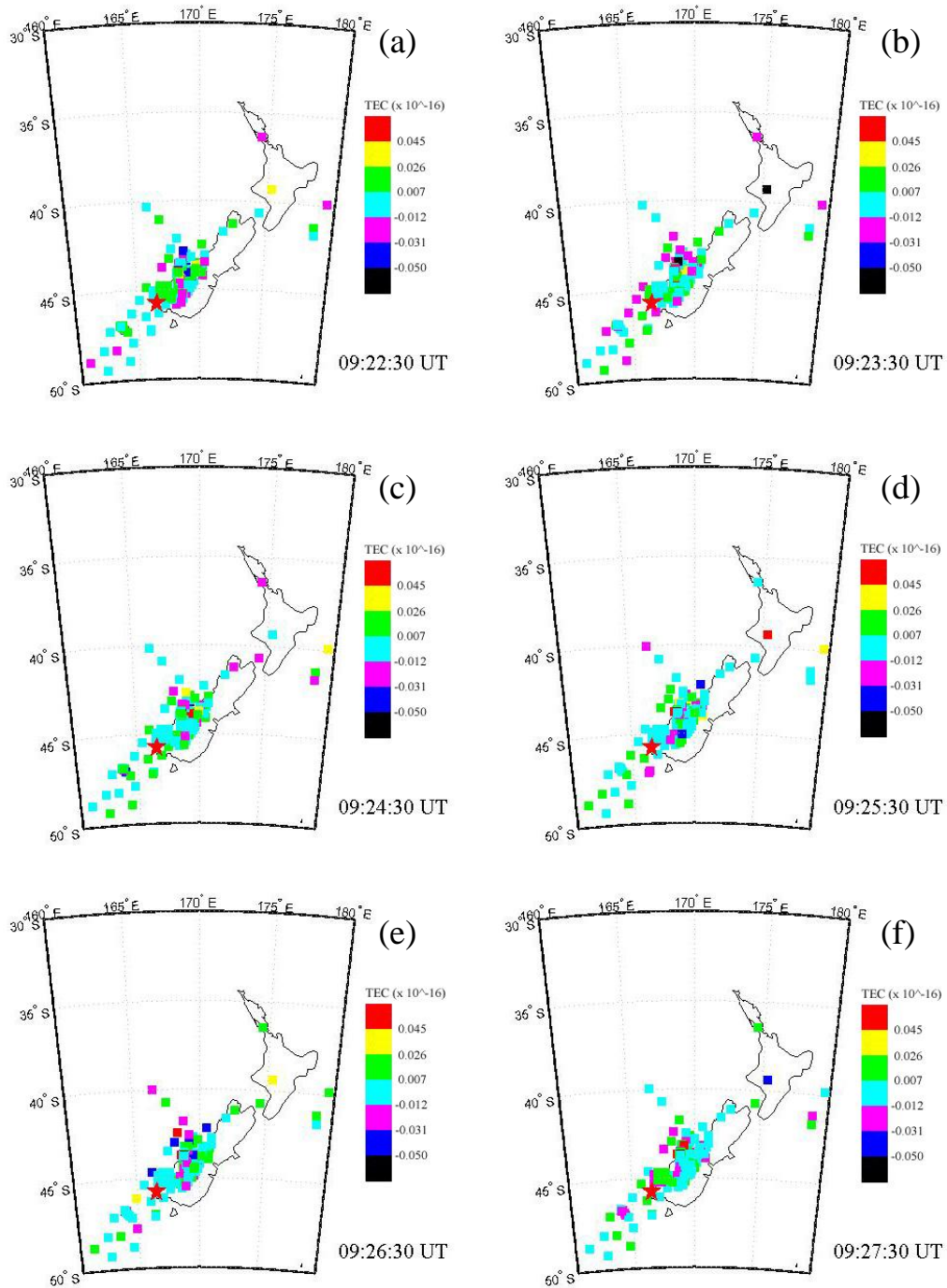
Figure 5-8 Two dimensional distributions of TEC variations on the IPP over New Zealand (a) 09:22:30 UT (b) 09:23:30 UT (c) 09:24:30 UT (d) 09:25:30 UT (e) 09:26:30 UT and (f) 09:27:30 UT.
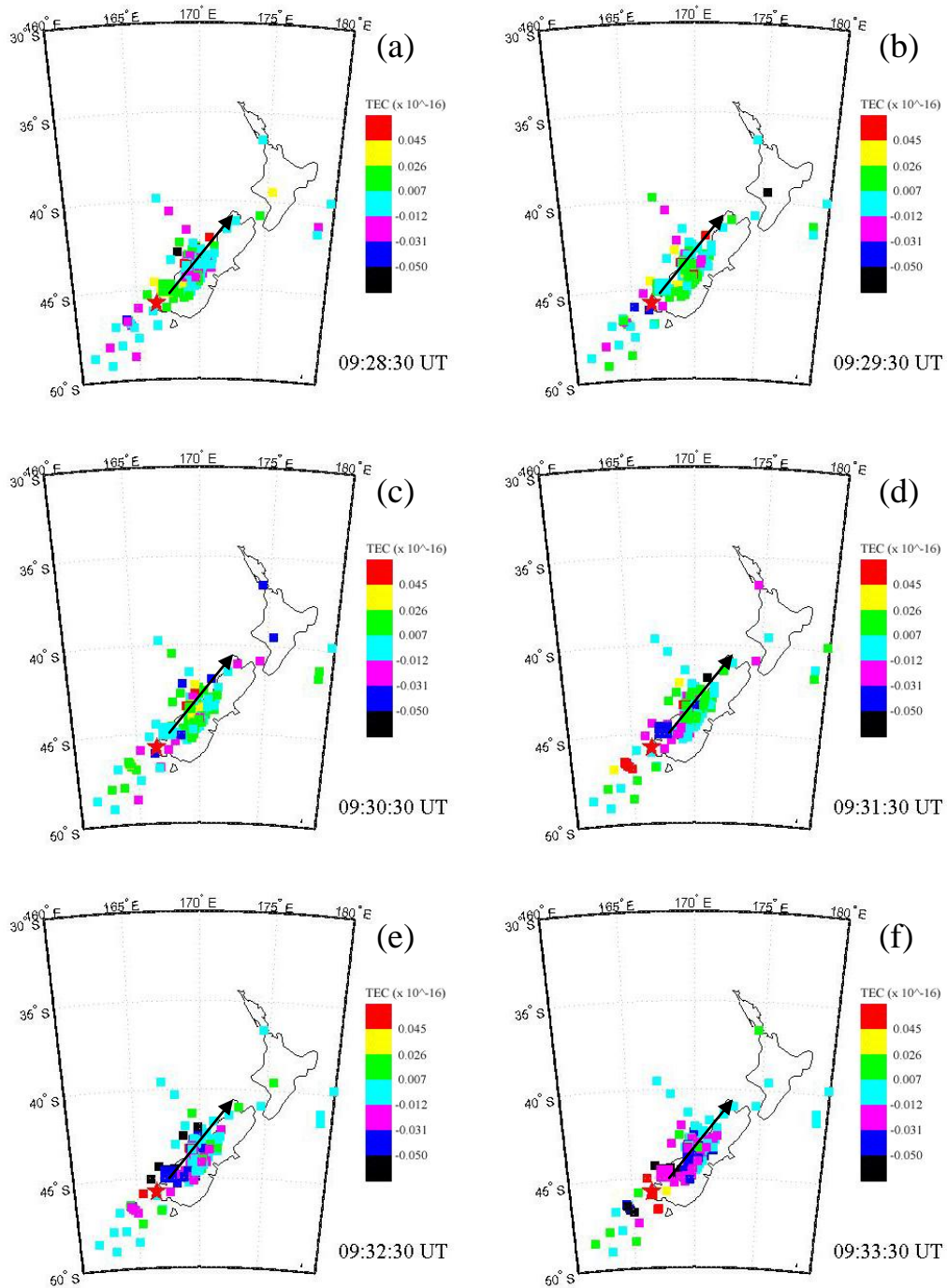
Figure 5-9 Two dimensional distributions of TEC variations on the IPP over New Zealand (a) 09:28:30 UT (b) 09:29:30 UT (c) 09:30:30 UT (d) 09:31:30 UT (e) 09:32:30 UT and (f) 09:33:30 UT.
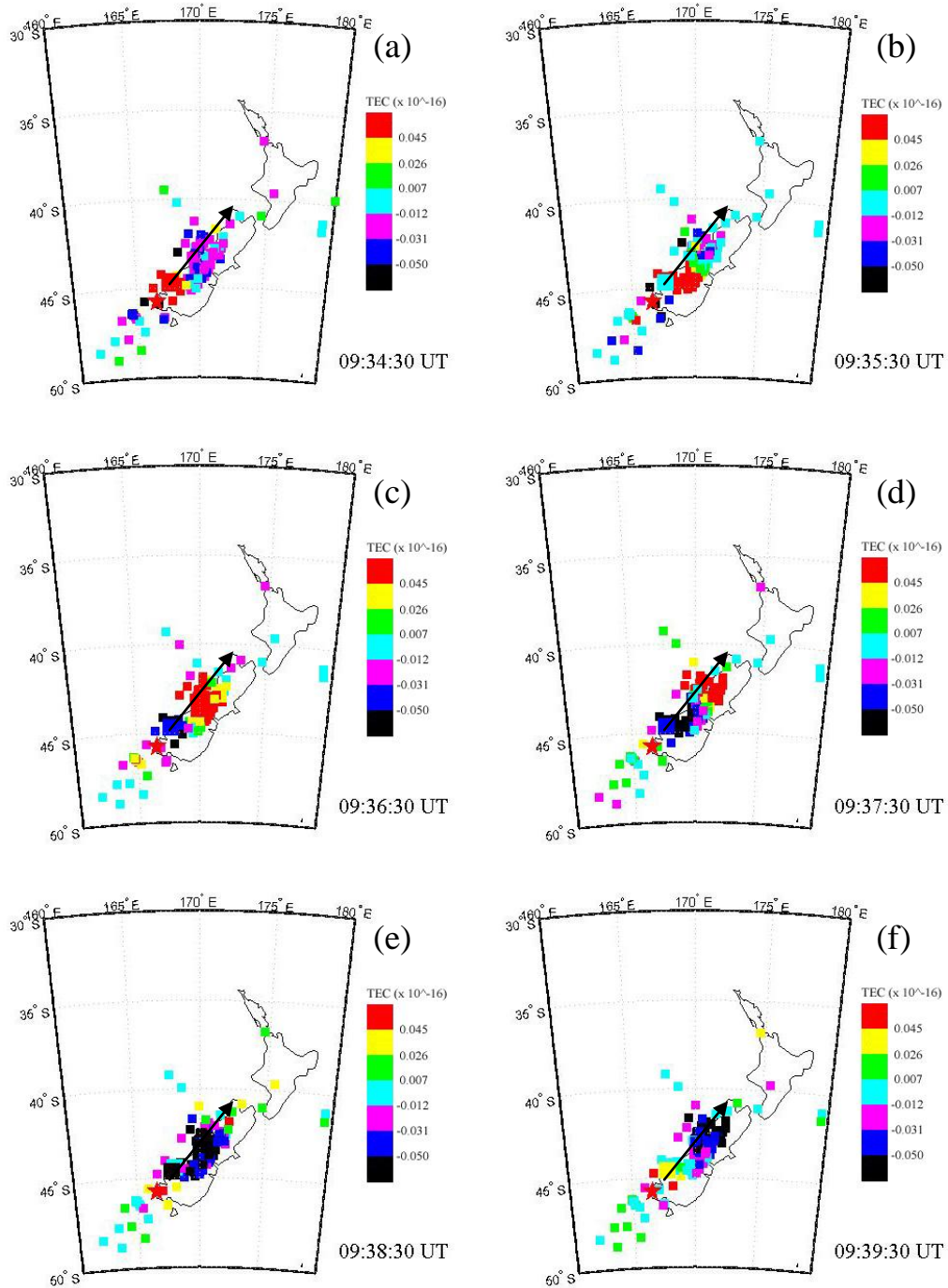
Figure 5-10 Two dimensional distributions of TEC variations on the IPP over New Zealand (a) 09:34:30 UT (b) 09:35:30 UT (c) 09:36:30 UT (d) 09:37:30 UT (e) 09:38:30 UT and (f) 09:39:30 UT.
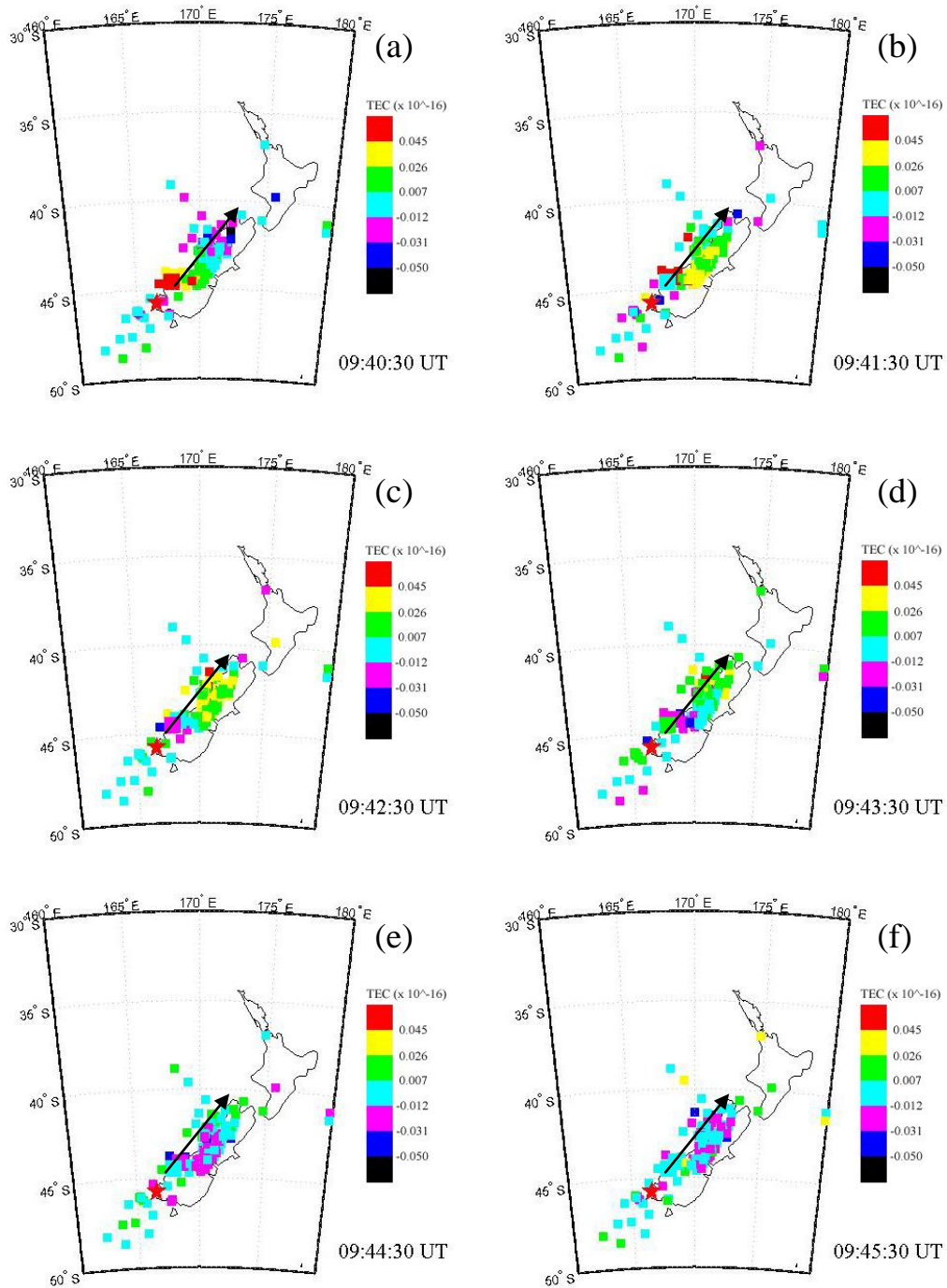
Figure 5-11 Two dimensional distributions of TEC variations on the IPP over New Zealand (a) 09:40:30 UT (b) 09:41:30 UT (c) 09:42:30 UT (d) 09:43:30 UT (e) 09:44:30 UT and (f) 09:45:30 UT.

Figure 5-12 illustrates the relationship between amplitudes of the TEC variations and distance of GPS receivers from the epicenter. It was clearly seen that the amplitude of the TEC variations increased from around 0.05 TECU at the distance around 250 km from the epicenter to approximately 0.35 TECU at the distance around 800 km from the epicenter. After that, there was a drop of the amplitudes of the TEC variations from 0.35 TECU at the distance about 800 km from the epicenter to below 0.1 TECU at the distance about 1,300 km from epicenter.
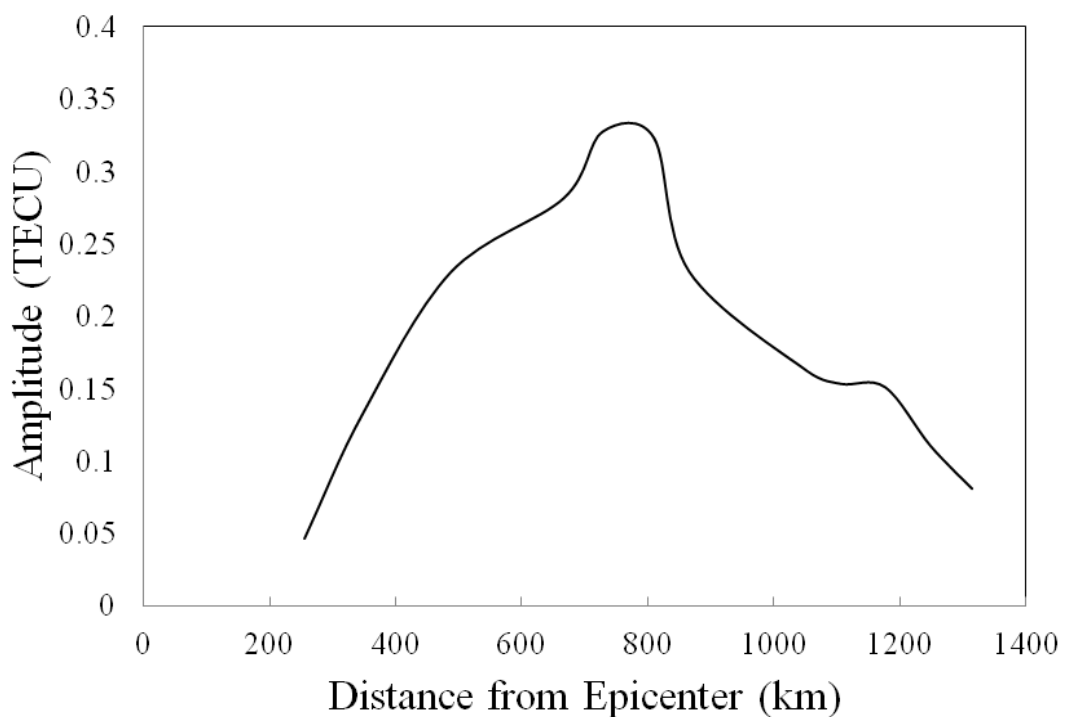
Figure 5-12 The observed amplitude of TEC variations at different distance between the epicenter zone and the GPS stations in New Zealand earthquake.

Figure 5-13 will clarify why GPS receivers near the epicenter can detect small amplitudes of the TEC variations. Heki *et al.* (2006) proposed that there are three factors that influence the amplitudes of the TEC variation such as 1) the distance from the epicenter and 2) the incident angle of the line of sight and 3) the directivity caused
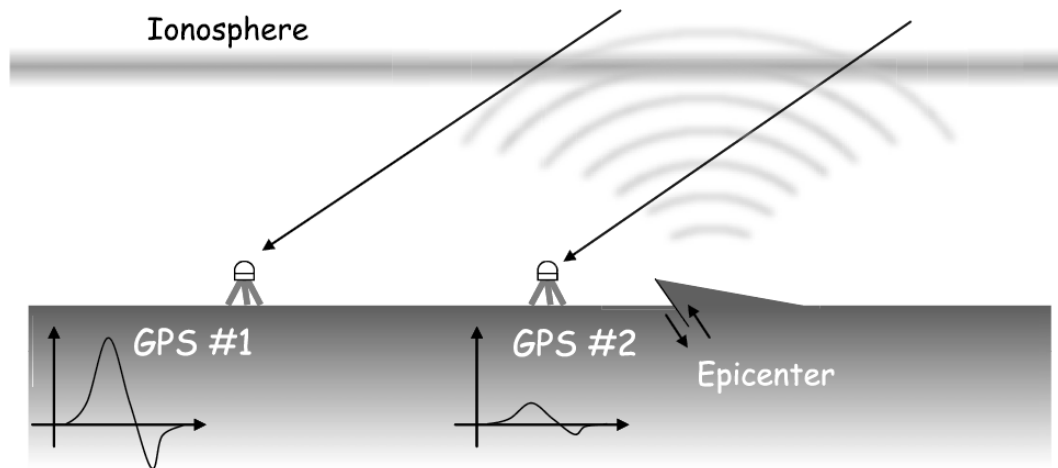
Figure 5-13 The amplitudes of TEC variations observed by GPS receivers located at different location (Heki *et al.*, 2006).

by geomagnetism. The amplitudes of the TEC variations decays as the waves travel away from the sources owing to the first factor. However, the second factor should be taken into account. The high amplitudes of the TEC variations can be detected when the line of sight is parallel with the wave front of the acoustic wave. Figure 5-13 shows that GPS #1 which is located far from the earthquake epicenter can detect a large amplitude of the TEC variations, compared to GPS #2 which is located near the earthquake epicenter. The GPS #2 can observe a small amplitude of the TEC variations. Figure 5-14 shows the Declination (D) of geomagnetic field which was 24.104° at the earthquake location. The charged particles on the ionosphere move only along geomagnetic field lines and are restricted to move across the geomagnetic field lines (Hooke, 1970; Kelley, 2009). Therefore, the acoustic wave front which is perpendicular with geomagnetic field line can survive in the ionosphere and drives charged particles to move along geomagnetic field lines. This gives the answer why the TEC variations move to northeast direction as can be seen from Figure 5-8 to 5-11. Figure 5-15 presents the locations which the lines of sight crossed the IPP on 15 July 2009 between 09:00:00 UT to 11:00:00 UT. It was clearly seen that PRN20 moved northeastward along New Zealand islands during the observation time. Therefore, PRN20 gives the clear signal because the radio waves passed through the acoustic wave fronts generated near the epicenter zone.
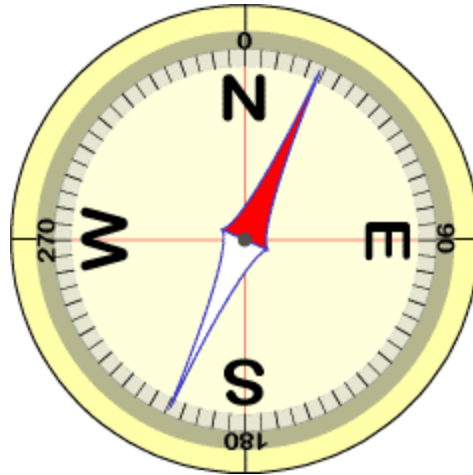
Figure 5-14 The Declination of geomagnetic field at 45.750°S, 166.577°E (World Data Center (WDC) for Geomagnetism, 1995).
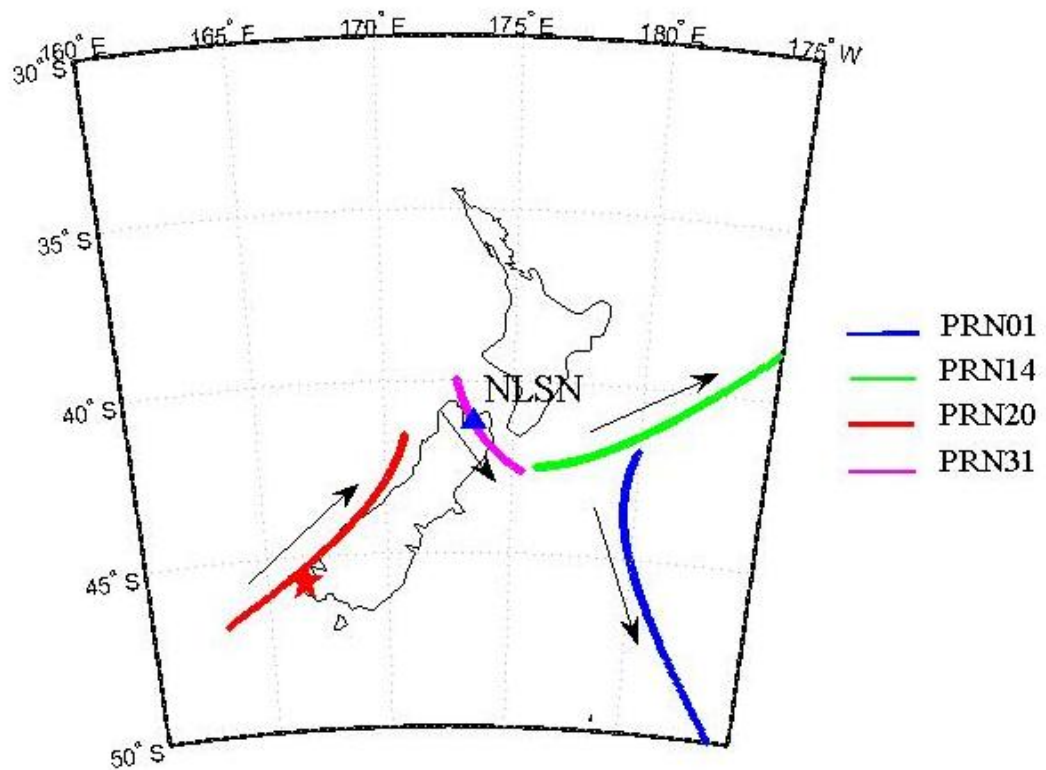
Figure 5-15 The locations on IPP which the lines of sight crossed between 09:00:00 UT to 11:00:00 UT on 15 July 2009 in New Zealand earthquake.

The earthquake origin time at New Zealand local time is 20:22:29 LT which is the nighttime. In principle, there is no the ionospheric E region after sunset. Since the acoustic wave plays the important role to disturb the lower ionosphere, if there is no the E region at the earthquake origin time, the TEC variations could not be detected. In this research, the ionospheric E region was referred from IRI-2007 model. Figure 5-16 presents the electron profile from IRI-2007 model over the earthquake epicenter zone. There was the ionospheric E region in the nighttime at the earthquake origin time.
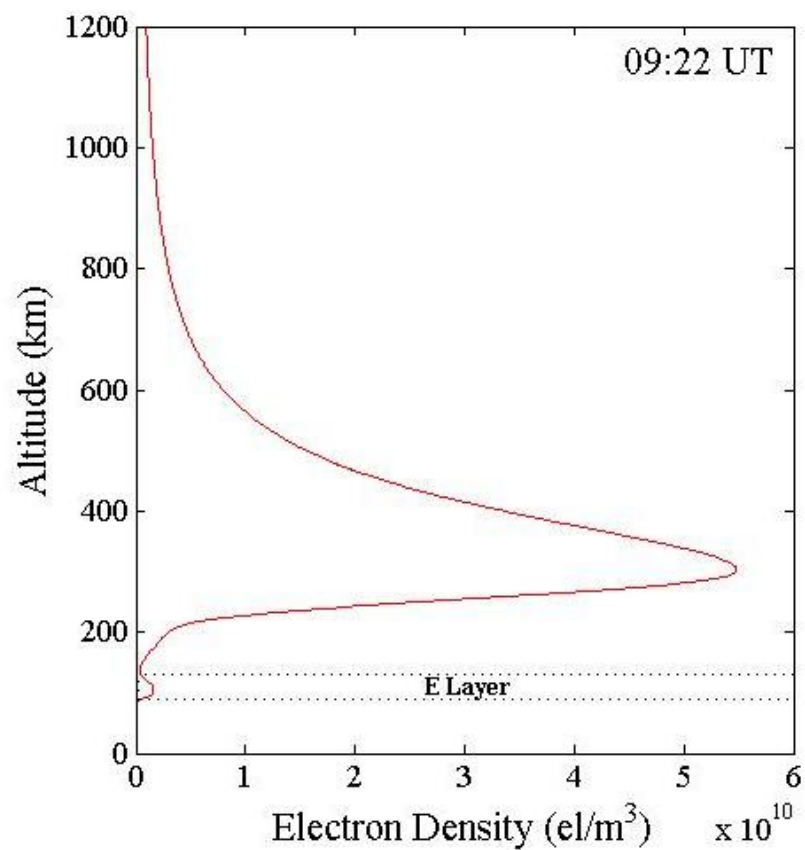
Figure 5-16 The electron profile from IRI-2007 model over the earthquake epicenter zone at 09:22 UT on 15 July 2009.

5.3 Samoa Islands Region

Geomagnetic and solar indices

The geomagnetic and solar indices were checked during the earthquake day. It can be seen from Figure 5-17(a) that Kp index at the earthquake origin time was one. Figure 5-17(b) shows the Dst index between 28 and 30 September 2009 which is higher than -15 nT. There was no solar flare which is larger than C class on 29 September 2009. The solar activity was classified as very low on 29 September 2009.

(a)

(b)
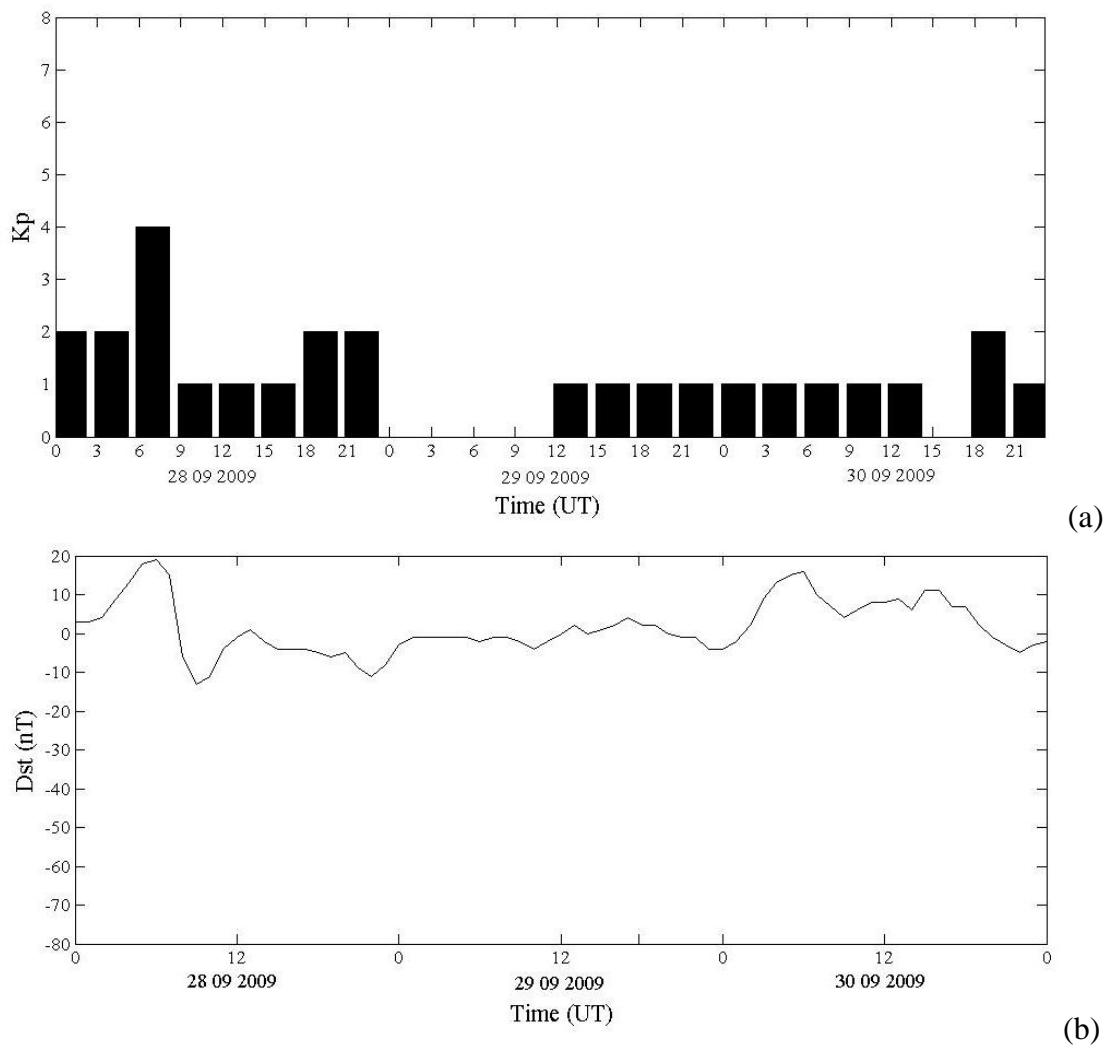
Figure 5-17 (a) Kp and (b) Dst indices from 28 to 30 September 2009.

TEC variations

The earthquake in Samoa Islands Region occurred on 29 September 2009 at 17:48:10 UT or 06:48:10 a.m. The magnitude of the earthquake is 8.1. The earthquake epicenter was at 15.509°S and 172.034°W and the depth of the focus is 18 km beneath the ground surface. Figure 5-18 illustrates the boundary of convergent plates between the Australian and the Pacific plates. The Pacific plate moves to the west direction at a speed of about 8.6 cm/yr and subducts to the Australian plate. The earthquake is the result of normal fault rupture near these tectonic plates (U.S. Geological Survey (USGS), 2010). Eight GPS receivers from IGS were used to observe the TEC variations including CKIS in Cook Islands, LAUT in Fiji, NRMD in France, KOUC in New Caledonia, NIUM in Niue, TONG in Tonga, TUVA in Tuvalu, and ASPA in the United States. The earthquake epicenter and GPS locations are shown in Figure 5-19.
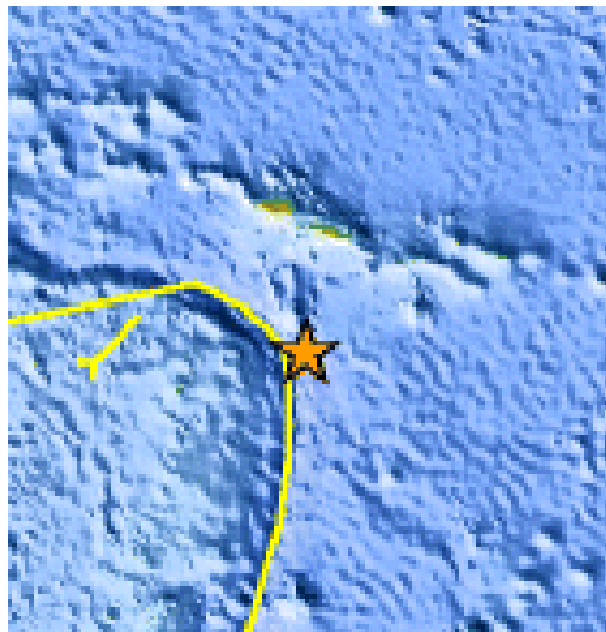
Figure 5-18 The boundary between the Australian and Pacific plates near Samoa Island region (U.S. Geological Survey (USGS), 2009).

The TEC variation was clearly seen after the earthquake origin time observed by PRN5. There was only one GPS receiver which could observe the TEC variations. ASPA station could detect the TEC variation after the earthquake time. The

geographic coordinate of ASPA station is at (14.3261°S, 170.7224°W) while the geomagnetic coordinate is at (15.51°S, 95.94°W). The distance between the epicenter and the GPS station is 193 km. Figure 5-20 shows the original data of the TEC at ASPA station between 28 and 30 September 2009. The vertical dot line shows the onset time of the earthquake which was at 17:48:10 UT. The locations which the satellite-receiver path crosses the IPP are (14.00°S, 172.15°W) at 17:30:00 UT and (15.73°S, 171.59°W) at 19:30:00 UT. The observation point moved to northeast direction during the observation time. The TEC variations occurred at 17:59:00 UT and continued to fluctuate about 30 minutes.

Figure 5-21 shows the TEC after the data processing between 28 and 30 September 2009. It was clearly seen that there were no variations on 28 and 30 September 2009. The horizontal dash lines show $\pm$ twofold of standard deviation of the TEC data from 17:30:00 UT to 19:00:00 UT. The onset time of the TEC variations on 29 September 2009 was at 17:55:00 UT. The time lag of the TEC variation was 6.83 minutes. The maximum peak was 0.33 TECU at 18:00:00 UT and the minimum peak was -0.41 TECU at 18:04:00 UT. The TEC continued to fluctuate 30 minutes and returned to its normal value at about 18:30:00 UT. The earthquake in Samoa Island region was occurred by a normal fault on the Pacific plate. It can be seen from Figure 5-21(b) that there is a decreasing number of the TEC value to the first peak of the TEC variations at 17:59:00 UT at ASPA station before the TEC variations reached the maximum peak at 18:00:30 UT. The normal fault caused the increasing value of the TEC after the earthquake origin time.
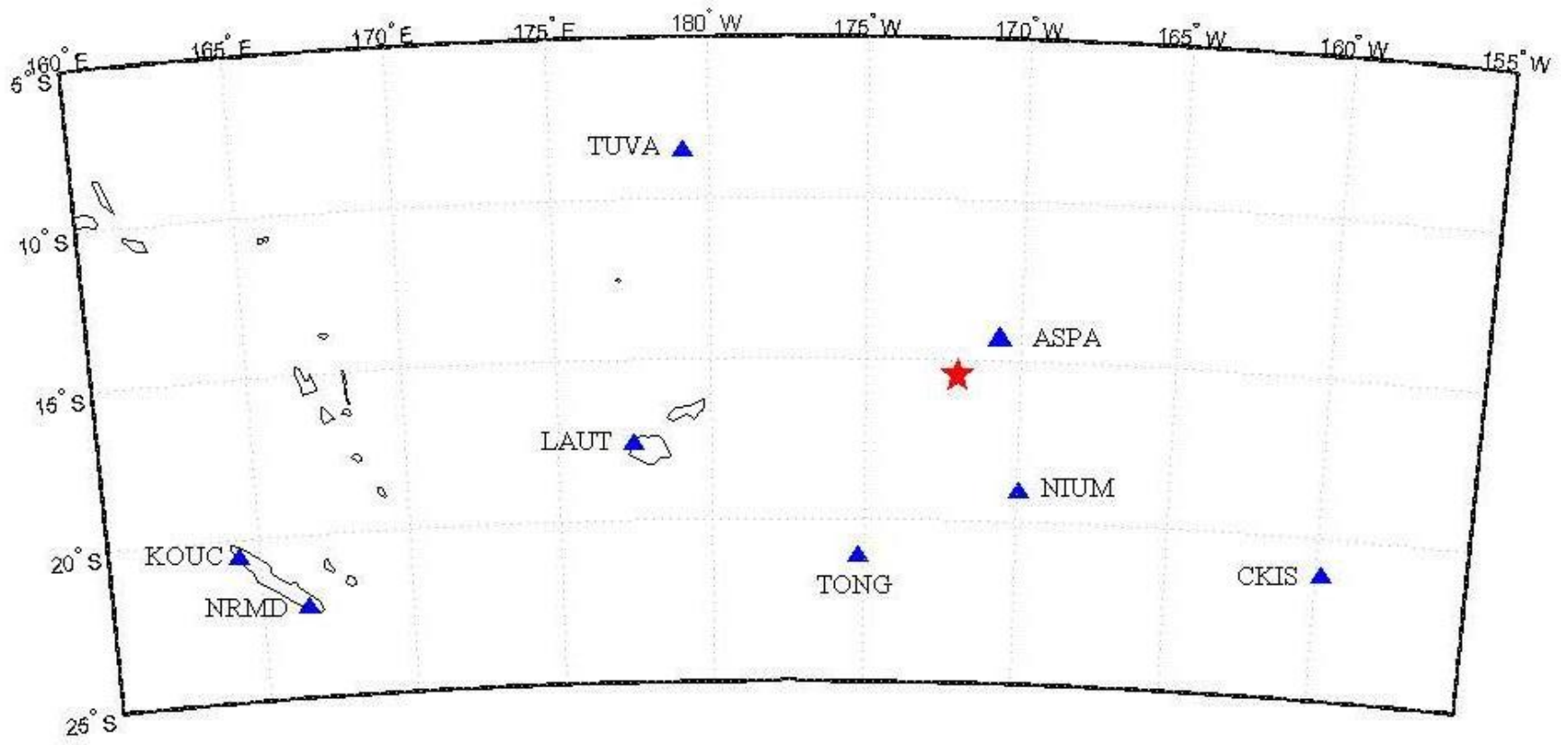
Figure 5-19 The locations of earthquake epicenter (red star) in Samoa Island Region

on 29 September 2009 and GPS stations (triangle).
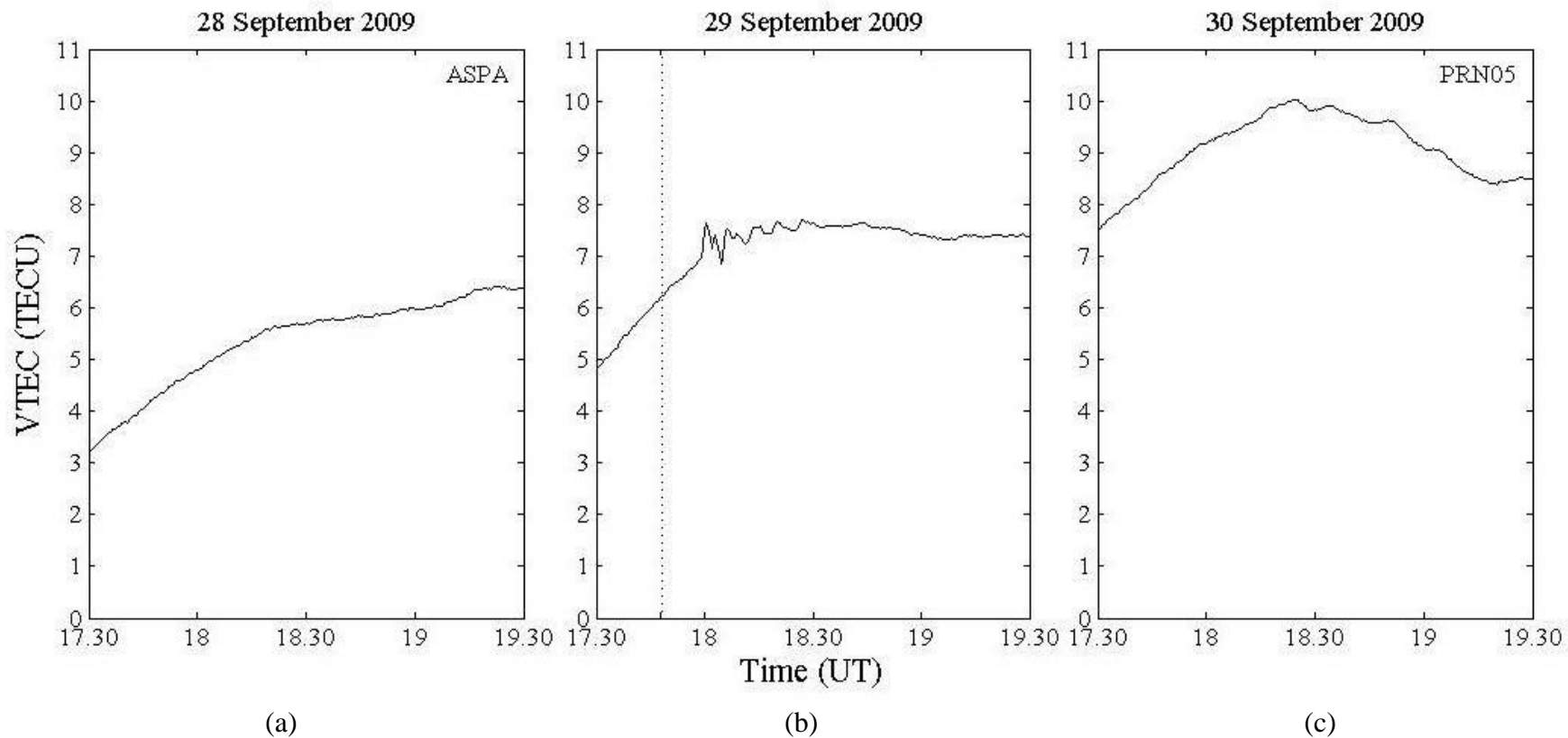
Figure 5-20 The observed TEC detected by PRN05 at ASPA station on (a) 28 September 2009 (b) 29 September 2009 and (c) 30 September 2009.
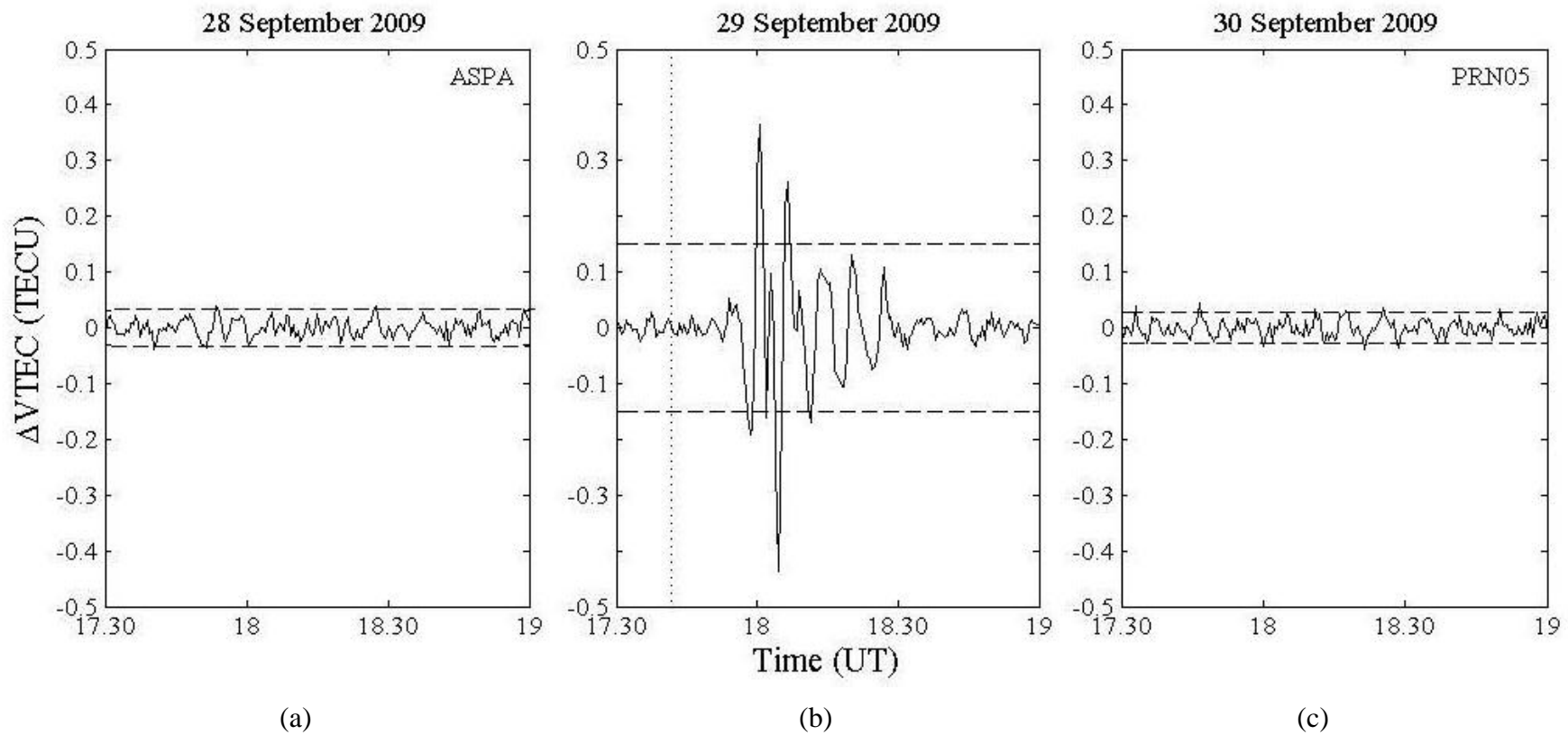
Figure 5-21 The filtered TEC data observed by PRN05 at ASPA station on (a) 28 September 2009 (b) 29 September 2009 and (c) 30 September 2009.

Figure 5-22 shows the power spectrum of the TEC variations between 17:30:00 UT and 19:00:00 UT obtained from FFT method. The vertical dot line indicates cut off frequency which is 1.67 mHz. The power spectrum shows the dominant frequency of 2.5 mHz. Therefore, the TEC variation period being found in this event is 6.40 minutes.
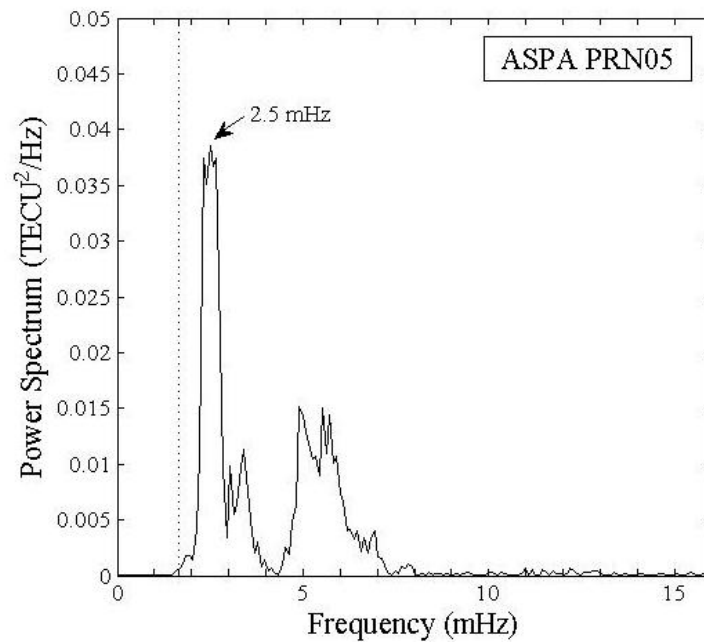
Figure 5-22 The power spectrum of TEC data observed by ASPA station on 29 September 2009.
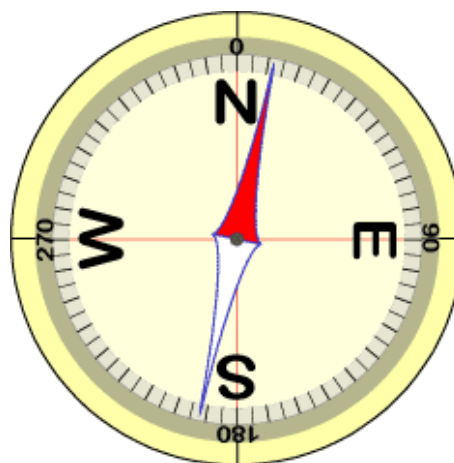
Figure 5-23 The Declination of geomagnetic field at 15.509°S, 172.034°W (World Data Center (WDC) for Geomagnetism, 1995).

The Declination of geomagnetic field of 11.847° at the earthquake epicenter was illustrated in Figure 5-23. The Declination pointed nearly north-northeast direction. Thus, the acoustic wave generated by the earthquake drove the charged particles to move to the direction of 11.847°. ASPA station which is located in the north-northeast direction could detect the TEC variations in this event, while the other GPS stations could not observe. The locations which the lines of sight crossed the IPP on 29 September 2009 between 17:30:00 UT to 19:00:00 UT are illustrated in Figure 5-24. It was clearly seen that there were six PRN during the observation time. PRN05 and PRN10 were moving and crossed the distance between the earthquake epicenter and ASPA station. Therefore, PRN05 and PRN10 could detect the TEC variations because the radio waves passed through the acoustic wave fronts generated near the epicenter zone, while the other GPS stations could not observe.
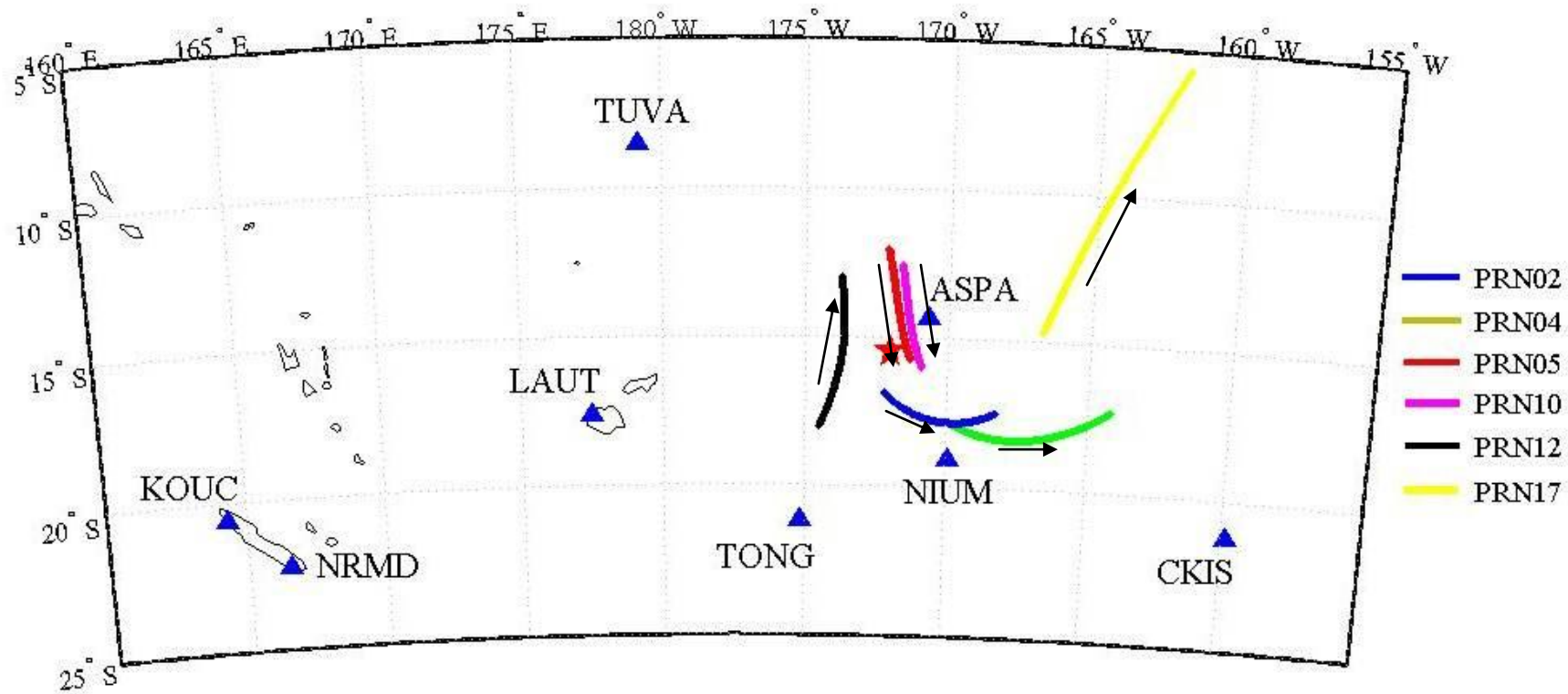
Figure 5-24 The locations on IPP which the lines of sight crossed between 17:30:00 UT to 19:00:00 UT on 29 September 2009 in Samoa Islands earthquake.

Figure 5-25 illustrates the electron profile over the earthquake epicenter zone from IRI-2007 model. The IRI model shows dominant peak of the ionospheric E region at the earthquake origin time.
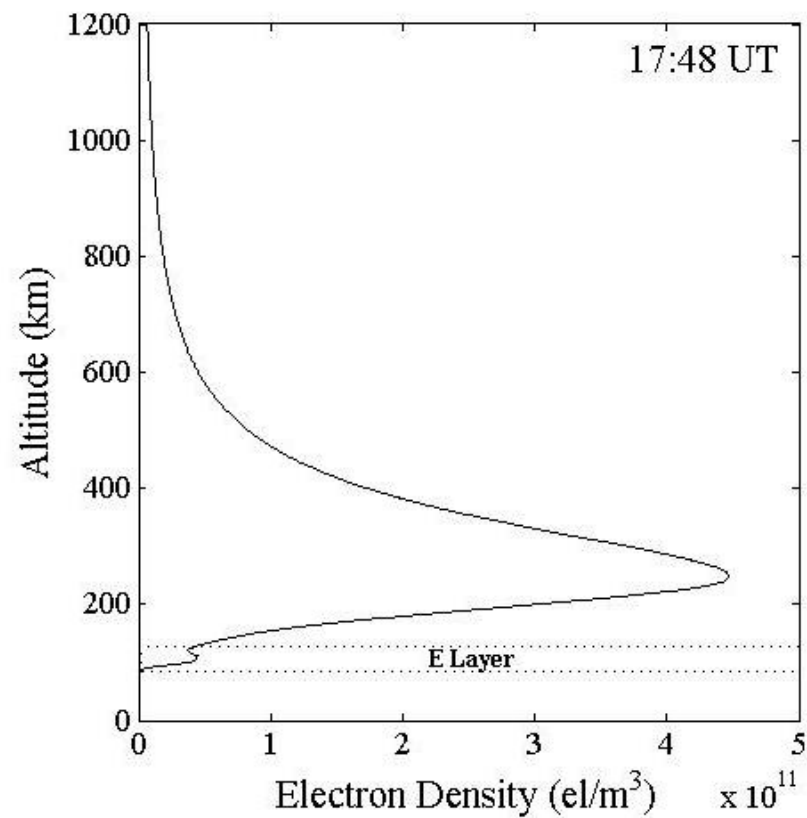
Figure 5-25 Electron profile from IRI-2007 model over the earthquake epicenter zone at 17:48 UT on 29 September 2009.

5.4   Kepulauan mentawai region, Indonesia

Geomagnetic and solar indices

Figure 5-26 shows Kp and Dst indices between 24 and 26 October 2010. It can be seen from Figure 5-26(a) that Kp index was two during the earthquake time. The Dst index during three days was higher than -35 nT. The geomagnetic activity level on 25 October 2010 was classified as quiet. No solar flares which are larger than C class were reported during the earthquake day. The solar activity level was classified as low on 25 October 2010.

(a)

(b)
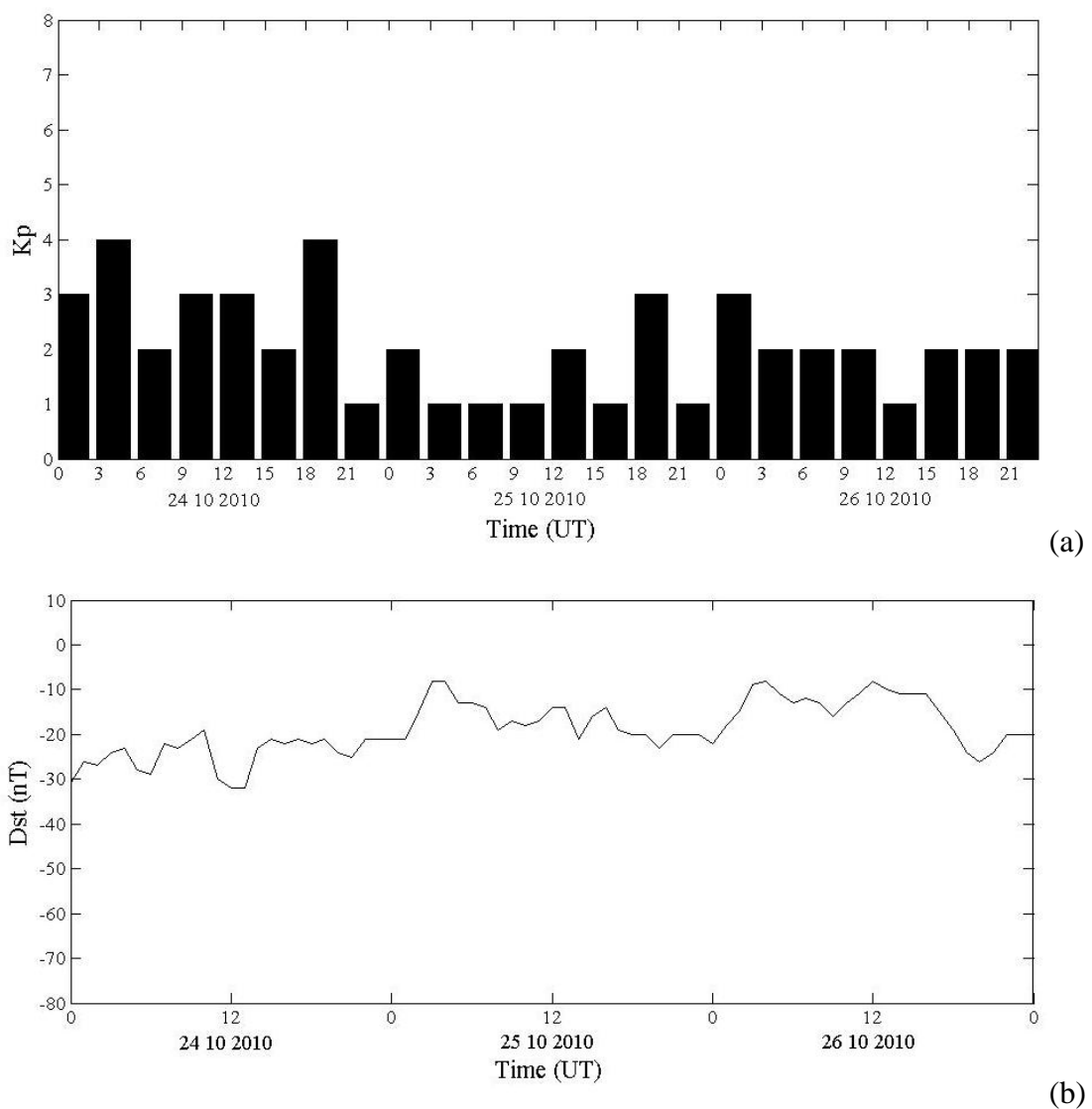
Figure 5-26 (a) Kp and (b) Dst from 24 to 26 October 2010.

TEC variations

The Kepulauan Mentawai Region earthquake with magnitude 7.7 in Indonesia occurred on 25 October 2010. The earthquake origin time is 14:42:22 UT or 09:42:22 p.m. The earthquake epicenter was at 3.484°S and 100.114°E and the depth of focus was 20.6 km beneath the ground surface. At the earthquake latitude, there is a convergence between Australian and Sunda plates. The Australian plate moves to the north-northeast direction relative to the Sunda plate at a speed of about 5.7-6.9 cm/yr. The thrust fault on or near the subduction interface plate boundary between the Sunda and Australian plates is the cause of this earthquake. Figure 5-27 shows the boundary between the Australian plate and the Sunda plate at the earthquake epicenter zone. There were seven GPS stations being used to observe the TEC variations in this event. These stations are IISC in India, CUSV in Thailand, DGAR of United Kingdom territory, NTUS in Singapore, BAKO in Indonesia, and COCO and XMIS in Australia. The earthquake epicenter and GPS receiver locations were shown in Figure 5-28.
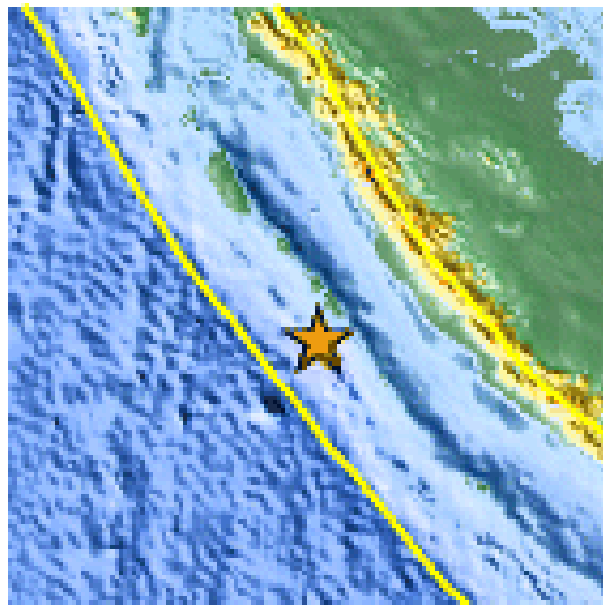
Figure 5-27 The boundary between Australian and Sunda Plates in Kaulauan Mentawai region (U.S. Geological Survey (USGS), 2010).
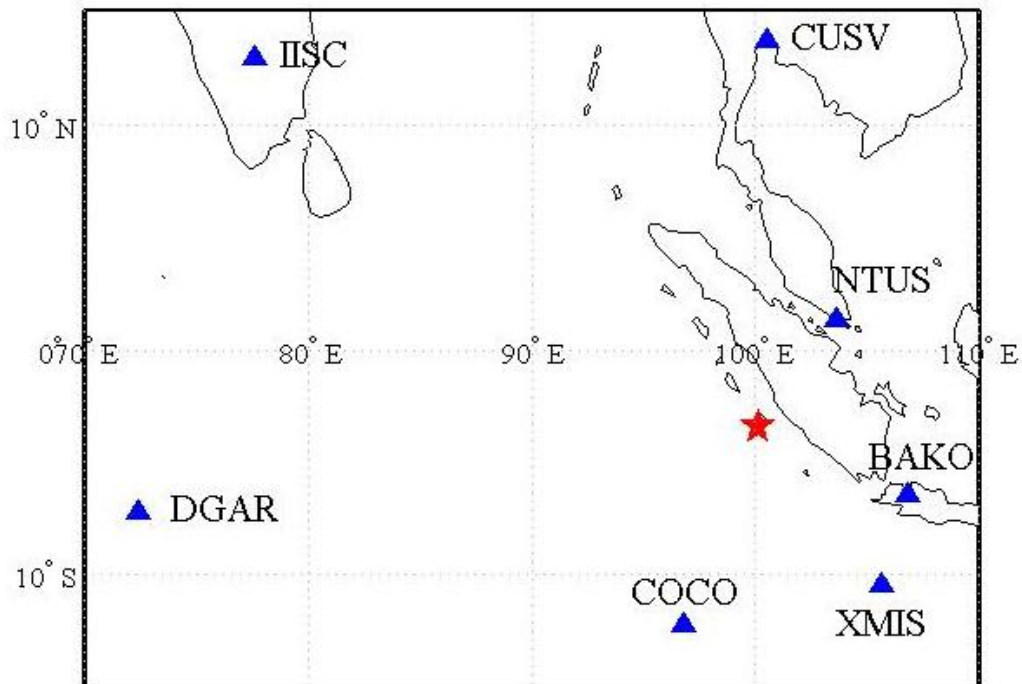
Figure 5-28 The locations of the earthquake epicenter (red star) in Kepulauan Mentawai region in Indonesia on 25 October 2010 and GPS stations (triangle).

The locations that the lines of sight crossed the IPP between 14:00:00 UT to 17:00:00 UT on 25 October 2010 at NTUS station were checked and shown in Figure 5-29. There were seven GPS satellites during the observation time. As can be seen from Figure 5-29, the line of sight between PRN29 and NTUS station crossed the distance between the earthquake epicenter and NTUS station. It is expected that PRN29 could observe the TEC variations at NTUS station. Figure 5-30 shows the TEC data between 24 and 26 October 2010. The horizontal dot line indicates the origin time of the earthquake of 14:42:22 UT. There were no TEC variations seen in this earthquake event. It can be seen from Figure 5-30(b) that there was a hole of the TEC data before the earthquake origin time. This TEC hold can be interpreted as plasma bubble (Burke, 2004 and Nishioka, 2009). Plasma bubbles are the depletion of the plasma density in the equatorial ionosphere. Plasma bubbles occur after sunset at the bottom of the F region. Normally, plasma bubbles always occur during the equinoxes at night time.
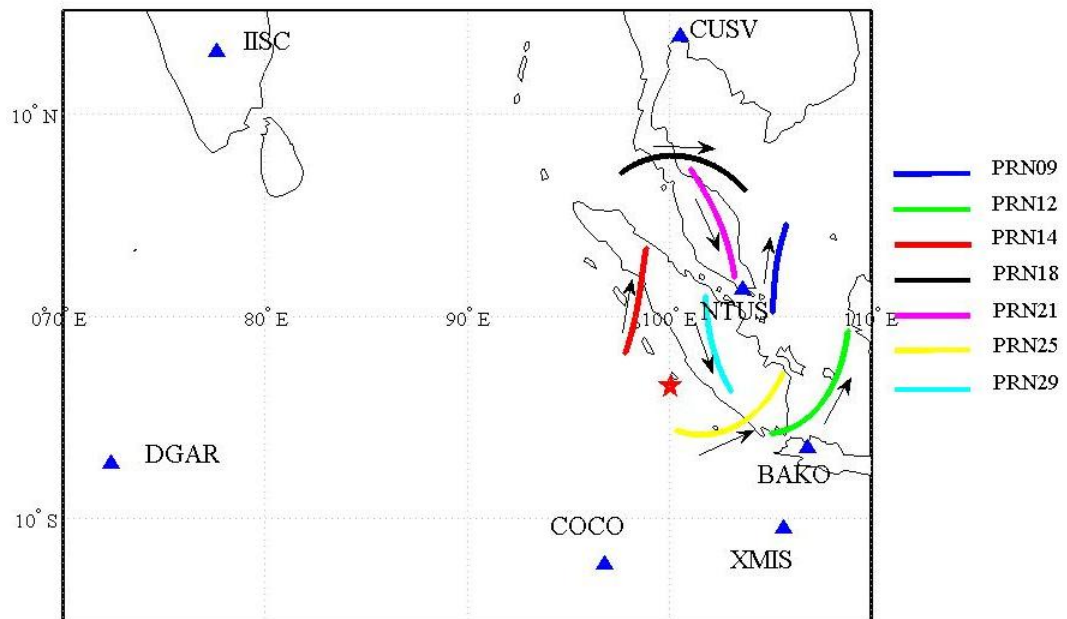
Figure 5-29 The locations on IPP which the lines of sight crossed between 14:00:00 UT to 17:00:00 UT at NTUS station on 25 October 2010 in Indonesia earthquake.
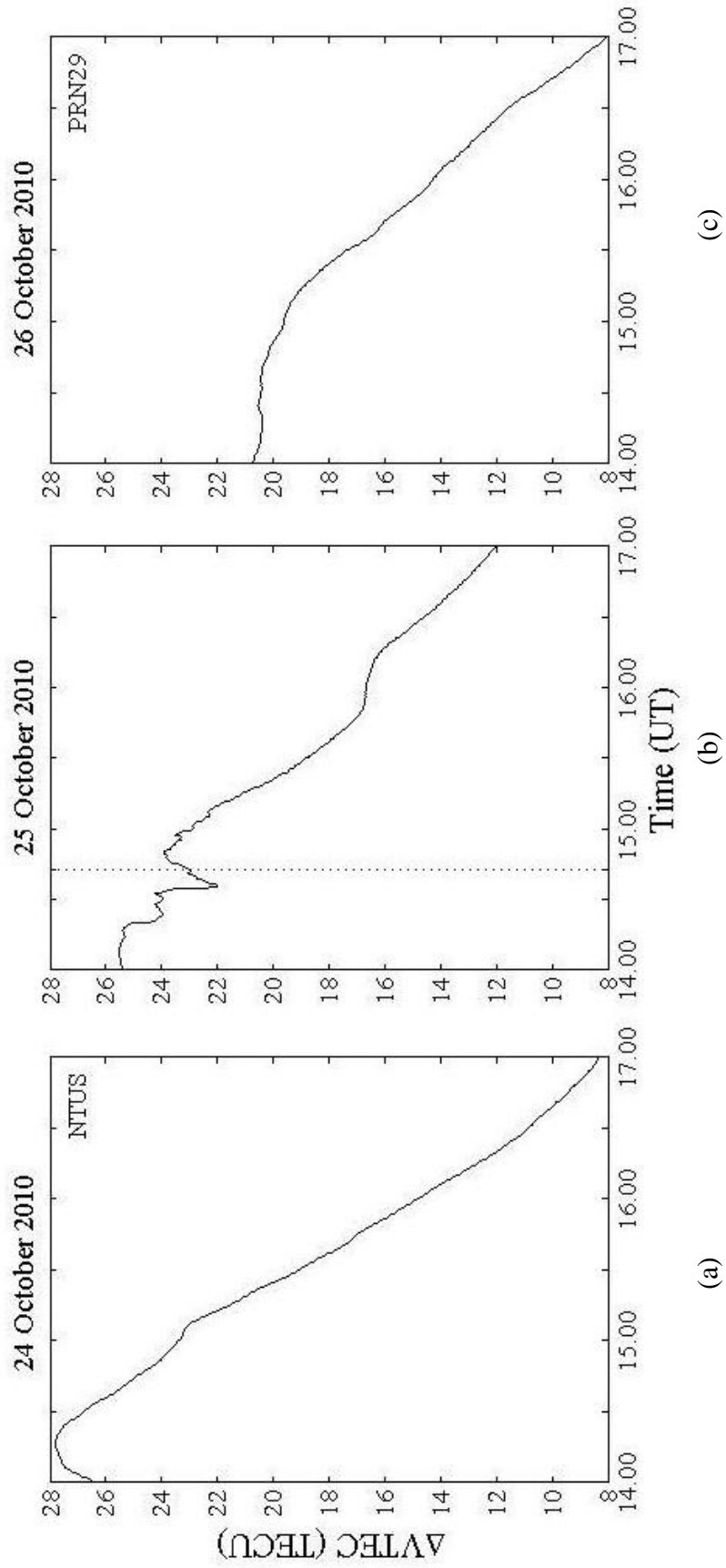
Figure 5-30 The observed TEC detected by PRN29 at NTUS station on (a) 24 October 2010 (b) 25 October 2010 and (c) 26 October 2010.

In this event, the TEC variations could not be observed by seven GPS stations. The electron density on the ionosphere at the earthquake origin time was checked from the IRI-model 2007 as shown in Figure 5-31. There was no ionospheric E layer at 09:42:22 p.m. The earthquake magnitudes between these two events are almost similar. In practical, there was no the E layer after sunset. However, there was the E layer at 08:22:29 p.m. in the earthquake in section 4.2 in New Zealand. Thus, it can be interpreted that the ionospheric E region is the major source which responds to the acoustic wave.

Heki *et al.* (2006) proposed that the vertical motions of the ground shake at the epicenter zones induced a kind of atmospheric wave called direct acoustic wave. The direct acoustic wave propagates upward to the Ionosphere with the speed of sound wave. There are three kinds of atmospheric wave including direct acoustic wave, gravity wave, and secondary acoustic wave. In the case of the earthquake in Indonesia, there was no enough energy to induce the high energy direct acoustic wave to the F layer at height about 200 km. The direct acoustic wave might lose all energy while it was travelling to the F layer. In contrast with the earthquake in New Zealand, there was the E layer at height about 100 km which responds to the direct acoustic wave. This is the reason why there were no TEC variations in the case of the earthquake in Kepulauan Mentawai Region.

(a)   (b)
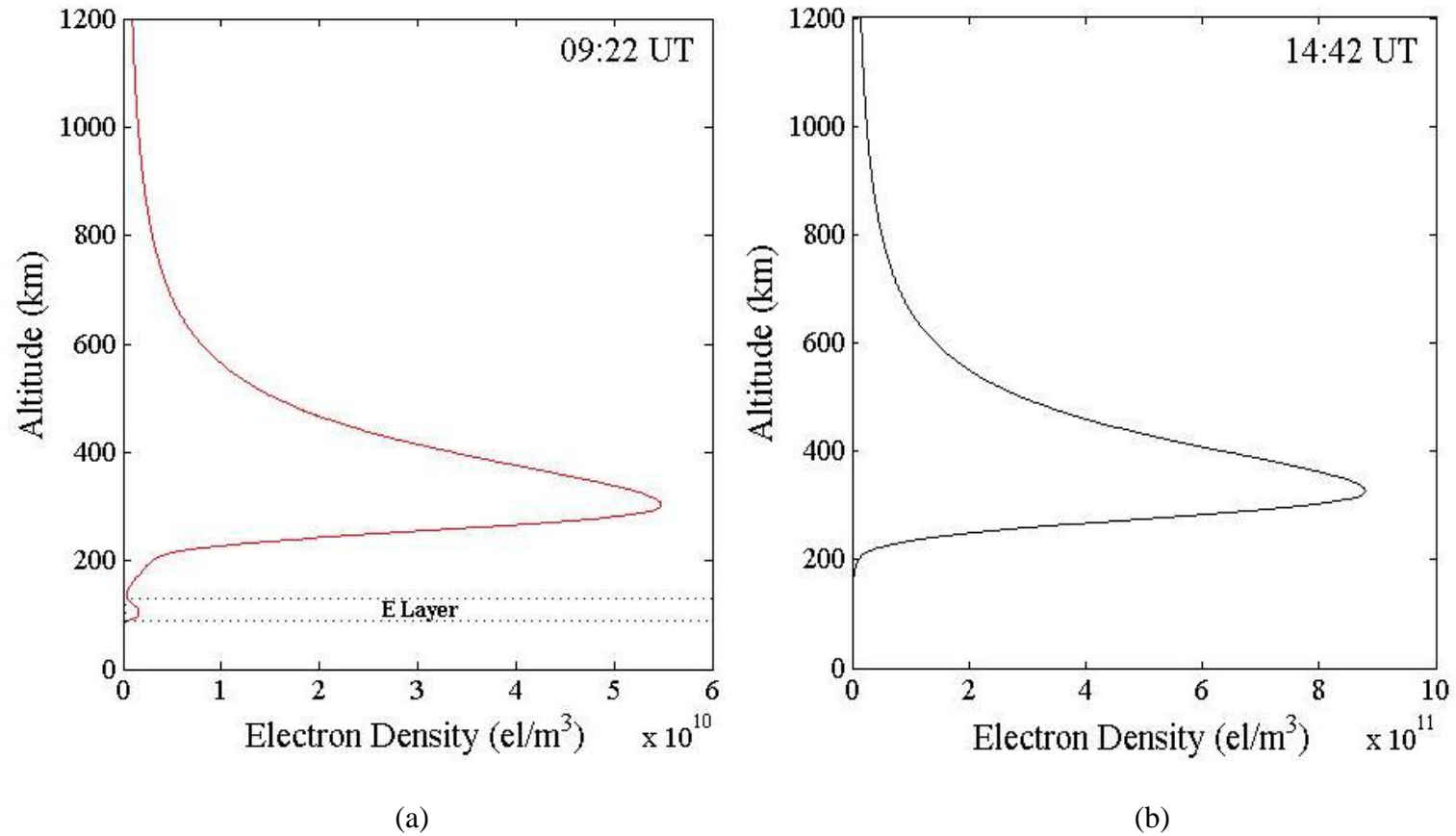
Figure 5-31 Electron profile from IRI-2007 model over the earthquake epicenter zone (a) Off west coast of the south island, New Zealand on 29 September 2009 at 09:22 UT and (b) Kepulauan mentawai region, Indonesia on 25 October 2010 at 14:42 UT.
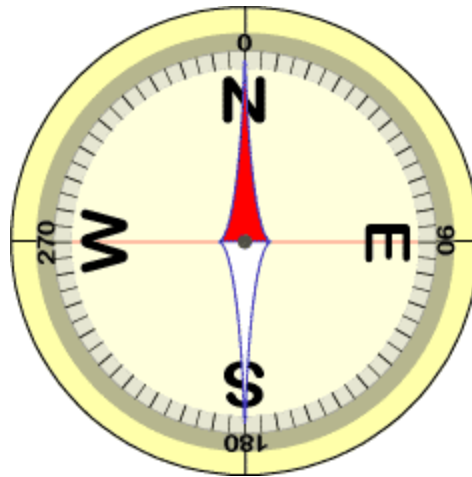
Figure 5-32 The Declination of geomagnetic field at 45.750°S, 166.577°E (World Data Center (WDC) for Geomagnetism, 1995).

The Declination of geomagnetic field was -0.371 degree at the earthquake location as shown in Figure 5-32. If there were TEC variations after the earthquake origin time, it is expected that GPS receivers at COCO, CUSV, NTUS and XMIS could detect the TEC variations because these stations are located where the acoustic wave front was perpendicular with the geomagnetic field line. Therefore, the acoustic wave will drive particles to move along geomagnetic field line. However, these GPS stations could not observe the TEC variations after the earthquake origin time.

5.5 Near the East Coast of Honshu, Japan

Geomagnetic and solar indices

Figure 5-33 shows the Dst and Kp indices from 10 to 12 March 2011. Kp index at the earthquake origin time is five, while Dst index reaches the minimum peak of -80 nT at 06:00:00 UT on 11 March 2011. The C-class flare on 11 March 2011 is 12. There were no M-class and X-class flares reported on the earthquake day. The solar activity levels were classified as "moderate" on 10 March 2011, "low" on 11 March 2011 and "moderate" on 12 March 2012.

(a)

(b)
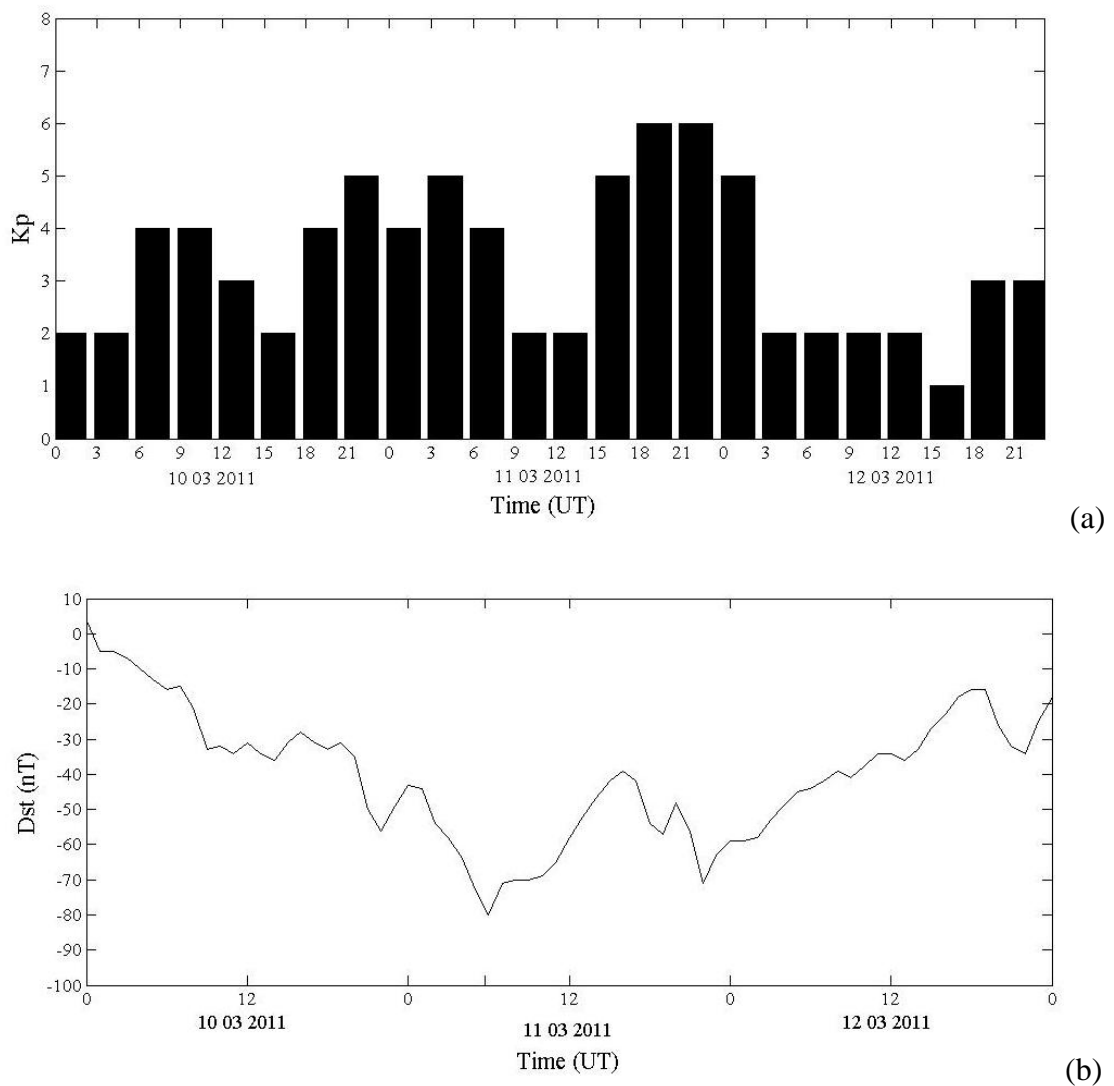
Figure 5-33 (a) Kp and (b) Dst indices from 10 to 11 March 2011.

TEC variations

The earthquake near the east coast of Honshu, Japan occurred on 11 March 2011 at 05:46:24 UT or 02:46:24 p.m. The earthquake magnitude was 9.0. The earthquake epicenter is at 38.297°N and 142.372°E. The depth of the earthquake focus is 30 km beneath the ground surface. At the earthquake area, the Pacific plate moves to the west with respect to North America plate with the speed of about 8.3 mm/yr. The Pacific plate subducts near Japan at the Japan Trench. Tohoku earthquake occurred as a result of thrust fault (reverse fault with low-angle) on or near the subduction zone boundary between Pacific and North America plates (U.S. Geological Survey (USGS), 2011). Figure 5-34 shows the boundary plates near the east coast of Honshu Island in Japan. The GPS stations being used to observe the TEC variations in this event are CHAN in China, MTKA, SMST, TSKB and USUD in Japan, DAEJ and SUWN in Korea, and KHAJ and YSSK in Russia. The GPS and epicenter locations are shown in Figure 5-35.

Figure 5-34 The boundary between North America and Pacific Plates near the east coast of Honshu Island in Japan (U.S. Geological Survey (USGS), 2011).
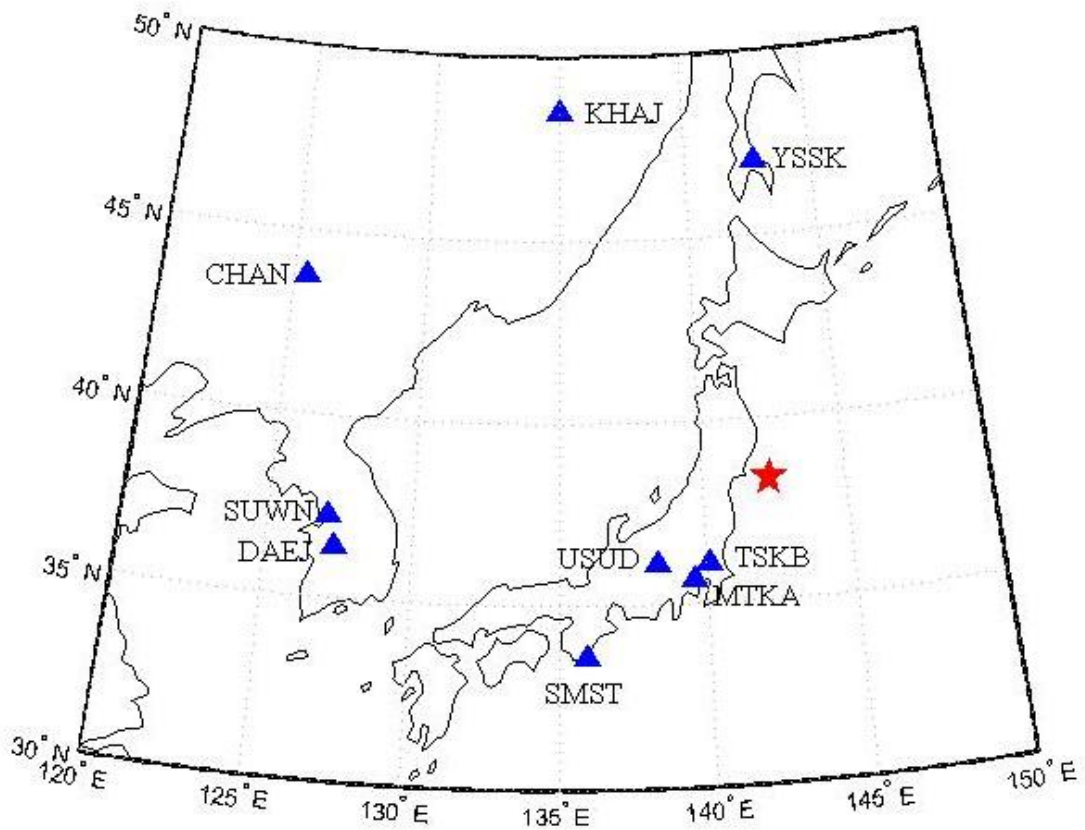
Figure 5-35 The locations of earthquake epicenter (red star) near the east coast of Honshu Island in Japan on 11 March 2011 and GPS stations (triangle).

Six GPS receivers including MTKA, SMST, TSKB, USUD, KHAJ, YSSK could observe the TEC variations. The locations of the GPS receivers and the distances between the earthquake epicenter and the GPS receivers are shown in Table 5-2.

Table 5-2 the GPS locations and their distances from the earthquake epicenter.

GPS Station	Geographic Coordinate		Country	Distance from epicenter (Km) [a]
	Lat.	Lon.		
MTKA	35.68°N	139.56°E	Japan	383
SMST	33.58°N	135.94°E	Japan	780
TSKB	36.11°N	140.09°E	Japan	316
USUD	36.13°N	138.36°E	Japan	429
KHAJ	48.52°N	135.05°E	Russia	1,279
YSSK	47.03°N	142.72°E	Russia	970

[a] National Oceanic and Atmospheric Administration (NOAA), 2010

MTKA Station

The geomagnetic coordinate of MTKA station is at (26.92°N, 151.19°E). Figure 5-36 illustrates the TEC variations between 10 and 12 March 2011 from 05:00:00 UT to 10:00:00 UT observed by MTKA station. The vertical dot line shows the earthquake origin time. There were no TEC variations occurred on 10 and 12 March 2011 as shown in Figure 5-36(a) and 5-36(c). On 11 March 2011, the TEC showed significant perturbation after the earthquake origin time and continued to fluctuate around one hour as shown in Figure 5-36(b). The maximum amplitude of the variations is around 0.13 TECU. The observation point on the IPP is (40.72°N, 130.26°E) at 05:12:00 UT and (28.76°N, 138.22°E) at 10:00:00 UT. The observation point moved to the southeast direction during the period of observation.

Figure 5-37 presents the TEC data after being processed the data processing between 10 and 12 March 2011. The vertical dot line indicates the origin time of the earthquake and the horizontal dash lines present $\pm$ twofold of the standard deviation (σ) of the TEC data from 06:30:00 UT to 07:30:00 UT. Figure 5-37(b) shows that the TEC started to fluctuate at 05:56:00 UT. It reached the first peak of variations at 05:58:00 UT. Then, there was a rapid decrease to the minimum value of -0.17 TECU at 06:02:00 UT. After that, it increased rapidly and reached the highest peak of 0.20 TECU at 06:05:00 UT and continued to fluctuate for an hour. Then, it returned to the

normal state. Figure 5-37(a) and 5-37(b) show that there were no TEC variations on 10 and 12 March 2011. The time lag of variation was 9.36 minutes. Figure 5-38 shows the power spectrum of TEC data between 05.30UT and 07:30UT. The dominant frequency is 2.2 mHz and the period of the TEC variations is 7.35 minutes.

Figure 5-36 The observed TEC detected by PRN18 at MTKA station on (a) 10 March 2011 (b) 10 March 2011 and (c) 11 March 2011.

Figure 5-37 The filtered TEC data observed by PRN18 at MTKA station on (a) 10 March 2011 (b) 11 March 2011 and (c) 12 March 2011.

Figure 5-38 The power spectrum of TEC data observed by MTKA station on

11 March 2011.

SMST Station

SMST station is located 780 km from the epicenter zone. The geomagnetic coordinate of SMST station is at (24.55°N, 154.26°W). The TEC variations could be detected by SMST station on 11 March 2011 as shown in Figure 5-39(b). However, the signal is broad and blur because the GPS receiver site is far from the epicenter. There were no TEC variations on 10 and 12 March 2011 as shown in Figure 5-39(a) and 5-39(c). The vertical dot line indicates the earthquake origin time. The TEC shows significant perturbation after the earthquake origin time and continued to fluctuate around one hour on 11 March 2011. The line of sight crossed the IPP at (38.44°N, 127.15°E) at 05:11:30 UT and at (27.32°N, 135.23°E) at 10:00:00 UT. The observation point moved to the southeast direction during the observation time.

The TEC data between 05:30:00 UT and 07:30:00 UT from 10 to 12 March 2011 were applied highpass-filter with 10 minutes cutoff period. After that it was smoothed using Savitzky-Golay method with 5 order polynomial and the windows size of 33 points. The filtered TEC data are shown in Figure 5-40. The origin time of the earthquake was indicated by the vertical dot line. The upper and lower horizontal dash lines present $\pm$ twofold of standard deviation (σ) of the TEC data from 05:30:00 UT to 07:30:00 UT. Figure 5-40(b) shows that the TEC started to fluctuate at 05:59:00 UT. It reached the first peak of 0.14 TECU at 06:00:00 UT. Then, there was a rapid decrease to the minimum value of -0.12 TECU at 06:04:00 UT. Then, it turned to the normal state. As can be seen from Figure 5-40(a) and 5-40(c), there were no TEC variations on 10 and 12 March 2011. The time lag of variation was 12.36 minutes. Figure 5-41 shows the power spectrum of the TEC data between 05.30:00 UT and 07:30:00 UT. The dominant frequency from power spectrum is 2.4 mHz and the period of the TEC variations is 6.57 minutes.

Figure 5-39 The observed TEC detected by PRN18 at SMST station on (a) 10 March 2011 (b) 10 March 2011 and (c) 11 March 2011.

Figure 5-40 The filtered TEC data observed by PRN18 at SMST station on (a) 10 March 2011 (b) 11 March 2011 and (c) 12 March 2011.

Figure 5-41 The power spectrum of TEC data observed by SMST station on 11 March 2011.

TSKB Station

TSKB is the nearest station where is located 316 km from the epicenter zone. The geomagnetic coordinate of TSKB station is at (27.39°N, 150.76°W). The TEC variations could be detected by TSKB station on 11 March 2011 as shown in Figure 5-42(b). There were no TEC variations on 10 and 12 March 2011 as shown in Figure 5-42(a) and 5-42(c). The vertical dot line indicates the earthquake origin time. The TEC shows significant perturbation after the earthquake origin time and continued to fluctuate around one hour on 11 March 2011. The satellite-receiver path crossed the IPP at (41.78°N, 128.28°E) at 05:00:00 UT and at (29.04°N, 138.64°E) at 10:00:00 UT. The observation point moved to the southeast direction during the period of observation.

Figure 5-43 shows the filtered TEC data between 10 and 12 March 2011 from 05:30:00 UT to 07:30:00 UT. The vertical dot line indicates the origin time of the earthquake. Figure 5-43(b) shows that the TEC started to fluctuate at 05:53:00 UT. It reached the first peak of 0.13 TECU at 05:58:00 UT. Then, there was a rapid decrease to the minimum value of -0.18 TECU at 06:00:00 UT. It continued to fluctuate and reached the maximum value of 0.20 TECU at 06:32:00 UT. It recovered to the normal level at about 07:15:00 UT. There were no TEC variations on 10 and 12 March 2011 as shown in Figure 5-43(a) and 5-43(c) The time lag of variation was 6.36 minutes. Figure 5-44 shows the power spectrum of TEC data between 05:30:00 UT and 07:30:00 UT. The dominant frequency from power spectrum is 1.8 mHz and the period of the TEC variations is 9.16 minutes.
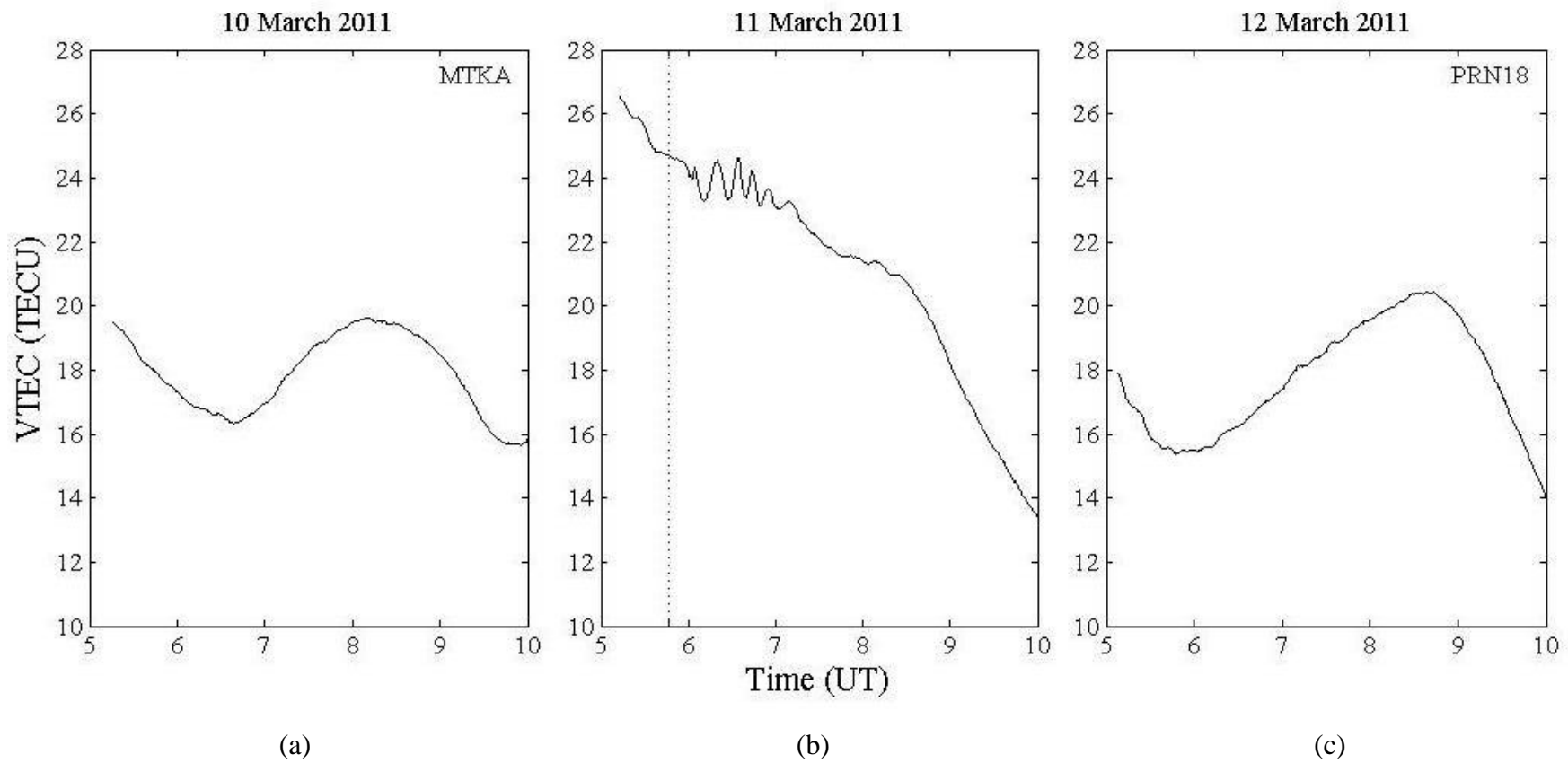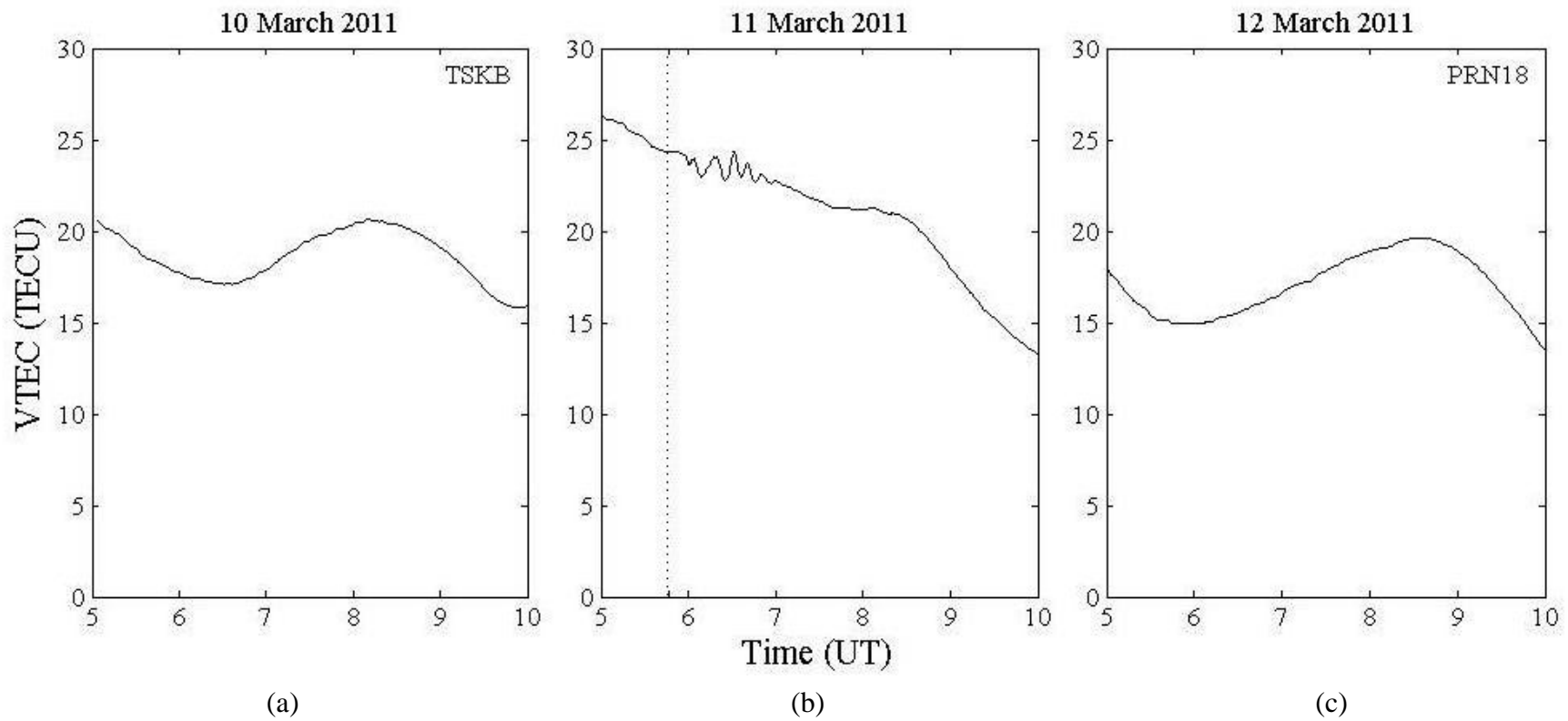
Figure 5-42 The observed TEC detected by PRN18 at TSKB station on (a) 10 March 2011 (b) 10 March 2011 and (c) 11 March 2011.
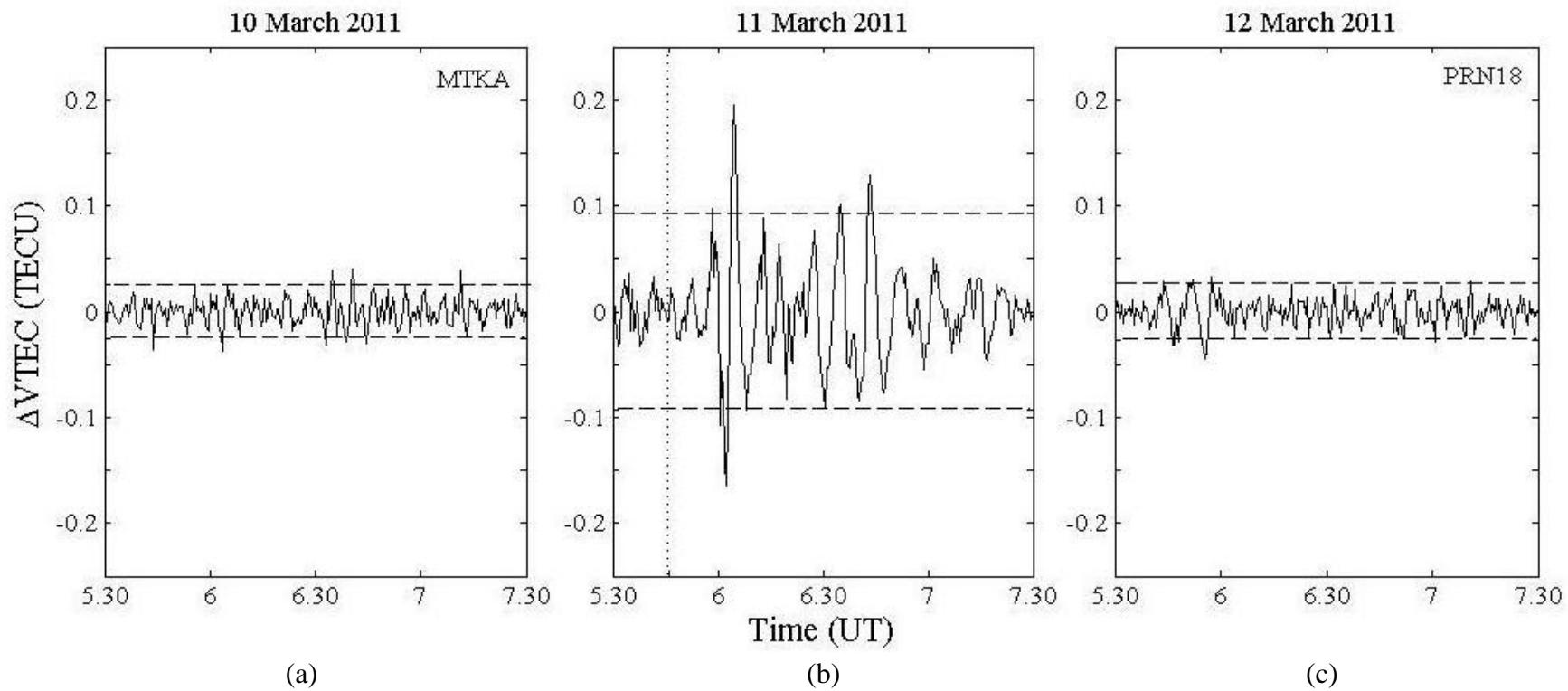
Figure 5-43 The filtered TEC data observed by PRN18 at TSKB station on (a) 10 March 2011 (b) 11 March 2011 and (c) 12 March 2011.
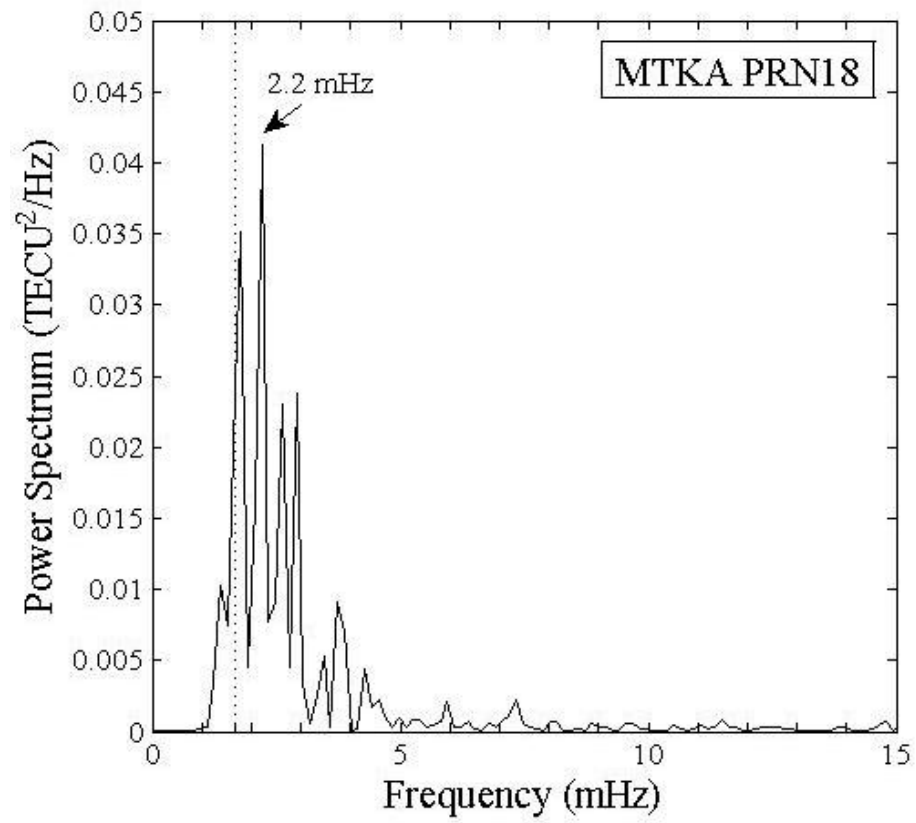
Figure 5-44 The power spectrum of TEC data observed by TSKB station on 11 March 2011.

USUD Station

USUD is located 429 km away from the epicenter zone. The geomagnetic coordinate of USUD station is at (27.27°N, 152.33°W). The TEC variations could be detected by USUD station on 11 March 2011 as shown in Figure 5-45(b). No TEC variations could be seen on 10 and 12 March 2011 as shown in Figure 5-45(a) and 5-45(c). The vertical dot line indicates the earthquake origin time at 05:46:24 UT. The TEC shows significant perturbations after the earthquake origin time and continued to fluctuate around one hour on 11 March 2011. The line of sight crossed the IPP at (40.77°N, 129.74°E) at 05:14:00 UT and at (29.09°N, 137.19°E) at 10:00:00 UT. The observation point moved to the southeast direction during the time of observation.

As can be seen from Figure 5-46(b), the TEC variations occurred after the earthquake origin time about 11.36 minutes on 11 March 2011. It reached the minimum value of -0.15 TECU at 06:28:00 UT and hit the maximum value of 0.14 TECU at 06:41:00 UT. The upper and lower horizontal dash lines show $\pm 2\sigma$ of the TEC data from 05:30:00 UT to 07:30:00 UT. There were no TEC variations on 10 and 12 March 2011 as shown by the narrow gap of $\pm 2\sigma$ in Figure 5-46(a) and 5-46(c). Figure 5-47 presents the dominant frequency of the TEC variation which is 1.9 mHz. The period of the TEC variations observed by USUD station is 8.46 minutes.
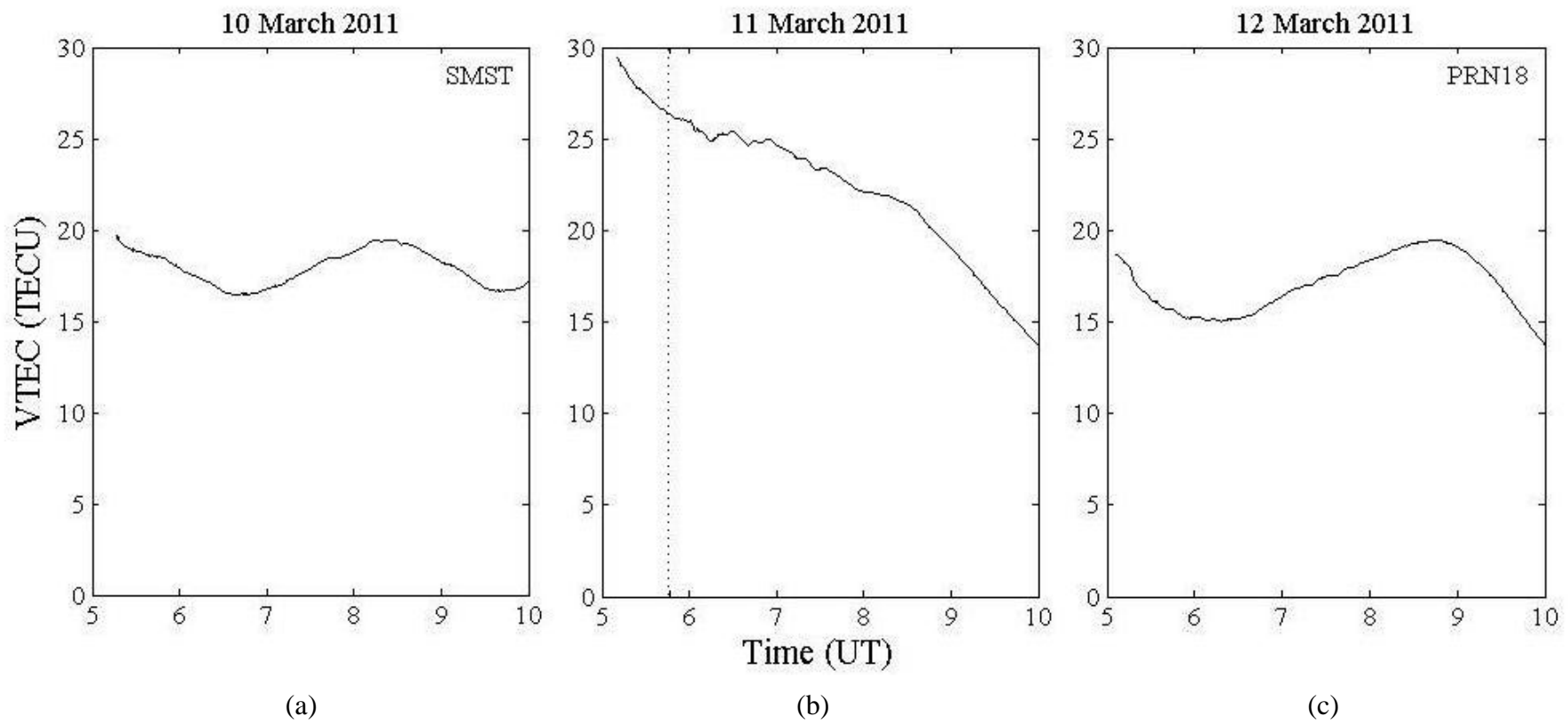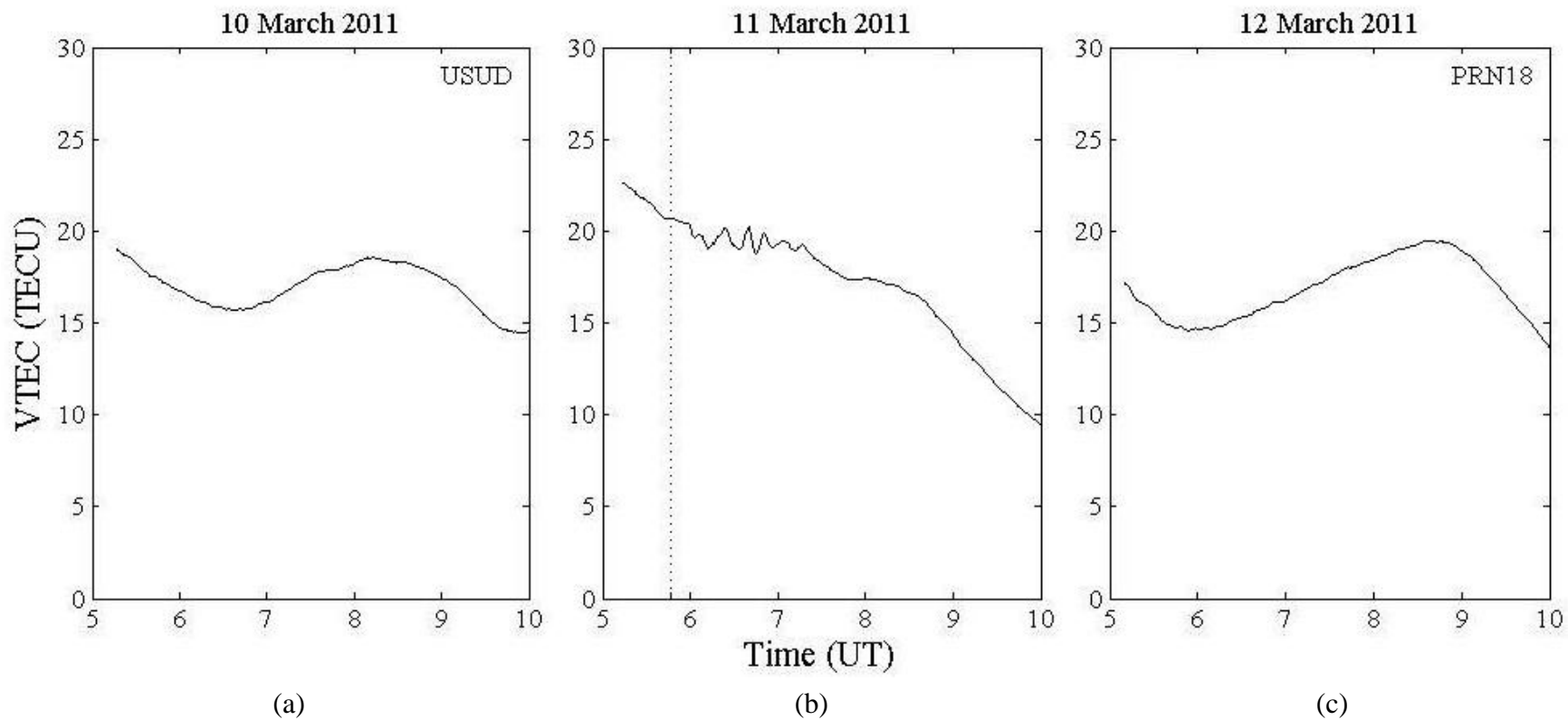
Figure 5-45 The observed TEC detected by PRN18 at USUD station on (a) 10 March 2011 (b) 10 March 2011 and (c) 11 March 2011.
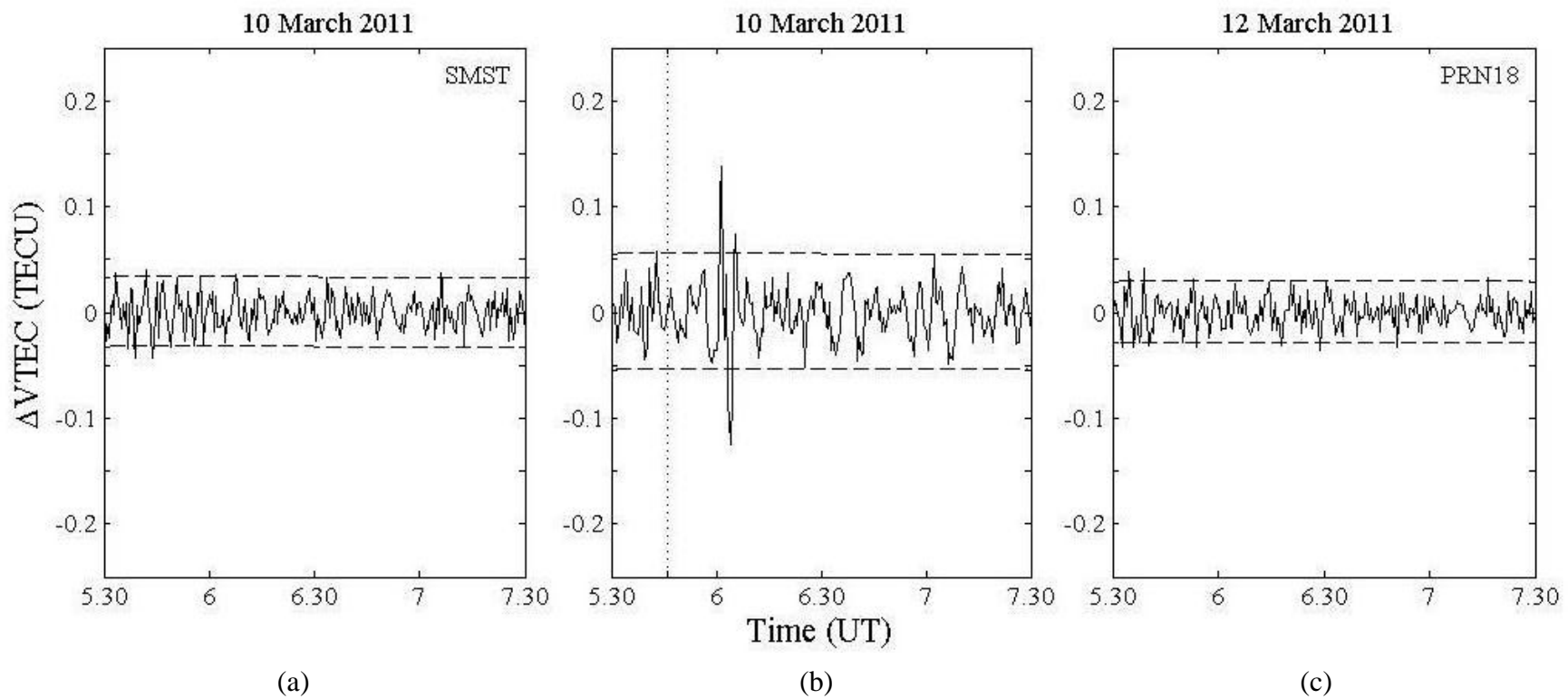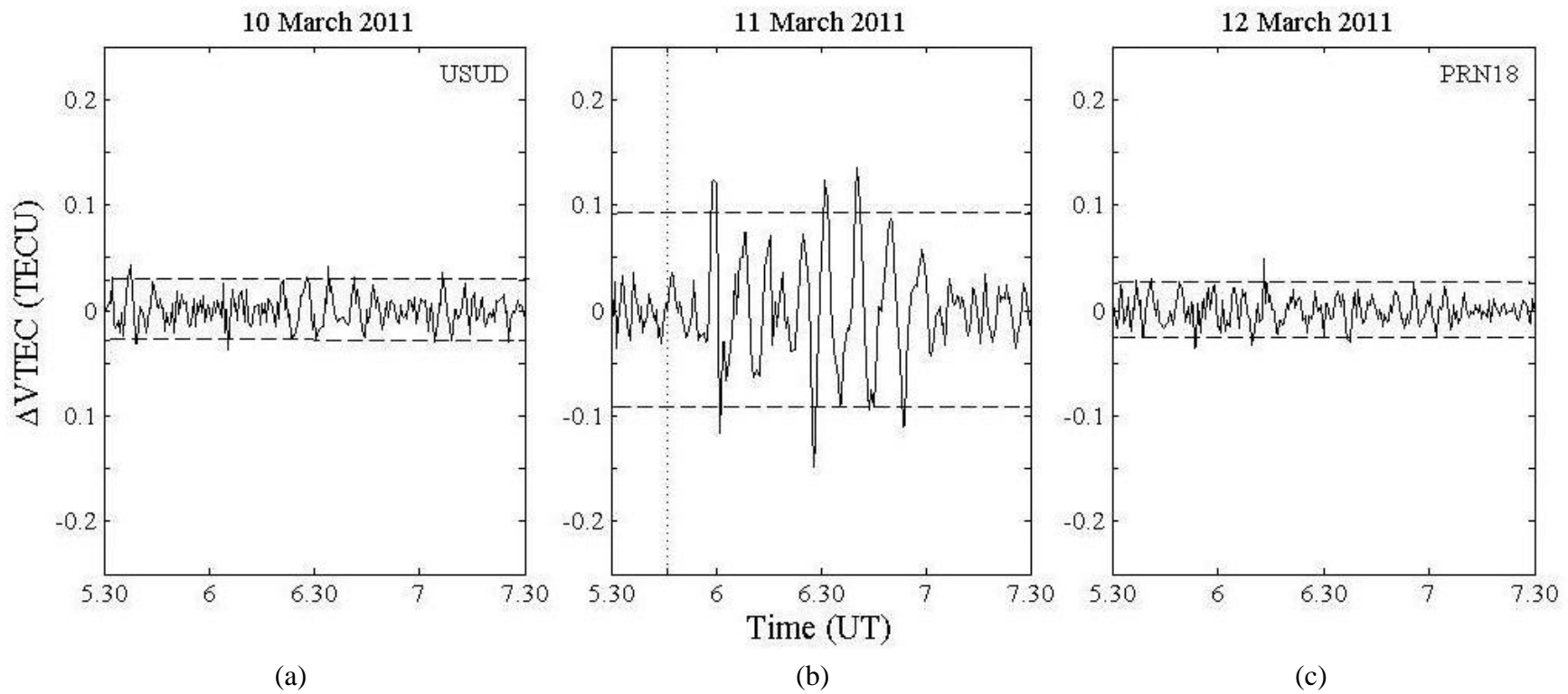
Figure 5-46 The filtered TEC data observed by PRN18 at USUD station on (a) 10 March 2011 (b) 11 March 2011 and (c) 12 March 2011.
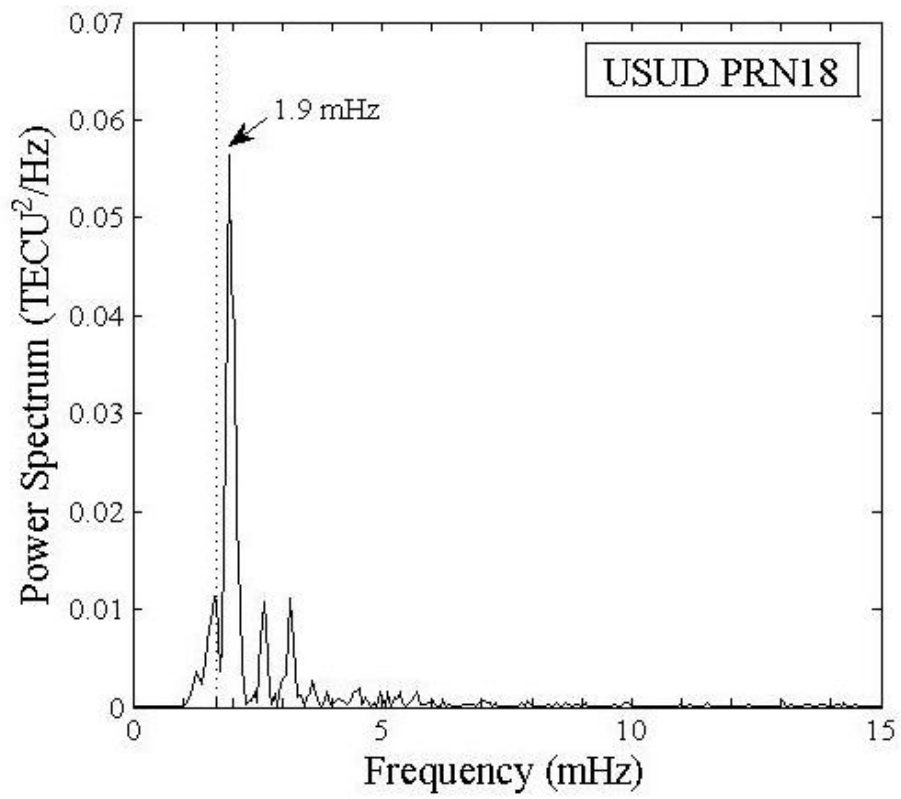
Figure 5-47 The power spectrum of TEC data observed by USUD station on 11 March 2011.

KHAJ Station

KHAJ is located in Russia. The distance between the earthquake epicenter and KHAJ station is 1,279 km. The geomagnetic coordinate of KHAJ station is at (39.35°N, 156.74°W). Figure 5-48 shows the TEC data between 05:00:00 UT and 10:00:00 UT from 10 to 12 March 2011. It can be seen the TEC variations at KHAJ station on 11 March 2011 as shown in Figure 5-48(b). There were no TEC variations on 10 and 12 March 2011 as shown in Figure 5-48(a) and 5-48(c). The vertical dot line indicates the earthquake origin time. The TEC shows significant perturbations after the earthquake origin time on 11 March 2011. The TEC continued to fluctuate around one hour and turned to the normal state. The satellite and receiver path crossed the IPP at (48.39°N, 133.36°E) at 05:00:00 UT and at (42.28°N, 147.92°E) at 09:01:30 UT on 11 March 2011. The observation point moved to the southeast direction during the time of observation.

It was clearly seen the TEC variations from the filtered TEC data at KHAJ station on 11 March 2011 as shown in Figure 5-49(b). The fluctuation started at 06:03:00 UT. The time lag of the TEC variations is 16.36 minutes after the earthquake origin time. There was the maximum value of 0.08 TECU at 06:30:00 UT. It reached the minimum value of -0.07 TECU at 06:54:00 UT. The TEC fluctuated for one and half hours. Then, it recovered to its normal level. As can be seen from Figure 5-49(a) and 5-49(c), the TEC variations could not be observed on 10 and 12 March 2011. Figure 5-50 shows the power spectrum of TEC data between 05:30:00 UT and 07:30:00 UT. The power spectrum from FFT method is 2.4 mHz. The period of oscillations is 6.57 minutes.
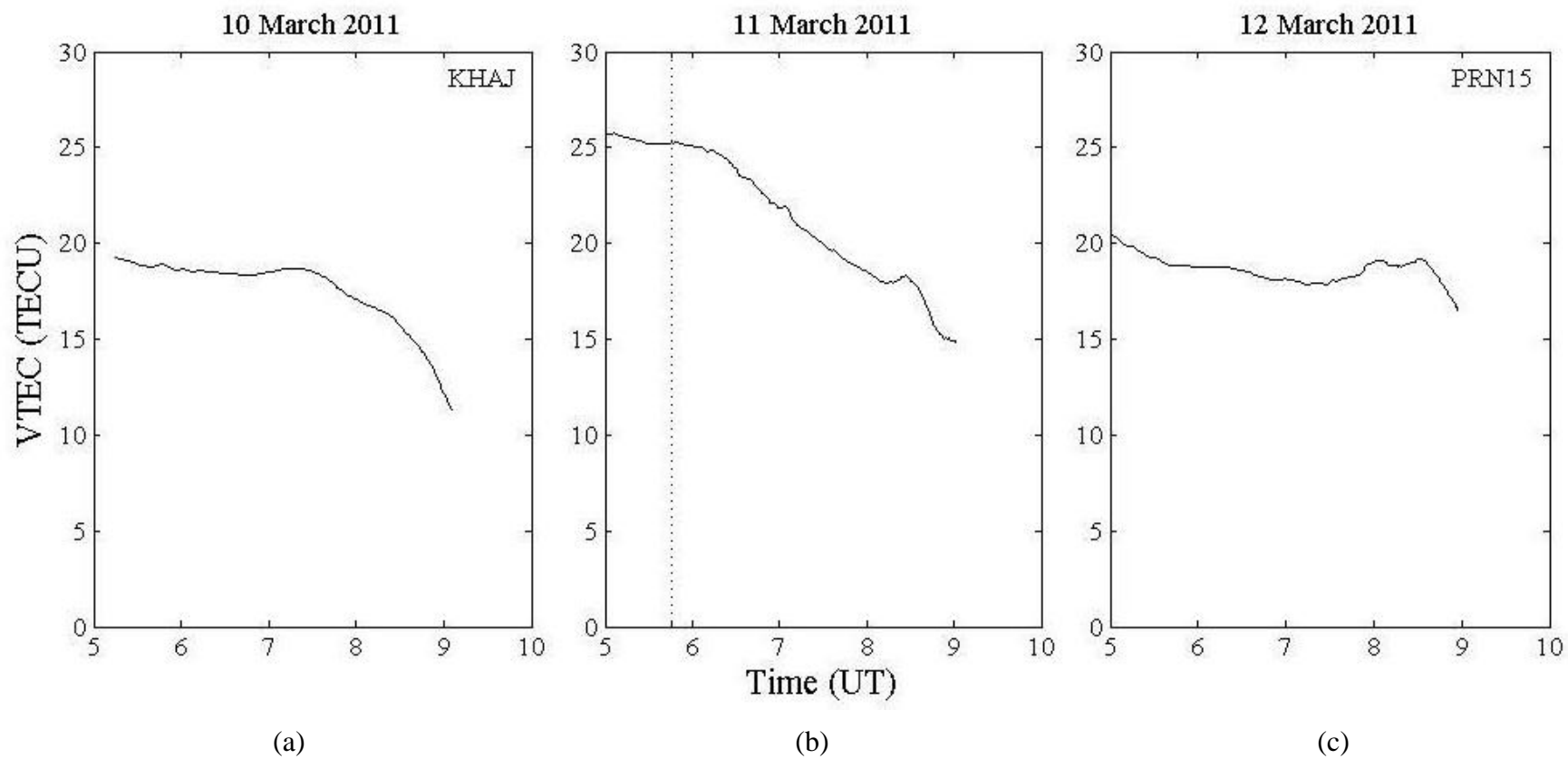
Figure 5-48 The observed TEC detected by PRN15 at KHAJ station on (a) 10 March 2011 (b) 10 March 2011 and (c) 11 March 2011.
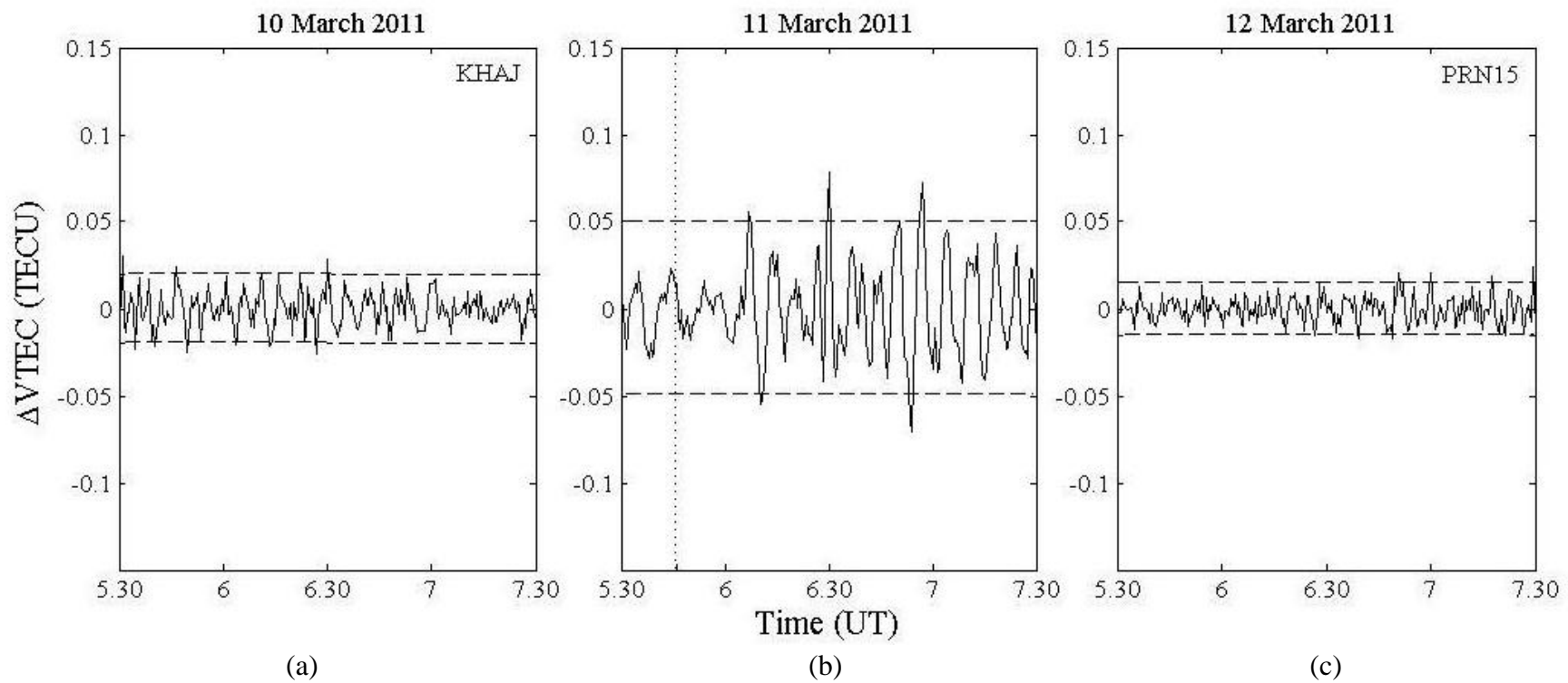
Figure 5-49 The filtered TEC data observed by PRN05 at KHAJ station on (a) 10 March 2011 (b) 11 March 2011 and (c) 12 March 2011.
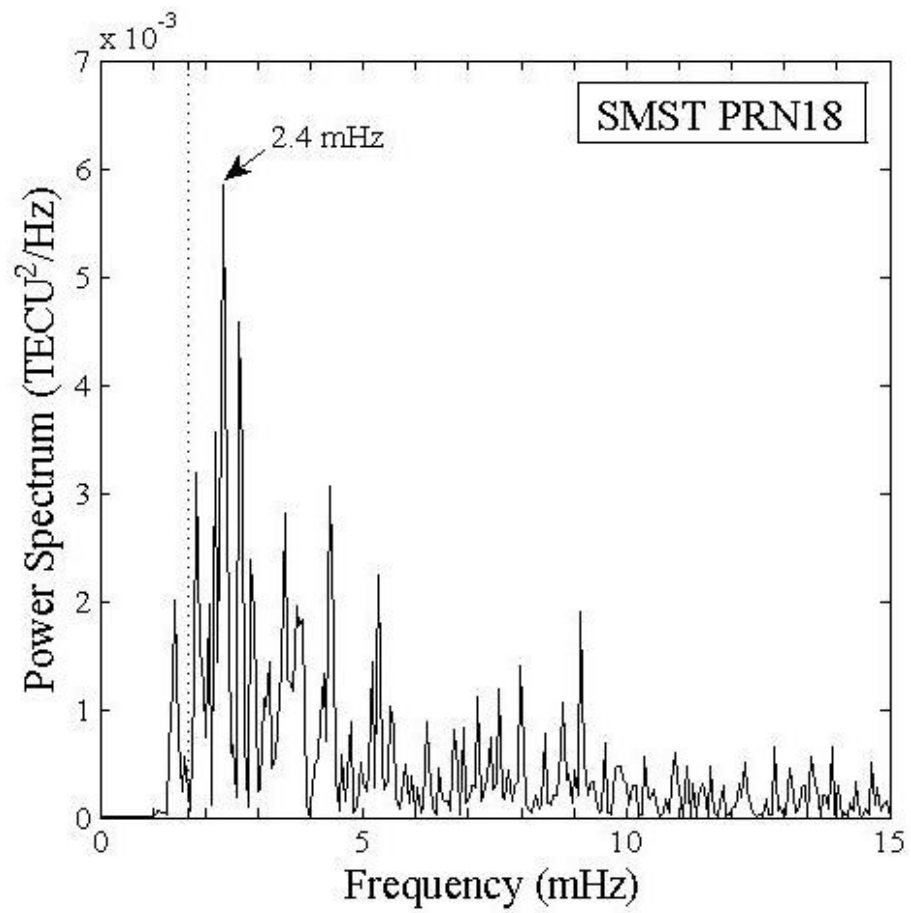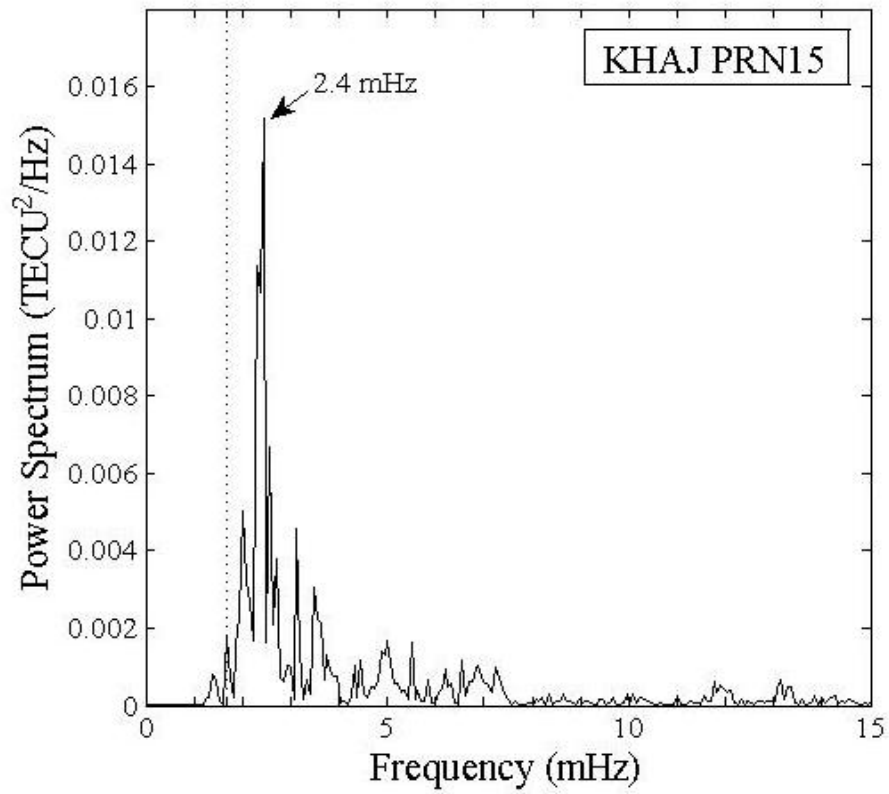
Figure 5-50 The power spectrum of TEC data observed by KHAJ station on 11 March 2011.

YSSK Station

YSSK station is located in Russia. The distance between YSSK station and the earthquake epicenter zone is 970 km. The geomagnetic coordinate of YSSK station is at (38.46°N, 149.92°W). The TEC variations could be detected by YSSK station on 11 March 2011 as shown in Figure 5-51(b). There were no TEC variations on 10 and 12 March 2011 as shown in Figure 5-51(a) and 5-51(c). The vertical dot line indicates the earthquake origin time. The TEC shows significant perturbation after the earthquake origin time and continued to fluctuate around one hour on 11 March 2011. The line of sight crossed the IPP at (51.06°N, 131.00°E) at 05:00:00 UT and at (34.91°N, 139.65°E) at 10:00:00 UT. The observation point moved southeastward during the time of observation.

Figure 5-52(b) shows the TEC variations observed by YSSK station from 05:30:00 UT to 07:30:00 UT. The time lag of the TEC variations is 14.36 minute after the earthquake origin time. It reached the maximum peak of 0.08 TECU at 06:45:00 UT and dropped suddenly to the minimum peak of -0.06 TECU at 06:49:00 UT. As can be seen from Figure 5-52(a) and 5-52(c), there were no TEC variations on 10 and 12 March 2011. The dominant frequency obtained from FFT method is 1.9 mHz. The period of TEC variations is 8.46 minutes.
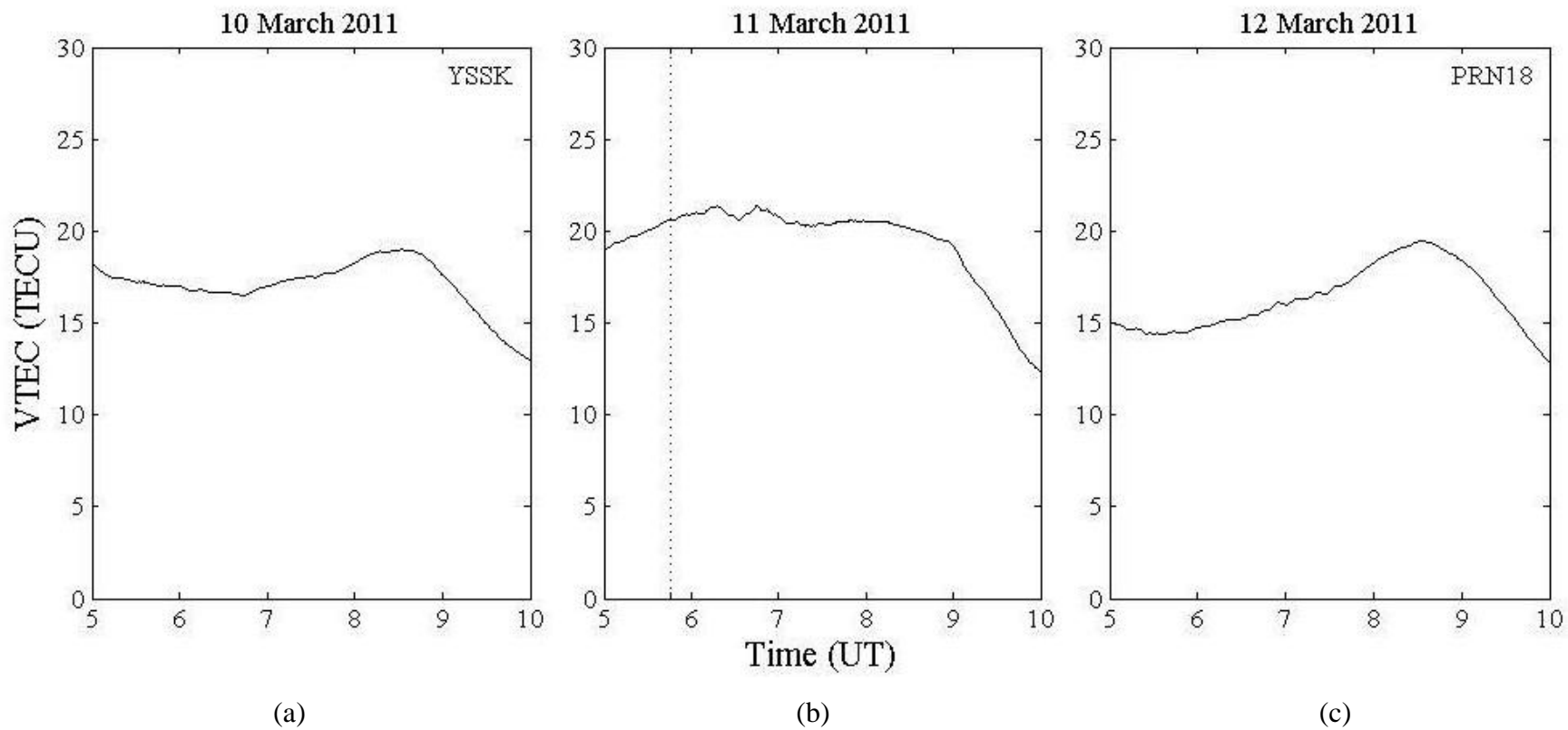
Figure 5-51 The observed TEC detected by PRN18 at YSSK station on (a) 10 March 2011 (b) 10 March 2011 and (c) 11 March 2011.
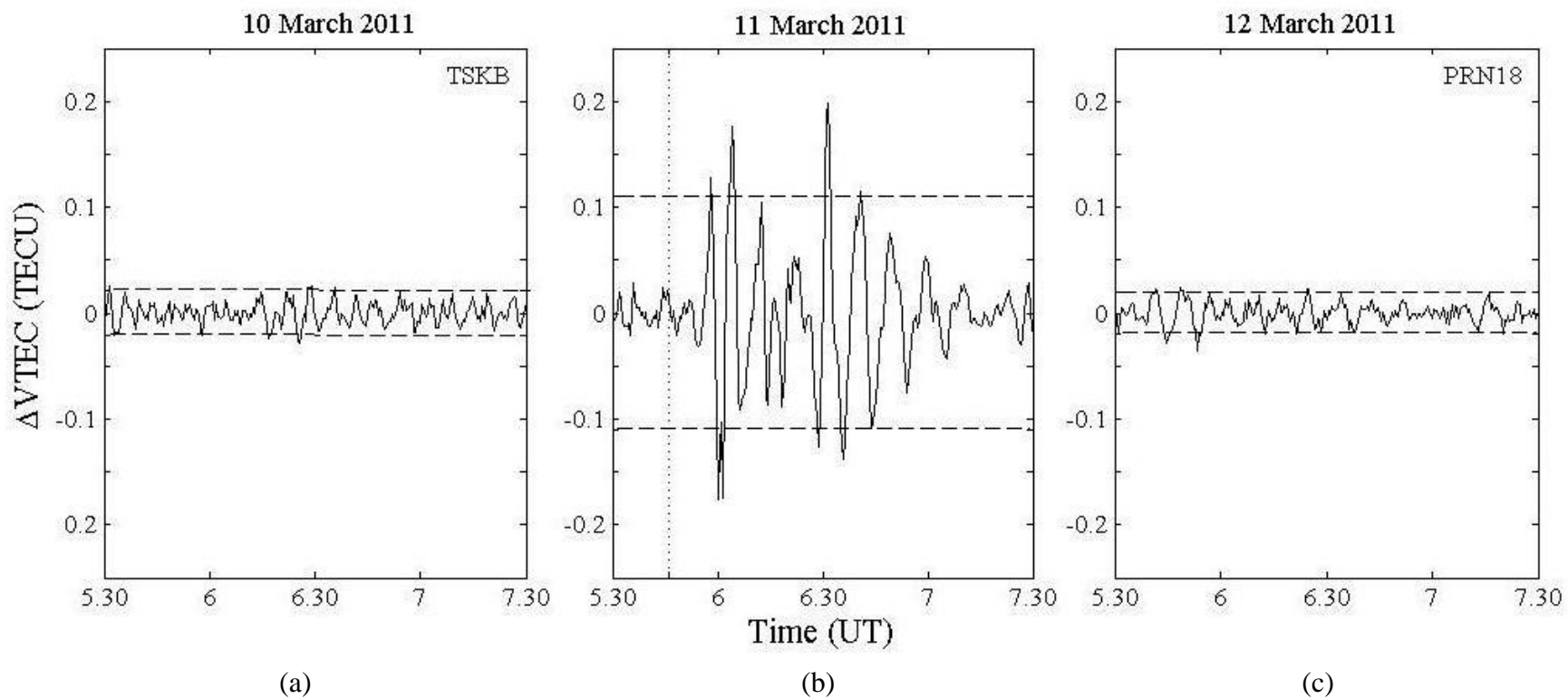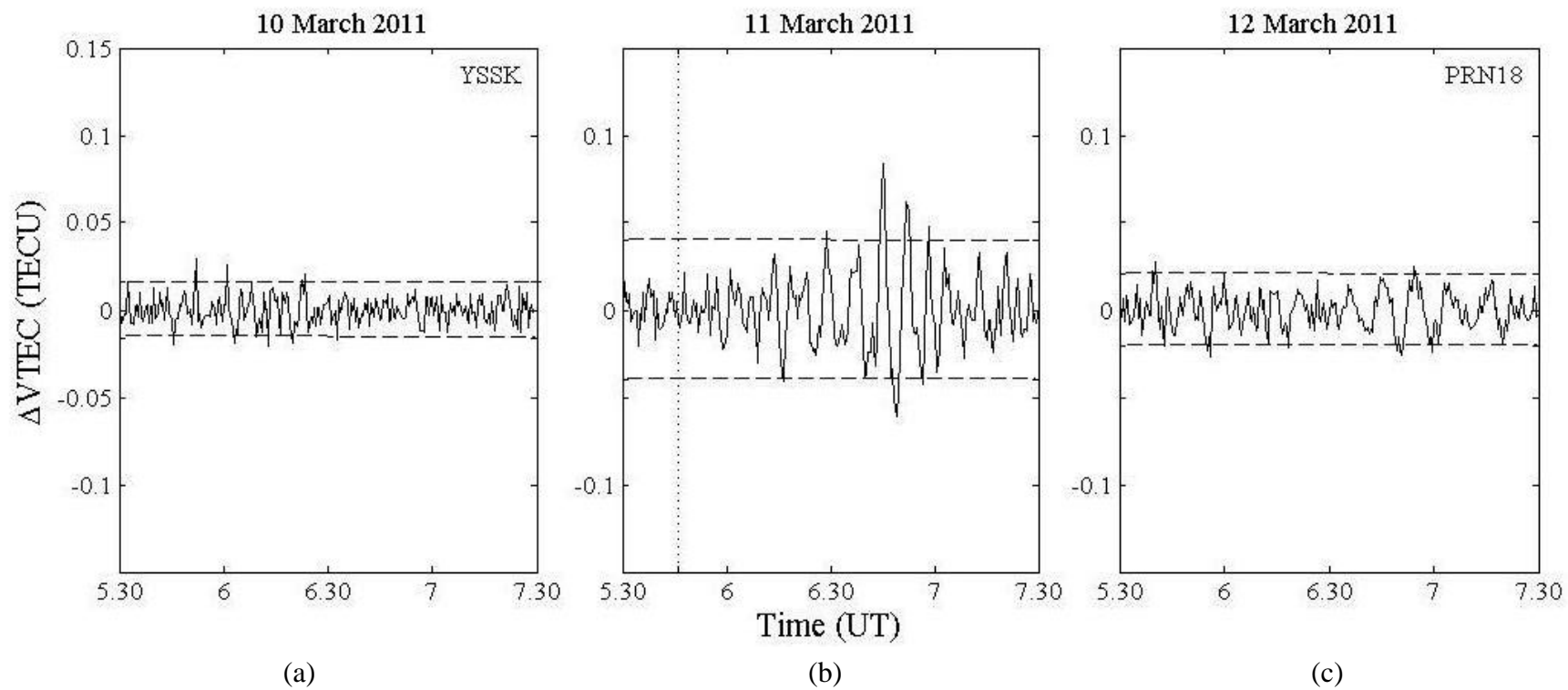
Figure 5-52 The filtered TEC data observed by PRN18 at YSSK station on (a) 10 March 2011 (b) 11 March 2011 and (c) 12 March 2011.
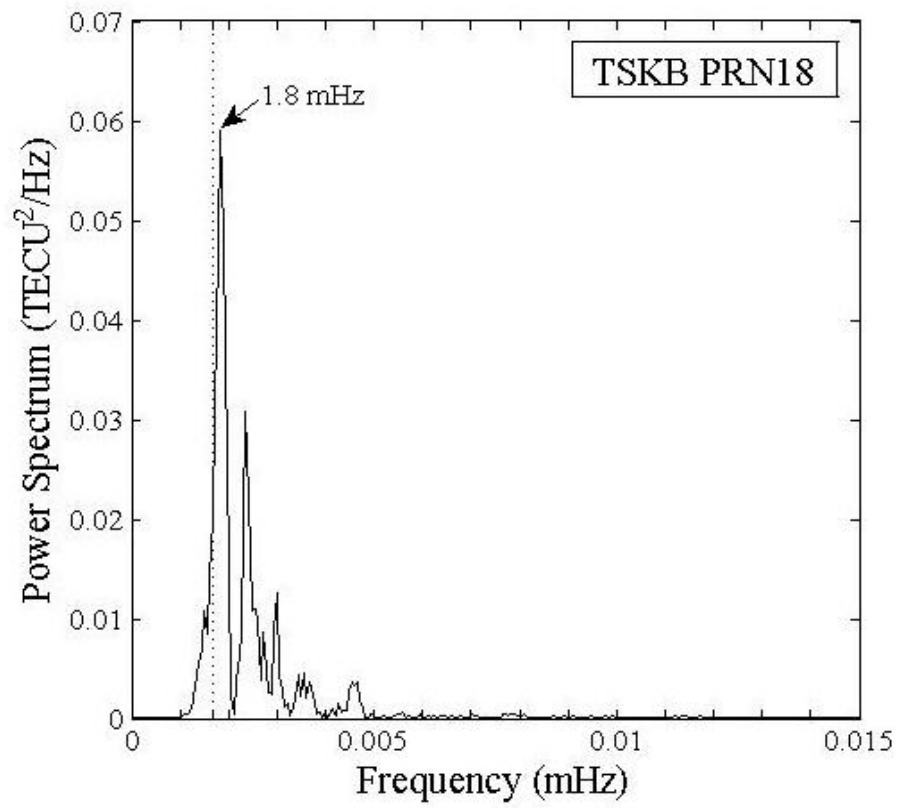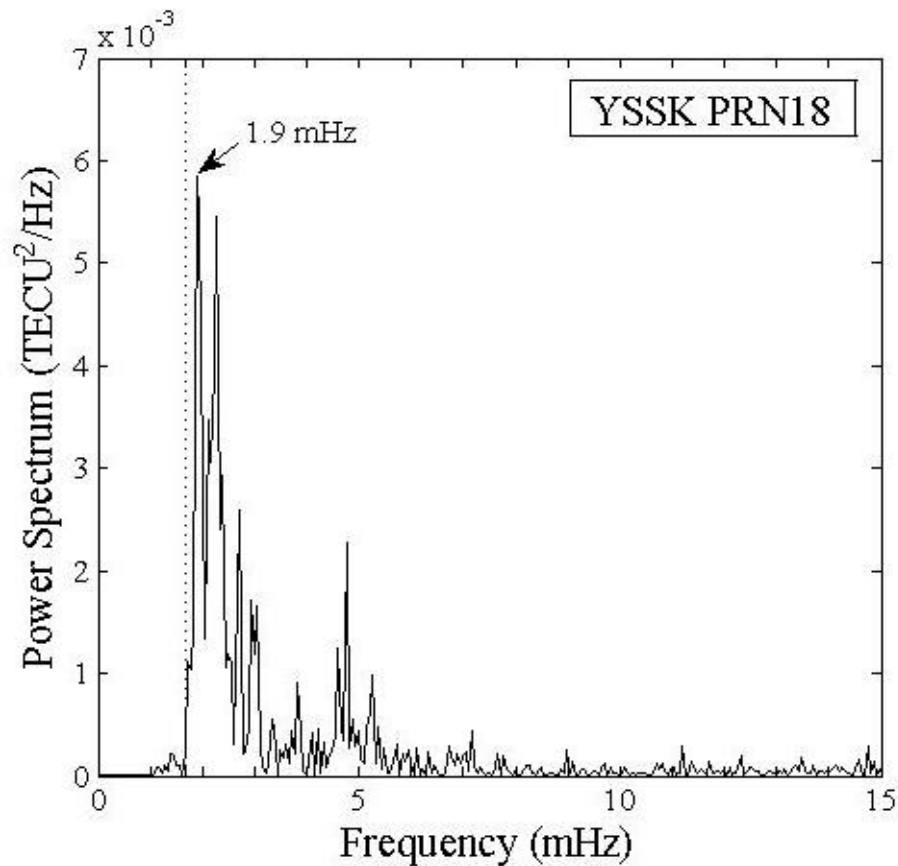
Figure 5-53 The power spectrum of TEC data observed by YSSK station on
11 March 2011.

From the results of the Tohoku earthquake, there were no TEC variations on 10 and 12 March 2011, while it was clearly seen the TEC variations on 11 March 2011 after the earthquake origin time. It can be concluded that the source of the TEC variations is the earthquake. Furthermore, the filtered TEC data from all GPS stations on 11 March 2011 illustrate the increasing number of the TEC value to the first peak of the TEC variations after the earthquake origin time. The increasing value of the TEC is the result of thrust fault at the earthquake latitude. The earthquake in section 4.2 was occurred by the similar fault with this event. Therefore, these two earthquakes show the same significant results.

The summarized periods of the TEC variations observed by all GPS receivers around the epicenter zone are shown on Table 5-3. The observed minimum period is 6.57 minutes while the maximum period is 9.16 minutes. These observed periods correspond to the periods of the acoustic wave mode.

Table 5-3 The periods of TEC variation observed by GPS receivers around the epicenter zone.

Station Names	Country	PRN	Dominant Frequency (mHz)	Variation Period (min)
MTKA	Japan	18	2.2	7.35
SMST	Japan	18	2.4	6.57
TSKB	Japan	18	1.8	9.16
USUD	Japan	18	1.9	8.46
KHAJ	Russia	15	2.4	6.57
YSSK	Russia	18	1.9	8.46
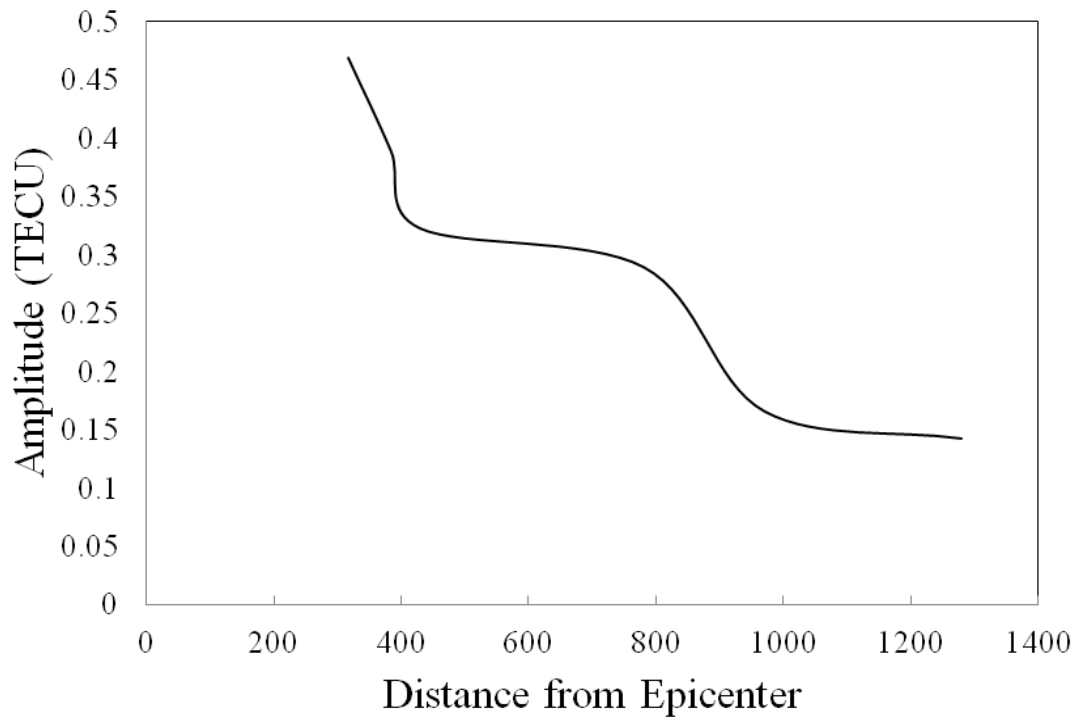
Figure 5-54 The observed amplitude of TEC variations at different distance between the epicenter zone and the GPS stations in Tohoku earthquake.

As can be seen from Figure 5-54, the amplitude of TEC variations decrease when the distance between the epicenter and the GPS receivers increases. The amplitude decreases from about 0.45 TECU at the distance around 350 km (from epicenter) to about 0.15 TECU at approximately 1,300 km (from epicenter). This result confirms that the acoustic wave decays when it travels far away from the earthquake epicenter. Therefore, the GPS stations where are located very far from the epicenters can detect the small amplitudes of the TEC variations. However, the factor of the satellite-receiver path which is parallel with the acoustic wave front should be taken into account. The locations on the IPP are discussed later.

The Declination of the geomagnetic field lines at the earthquake epicenter zone was -7.519° as shown in Figure 5-55. The horizontal component of geomagnetic field line pointed to north-northwest direction. Therefore, MTKA, SMST, TSKB, USUD, KHAJ and YSSK could detect the TEC variations because the component of acoustic wave front which is perpendicular with geomagnetic field lines passed these GPS stations as illustrated in Figure 5-56. The solid and dash circles in Figure 5-56 are the sample of acoustic wave front which propagated away from above the epicenter zone on the ionospheric height. The solid circle indicates "Crest" and the dash circle illustrates "Trough" of acoustic wave. The wave front of acoustic wave which propagated westward is parallel with geomagnetic field lines. Therefore, the acoustic wave could not survive when it travelled to the west direction because the charged particles are restricted to move across the geomagnetic field lines (Kelley, 2009). These are reasons why CHAN, SUWN and DAEJ could not detect the TEC variations. The red, pink, green, back and yellow lines show the locations of the observation points that satellite (PRN18) and receiver paths cross the IPP observed by SMST, USUD, MTKA, TSKB and KHAJ, respectively. The points of observation move southeastward. In the case of KHAJ station, the point of observation of PRN15 (blue line) moved to the east direction.
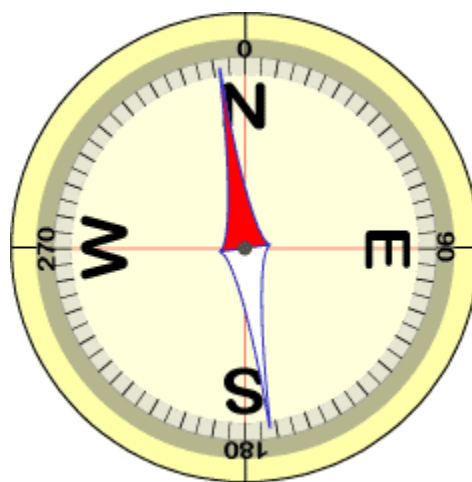
Figure 5-55 The Declination of geomagnetic field at 38.297°N, 142.372°E (World Data Center (WDC) for Geomagnetism, 1995).
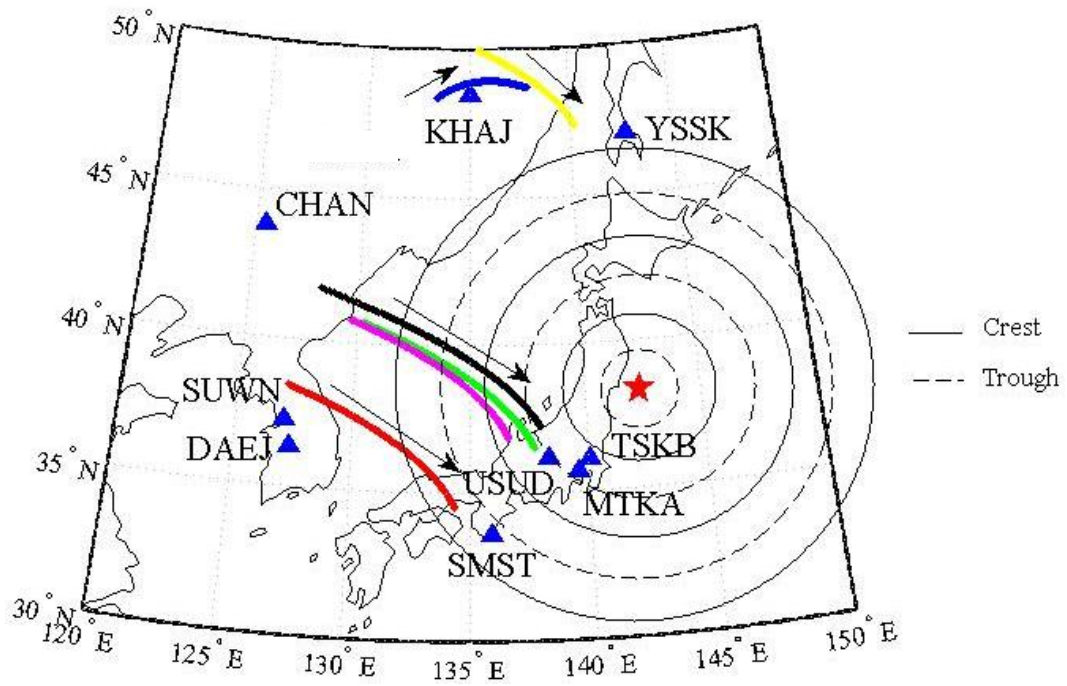
Figure 5-56 The ionospheric disturbance propagated from the epicenter zone.

Figure 5-57 shows the IRI-2007 model. It can be seen from Figure 5-57(a) that there was the E layer during the Tohoku earthquake process at 05:46:00 UT over the epicenter. In the case of Figure 5-53(b), there is no the ionospheric E region at 10:00 UT (after sunset) over the Tohoku earthquake epicenter.
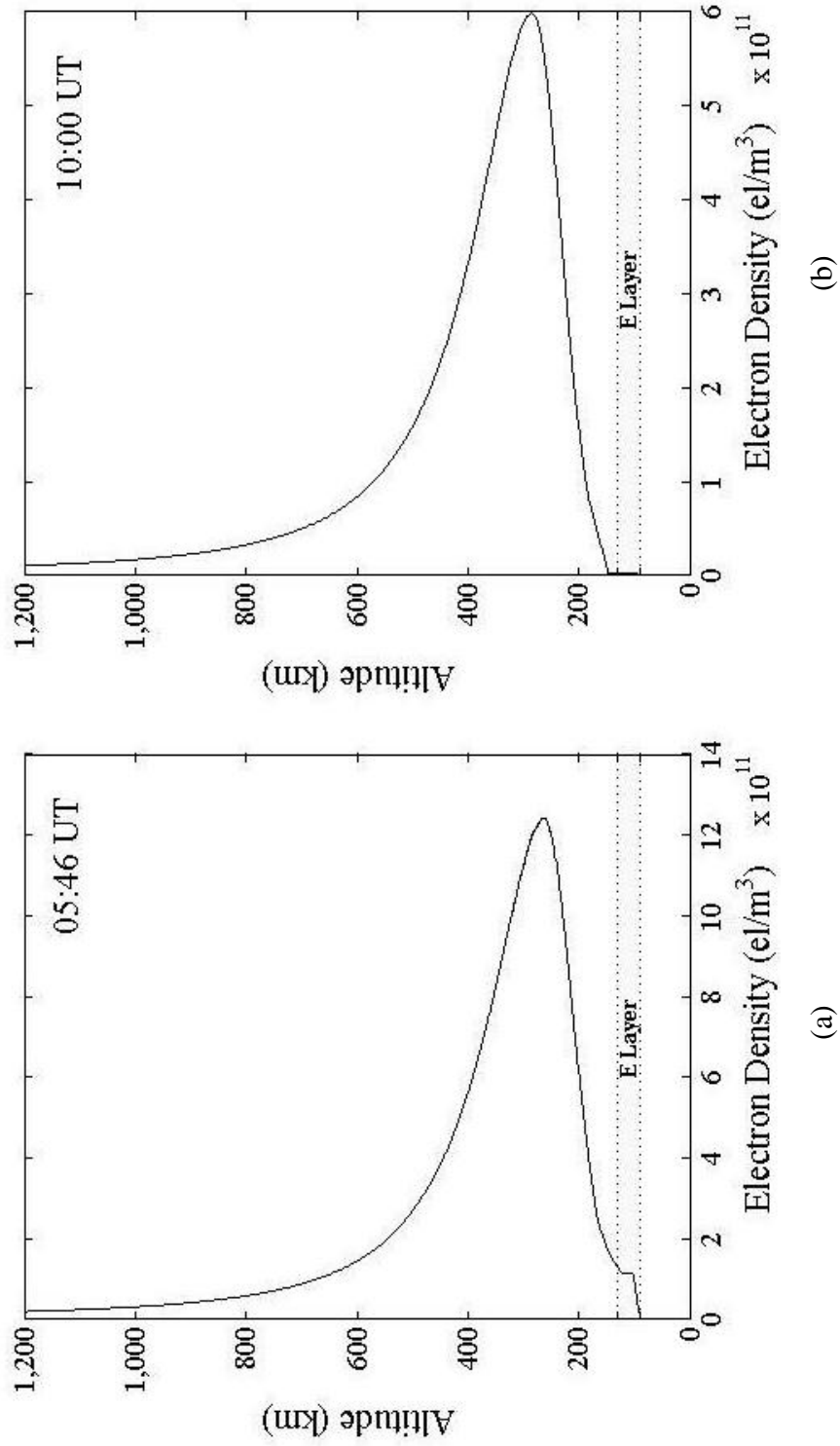
Figure 5-57 Electron profile from IRI-2007 model over the earthquake epicenter zone (a) at 05:46 UT on daytime (b) 10:00 UT after sunset.

5.6 Kermadec islands region

Geomagnetic and solar indices

As can be seen from Figure 5-58(a) and 5-58(b), the Kp index was two and the Dst index was higher than -35 nT during the earthquake time. The geomagnetic activity level between 5 and 7 July 2011 were classified as "unsettled", "unsettled" and "quiet". There were no solar flares which were larger than C class being reported during 5 and 7 July 2011. The solar activity level on 6 July 2011 was classified as "very low".

(a)

(b)

Figure 5-58 (a) Kp and (b) Dst from 5 to 7 July 2011.

TEC variations

The earthquake with magnitude 7.6 in Kermadec Islands region occurred on 6 July 2011 at 19:03:16 UT or 07:03:16 a.m. The focus of the earthquake was 20 km beneath the ground surface. The location of this earthquake was 29.312°S and 176.204°W in the southern hemisphere. At the earthquake site, the Pacific plate subducts the Australian plate and is melted beneath the eastern edge of the Australian plate. The Pacific plate moves to the west direction at the speed of about 6.1 mm/yr. Figure 5-59 shows the boundary between the Australian and the Pacific plates at the earthquake epicenter zone. This earthquake was occurred by the rupture of the normal fault on the Pacific plate. There are eight GPS stations which were used to observe TEC variations. The GPS station names, their locations, and their distances from the epicenter are shown in Table 5-4. Figure 5-60 shows the locations of earthquake epicenter and GPS stations.

Figure 5-59 The boundary between the Australian and Pacific plates near Kermadec Island region (U.S. Geological Survey (USGS) 2011).

Table 5-4 The GPS locations and their distances from the earthquake epicenter.

GPS Station	Geographic Coordinate		Country	Distance from epicenter (km) [a]
	Lat.	Lon.		
ASPA	14.32°S	170.72°W	United State	1,758
CHTI	43.73°S	176.61°W	New Zealand	1,603
CORM	36.86°S	175.74°E	New Zealand	1,124
FAA1	17.57°S	149.60°W	Tahiti	2,999
HIKB	37.56°S	178.30°E	New Zealand	1,048
LAUT	17.60°S	177.44°E	N/A	1,452
NIUM	19.07°S	169.92°W	Niue	1,805
TONG	21.14°S	175.17°W	N/A	1,254

[a] National Oceanic and Atmospheric Administration (NOAA), 2010
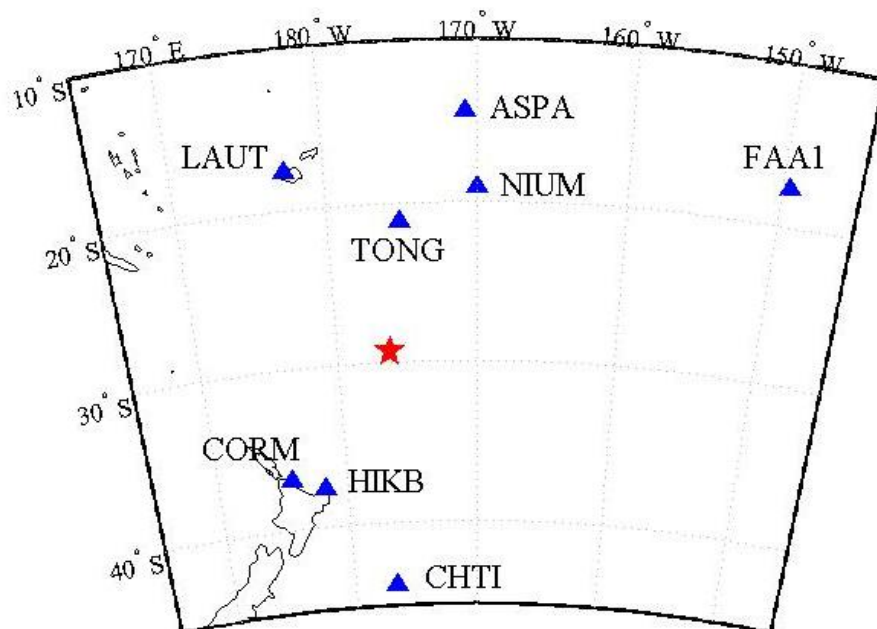
Figure 5-60 The locations of earthquake epicenter (red star) in Kermadec Island region on 15 July 2009 and GPS stations (triangle).

The TEC from 18:30:00 UT to 20:30:00 UT of TONG station observed by PRN17 is shown in Figure 5-61. The geographic coordinate of TONG station is at (21.145°S, 175.179°W), while the geomagnetic coordinates of TONG station was at (22.90°S, 98.94°W). The TEC perturbations are not clearly seen after the earthquake onset time as shown in Figure 5-61. It could not be concluded completely that there were no TEC variations from the original data of the TEC. The vertical dot line in Figure 5-61(b) indicates the time of the earthquake at 19:03:16 UT. The locations on the ionospheric pierce point (IPP) where the paths between satellites and receivers crossed were (23.64°S, 176.13°W) at 18:30:00 UT and (22.96°S, 172.15°W) at 20:30:00 UT. The points of observation moved nearly to the east.

The TEC data was applied high-pass filter which cut off period is 10 minutes. Then, it was smoothed using Savitzky-Golay method with 5 order polynomial and the window size of 33 points. As can be seen from Figure 5-62(b), the TEC started to fluctuate at 19:12:00 UT. The time lag of variation was 8.44 minutes. The maximum peak of variation was 0.1 TECU at 19:19:00 UT and the minimum peak of variation was -0.07 TECU at 19:24:00 UT. The fluctuation period of the TEC is approximately 12 minutes. After that, the TEC turned to the normal state. It could not be concluded that how the normal fault could disturb the TEC variations because the observed amplitude of the TEC variations at TONG station is too small. The reason for small amplitude at TONG station is that TONG station is located too far from the earthquake epicenter zone (1,254 km). The acoustic wave decayed as the distance increases (Heki *et al.* 2006). The GPS data from the nearest station and the second near stations which are HIKB and CORM stations were also studied. However, there were no variations seen at these stations. The acoustic wave tends to drive the charged particles to the equatorial zone because the geomagnetic fields at the equator are nearly horizontal. There are no effects from the geomagnetic fields to the plasma at the equator. Therefore, CORM station could detect the TEC variations in this event. With regards to HIKB and CORM stations, these stations are located in mid-latitude regions. The geomagnetic fields are not in the horizontal plane. Therefore, the charged particles might be affected by the geomagnetic fields. Therefore, the acoustic wave might decay all when it arrived these stations.
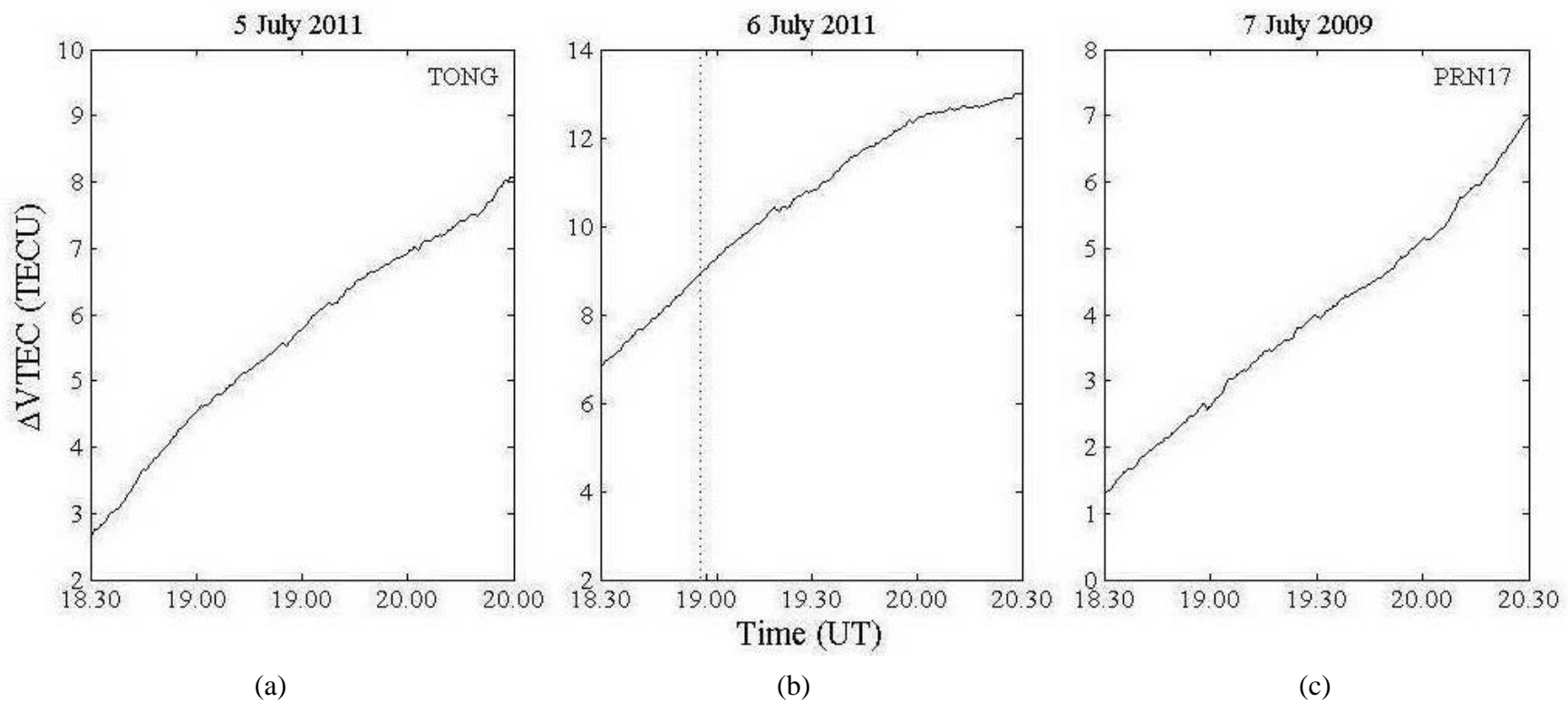
Figure 5-61 The observed TEC detected by PRN17 at TONG station on (a) 5 July 2011 (b) 6 July 2011 and (c) 7 July 2011.
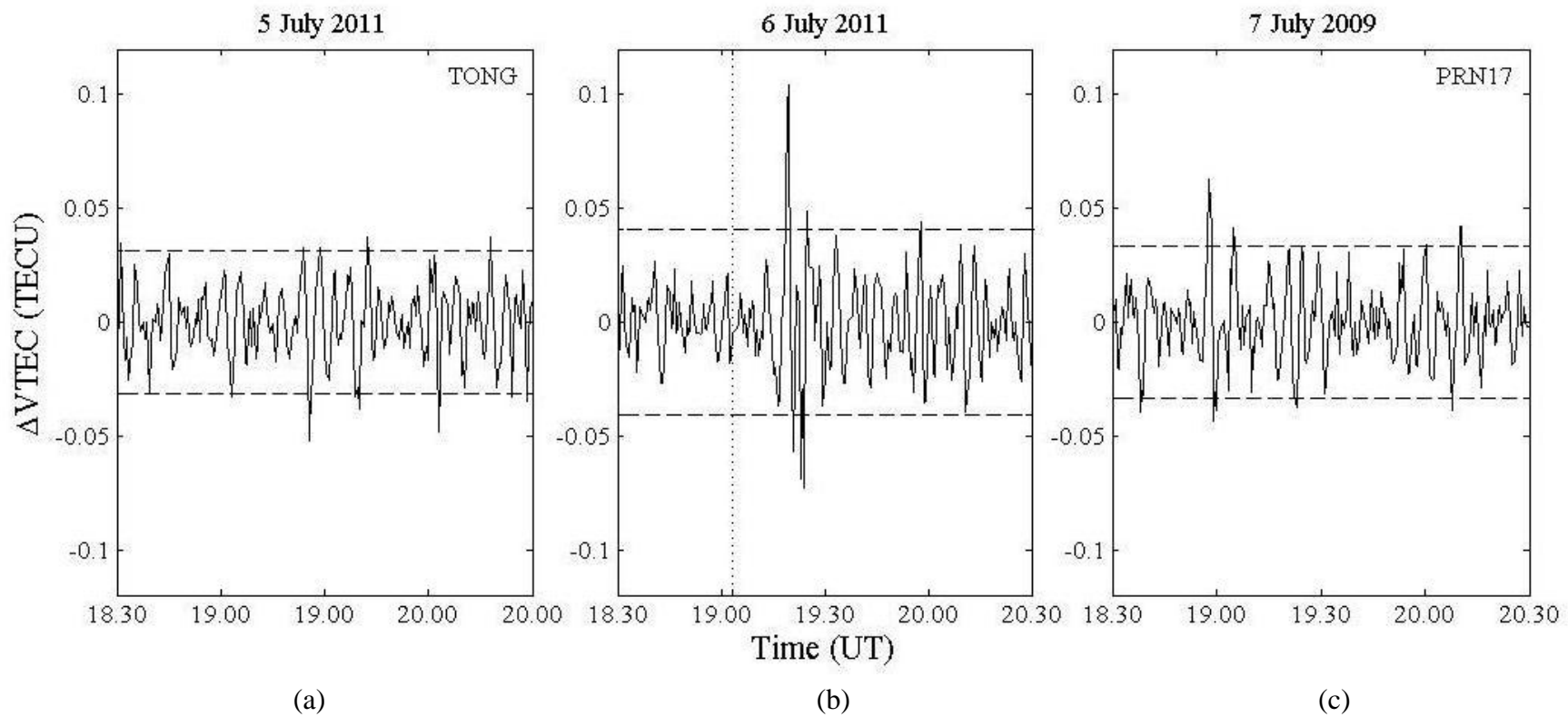
Figure 5-62 The filtered TEC data observed by PRN17 at TONG station on (a) 5 July 2011 (b) 6 July 2011 and (c) 7 July 2011.

The dominant frequency of the TEC variations obtained by FFT method was shown in Figure 5-63. The dominant frequency detected by TONG station is 4.3 mHz. The TEC oscillated with the period of about 3.53 minutes after the earthquake origin time.
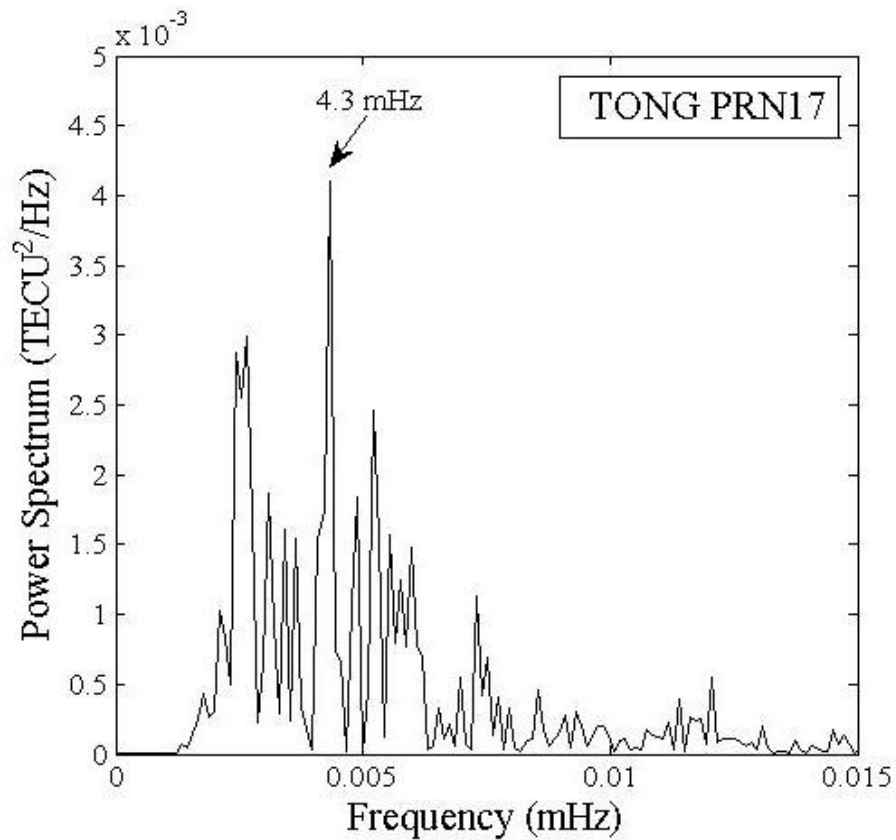
Figure 5-63 The power spectrum of TEC data observed by TONG station on 6 July 2011.

The Declination of the geomagnetic field line in the horizontal component was 16.384° at the earthquake location. The field pointed to north-northeast direction. Therefore, ASPA, NIUM, TONG, LAUT, CORM, HIKB and CHTI should detect the TEC variation because these GPS stations are located where the wave front of the acoustic wave is perpendicular with the field lines. However, only one station which is TONG could observe the TEC variations in this study. Figure 5-65 shows the locations on the IPP which the lines of sight crossed between 18:30:00 UT and 20:30:00 UT. There were four GPS satellites during the observation time at TONG station. The line of sight on the IPP between PRN17 and TONG stations crossed the distance between the epicenter and TONG station during the observation time. Therefore, PRN17 could observe the acoustic wave generated by this earthquake. The magnitude of this earthquake was small (M=7.6) and the depth of the focus was too deep (20 km beneath the ground surface) compared to the earthquake in section 4.2. Moreover, the GPS stations are located too far from the earthquake epicenter (> 1,000 km). This earthquake occurred on daytime which is 07:36:16 a.m. There was the ionospheric E layer at the earthquake origin time as shown in Figure 5-66. It might have the TEC variations on the E layer near the epicenter zone after the earthquake onset time. With the far distances of GPS stations from the epicenter, the acoustic wave might decay all before it arrived these GPS stations.
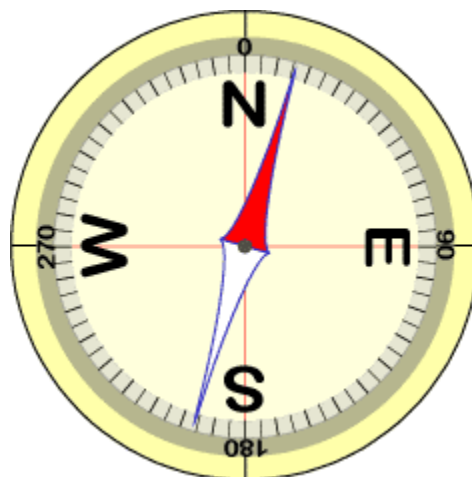
Figure 5-64 The Declination of geomagnetic field at 29.312°S, 176.204°W (World Data Center (WDC) for Geomagnetism, 1995).
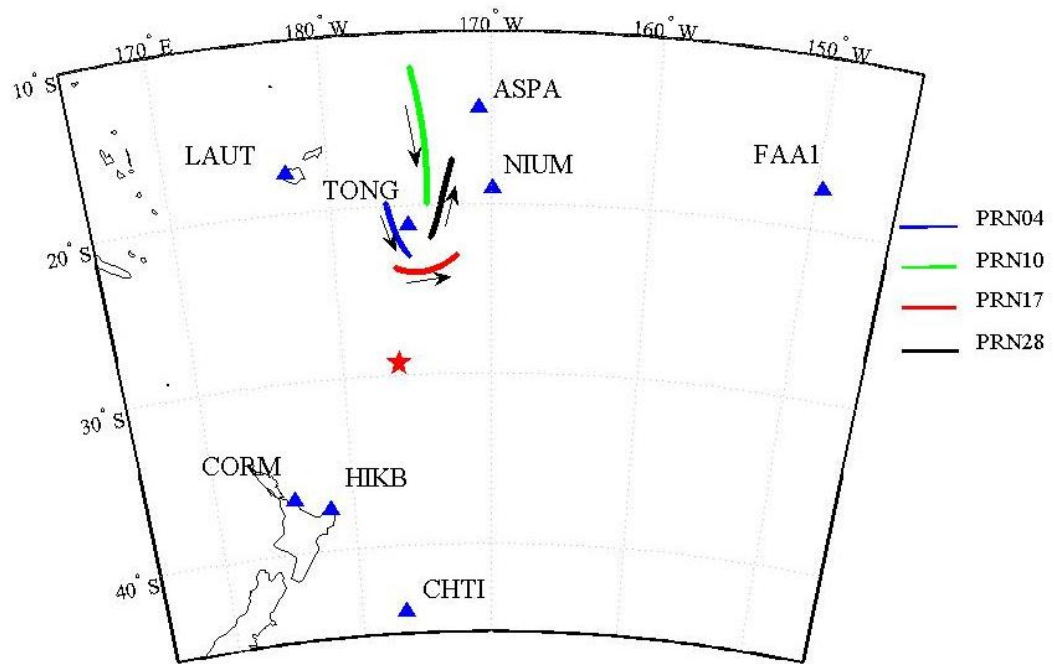
Figure 5-65 The locations on IPP which the lines of sight crossed between 18:30:00 UT to 20:30:00 UT on 6 July 2011 in Kermadec Islands earthquake.
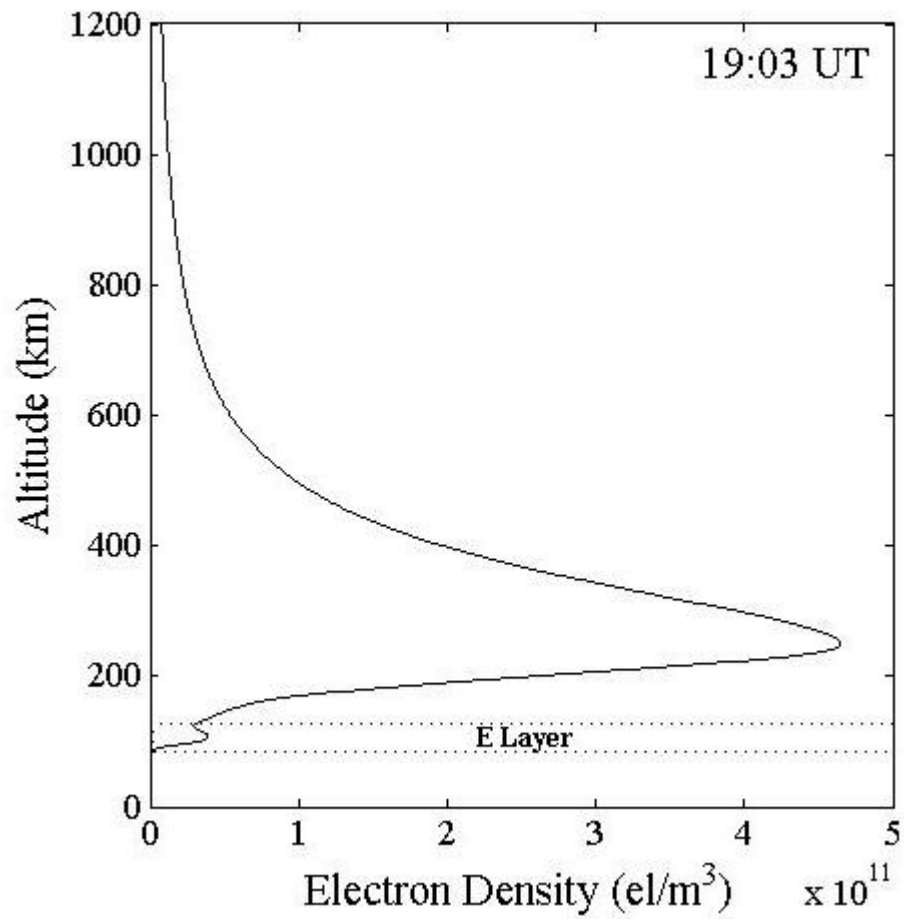
Figure 5-66 The electron profile from IRI-model 2007 at 19:03:00 UT.

CHAPTER VI
CONCLUSIONS

The program for the data analysis of the TEC data was developed by MATLAB in order to study the Earth Science phenomena. The program plays the role to apply highpass filter, Savitzky-Golay and Fast Fourier Transform (FFT) to the TEC data. The program was tested the accuracy with the results of Choosakul *et al.* (2009). The TEC data of Choosakul *et al*. (2009) were processed the data processing on the IDL. The results provided by MATLAB in this study are equal to the results of Choosakul *et al.* (2009). This program has the accuracy enough to analyze the TEC data. After applying this program to the TEC data after the large earthquakes, the significant TEC variations after the earthquake origin times could be observed.

The observations of the TEC variations after the large earthquakes show that the earthquake local times are the major factor which responds to the TEC variations. Most of earthquakes that their origin times are in the daytime could be observed the TEC variations. There is the ionospheric E layer in the daytime which responds to the acoustic wave from the earthquake. With regards to the earthquake that the origin time is in the nighttime, the TEC variations could not be observed in this event because there is no the E layer which responds to the acoustic wave. When the earthquakes occur, the ground shake in the vertical direction generates a mode of atmospheric waves called direct acoustic wave from the focal area. The other modes of atmospheric waves are secondary acoustic wave generated by surface Rayleigh wave and gravity wave generated by Tsunami wave (Heki *et al.*, 2006). The source of the TEC variations in this research is the direct acoustic wave generated by the earthquakes from the focal area. The periods of the acoustic wave which were detected in this study are about 3.5 to 9.2 minutes. All earthquakes can be observed the TEC variations after the earthquake origin time about six minutes. The time lags of the variations which are larger than six minutes can be interpreted by Iyemori *et al*. 2005 report. Iyemori *et al.* (2005) proposed that the acoustic wave generated by the earthquake takes six minutes from the ground surface to the E layer at height about 120 km. The acoustic wave is a kind of compression waves. The speed of the direct

acoustic wave is about 343 m/s. From results of this study, there are many factors which let the researchers observe the TEC variations after the earthquake origin time as listed below.

1. Reverse and normal faults.

   The reverse fault causes the increasing number of the TEC value to the first peak of the TEC variations after the earthquake origin time. With regards to normal fault, the TEC depletion at the first peak of the TEC variations after the earthquake origin time is a result of normal fault.

2. Line of sight

   The satellite-receiver paths which cross the IPP are one of the factors which give the clear signal of the TEC variations. The high amplitude of the TEC variations can be detected when the line of sight is parallel with the acoustic wave front. If the line of sight is not parallel with the wave front, the amplitude partly cancels (Heki *et al.* 2006).

3. Distance from the epicenter

   The direct acoustic wave decays when it travels long distance. Therefore, the GPS stations which are located too far from the earthquake epicenters could detect the small amplitudes of the TEC variations or could not observe the TEC variations.

4. Geomagnetic field line and acoustic wave front

   The charged particles on the ionosphere move along the geomagnetic field lines. The particles are restricted to move across the geomagnetic field lines (Heki *et al.*, 2006; Kelley, 2009). Therefore, the GPS stations which are located where the acoustic wave front is perpendicular with the geomagnetic field lines could detect the TEC variations. The acoustic wave front which is parallel with the geomagnetic field line cannot survive. Therefore, the GPS receivers which are located where the acoustic wave front is parallel with the geomagnetic field lines could not detect the TEC variations.

REFERENCES

Artru, J., Ducic, V., Kanamori, H., Lognonné, P., and Murakami, M. Ionospheric detection of gravity waves induced by tsunamis. <u>Geophysical Journal International</u> 160, 3 (2005) : 840-848.

Bolt, B. A. Seismic Air Waves from the Great 1964 Alaskan Earthquake. <u>Nature</u> 202, 4937 (1964) : 1095-1096.

Burke, W. J., Huang, C. Y., Gentile, L. C., and Bauer, L. Seasonal-longitudinal variability of equatorial plasma bubbles. <u>Ann. Geophys.</u> 22 (2004) : 3089-3098.

Chen, C. H., Saito, A., Lin, C. H., Liu, J. Y., Tsai, H. F., Tsugawa, T., Otsuka, Y., Nishioka, M., and Matsumura, M. Long-distance propagation of ionospheric disturbance generated by the 2011 off the Pacific coast of Tohoku Earthquake. <u>Earth Planets Space</u> 63, 7 (2011) : 881-884.

Choosakul, N., Saito, A., Iyemori, T., and Hashizume, M. Excitation of 4-min periodic ionospheric variations following the great Sumatra-Andaman earthquake in 2004. <u>J. Geophys. Res.</u> 114, 10 (2009) : A10313.

Choosakul, N. <u>Study on the periodic ionospheric variations after large earthquakes using GPS data</u>. Doctoral dissertation (Science), Department of Earth and Planetary Science, Graduate School of Science, Kyoto University, 2009.

Dana, P. H. <u>Global Positioning System Overview</u> [Online]. (n.d.) Available from: http://www.colorado.edu/geography/gcraft/notes/gps/gps_f.html [2013, February 18]

Davies, K., and Baker, D. M. Ionospheric Effects Observed around the Time of the Alaskan Earthquake of March 28, 1964. <u>J. Geophys. Res.</u> 70, 9 (1965) : 2251-2253.

Ducic, V., Artru, J., and Lognonné, P. Ionospheric remote sensing of the Denali Earthquake Rayleigh surface waves. <u>Geophys. Res. Lett.</u> 30, 18 (2003) : 1951.

Hasbi, A. M., Momani, M. A., Ali, M. A. M., Misran, N., Shiokawa, K., Otsuka, Y., and Yumoto, K. Ionospheric and geomagnetic disturbances during the 2005 Sumatran earthquakes. <u>Journal of Atmospheric and Solar-Terrestrial Physics</u> 71, 17-18 (2009) : 1992-2005.

Hines C. O. Gravity-wave in atmosphere. <u>Nature</u> 239 (1960) : 73-78.

Heki, K., Otsuka, Y., Choosakul, N., Hemmakorn, N., Komolmis, T. and Maruyama, T. Detection of ruptures of Andaman fault segments in the 2004 great Sumatra earthquake with coseismic ionospheric disturbances. <u>J. Geophys. Res.</u> 111, B09313 (2006) : 1-11.

Heki, K. Large earthquakes shakes ionosphere. <u>Naifuru</u> 63, (2007) : 4-5.

Kanamori, H., and Mori, J. Harmonic excitation of mantle Rayleigh waves by the 1991 eruption of Mount Pinatubo, Philippines. <u>Geophys. Res. Lett.</u> 19, 7 (1992) : 721-724.

Kanamori, H., Mori, J., and Harkrider, D. G. Excitation of atmospheric oscillations by volcanic eruptions. <u>J. Geophys. Res.</u> 99, B11 (1994) : 21947-21961.

Kelley, M. C. <u>The earth's ionosphere : plasma physics and electrodynamics</u>. Second Edition. United States of America : Academic Press, 2009.

Ionospheric Prediction Service (IPS). <u>Glossary of Solar Terrestrial Terms</u> [Online]. 2009. Available from : http://www.ips.gov.au/Educational/1/2/1/S [2010, December 25].

Iyemori, T., Nose, M., Han, D., Gao, Y., Hashizume, M., Choosakul, N., Shinagawa, H., Tanaka, Y., Utsugi, Y., Saito, A., McCreadie, H., Odagi, Y., Yang, F. Geomagnetic perturbations caused by the Sumatra earthquake on December 26, 2004. <u>Geophys. Res. Lett.</u> 3, 20 (2005) : L20807.

Leonard, R. S., and Barnes, R. A. Jr. Observation of Ionospheric Disturbances Following the Alaska Earthquake. J. Geophys. Res. 70, 5 (1965) : 1250-1253.

Matsumura, M., Saito, A., Shinagawa, H., Tsugawa, T., Otsuka, Y., Nishioka, M., and Chen, C. H. Numerical simulations of atmospheric waves excited by the 2011 off the Pacific coast of Tohoku Earthquake. Earth Planets Space 63 (2011) : 885–889.

Michel, G. W., Becker, M., Angermann, D., Reigber, C., and Reinhart, E. Crustal motion in E-and SE-Asia from GPS measurements. Earth Planets Space 52 (2000) : 713-720.

Mikumo, T., Shibutani, T., Pichon, A. L., Garces, M., Fee, D., Tsuyuki, T., Watada, S., and Morii, W. Low-frequency acoustic-gravity waves from coseismic vertical deformation associated with the 2004 Sumatra-Andaman earthquake (Mw = 9.2). J. Geophys. Res. 113, B12 (2008) : B12402.

National Oceanic and Atmospheric Administration (NOAA). Latitude/Longitude Distance Calculator [Online]. 2010. Available from : http://www.nhc.noaa.gov/gccalc.shtml [2010, December 25].

National Oceanic and Atmospheric Administration (NOAA). SWPC Anonymous FTP Server [Online]. 2009. Available from : http://www.swpc.noaa.gov/ftpmenu/indices/old_indices.html [2010, December 25].

Nishioka, M. Plasma Bubble in the Ionosphere [Online]. 2009. Available from : http://www.geo.sc.chula.ac.th/espcu/activity/pdf/13100602.pdf [2013, April 28].

Norsuzila, Y., Abdullah, M., and Ismail, M. GPS Total Electron Content (TEC) Prediction at Ionosphere Layer over the Equatorial Region, Trends in Telecommunications Technologies, Christos J Bouras (Ed.) : InTech, 2010

Otsuka, Y., Kotake, N., Tsugawa, T., Shiokawa, K., Ogawa, T., Effendy, Saito, S., Kawamura, M., Maruyama, T., Hemmakorn, N., and Komolmis, T. GPS detection of total electron content variations over Indonesia and Thailand following the 26 December 2004 earthquake. Earth Planets Space 58, 2 (2006) : 159-165.

Rama Rao P.V.S., Niranjan, K., Prasad, D.S.V.V.D., Gopi Krishna, S., and Uma, G. On the validity of the ionospheric pierce point (IPP) altitude of 350km in the Indian equatorial and low-latitude sector. Ann. Geophys. 24 (2006) : 2159–2168.

Rama Rao P.V.S., Gopi Krishna, S., Niranjan, K., and Prasad, D.S.V.V.D. Temporal and spatial variations in TEC using simultaneous measurements from the Indian GPS network of receivers during the low solar activity period of 2004–2005. Ann. Geophys. 24 (2006) : 3279–3292.

Saito, A., Tsugawa, T., Otsuka, T., Nishioka, M., Iyemori, T., Matsumura, M., Saito, S., Chen, C.H., Goi, Y., and Choosakul, N. Acoustic resonance and plasma depletion detected by GPS total electron content observation after the 2011 Tohoku Earthquake. Earth Planets Space 63, 7 (2011) : 863-867.

Schunk, R. W., and Nagy, A. F. Ionospheric Physics, Plasma Physics, and Chemistry. Cambridge : Cambridge University Press, 2000.

Scripps Orbit and Permanent Array Center (SOPAC). Permanent GPS Site Arrays [Online]. 1990. Available from : http://sopac.ucsd.edu/cgi-bin/dbShowArraySitesMap.cgi [2011, September 1].

Theerapatpaiboon, P., Leelaruji, N., Hemmakorn, N., and Supnithi, P. The Effects of Sumatra-Andaman Earthquake on Total Ionospheric Electron Content (TEC) and Ionospheric Scintillation of GPS Signal in Thailand. The Fifth Int. Conf. on Information Communications and Signal Processing. ICICS 2005 (2005) : 1183-1186.

Tsugawa, T. Observational studies on large-scale traveling ionospheric disturbances using GPS receiver networks. Doctoral dissertation (Science), Department of Earth and Planetary Science, Graduate School of Science, Kyoto University, 2004.

Tsugawa, T., Zhang, S. -R., Coster, A. J., Otsuka, Y., Sato, J., Saito, A., Zhang, Y., and Paxton, L. J. Summer-winter hemispheric asymmetry of the sudden increase in ionospheric total electron content and of the O/N2 ratio: Solar activity dependence. J. Geophys. Res. 112, A8 (2007) : A08301.

Tsugawa, T., Saito, A., Otsuka, Y., Nishioka, M., Maruyama, T., Kato, H., Nagatsuma, T., and Murata, K. T. Ionospheric disturbances detected by GPS total electron content observation after the 2011 off the Pacific coast of Tohoku Earthquake. Earth Planets Space 63, 7 (2011) : 875-879.

Wellenhof, B. H., Lichtenegger, H., and Collins, J. GPS theory and practice. 5th ed. New York : Springer-Verlag Wien, 2001.

U.S. Geological Survey (USGS). Earthquake Harzards Program [Online].1998. Available from : http://earthquake.usgs.gov [2010, December 25].

U.S. Geological Survey (USGS). Magnitude 7.8 - OFF WEST COAST OF THE SOUTH ISLAND, N.Z. [Online]. 2009. Available from: http://earthquake.usgs.gov/earthquakes/recenteqsww/Quakes/us2009jcap.php#summary [2010, December 25].

U.S. Geological Survey (USGS). Magnitude 8.1 - SAMOA ISLANDS REGION [Online]. 2009. Available from: http://earthquake.usgs.gov/earthquakes/recenteqsww/Quakes/us2009mdbi.php#summary [2010, December 25].

U.S. Geological Survey (USGS). Magnitude 7.7 - KEPULAUAN MENTAWAI REGION, INDONESIA [Online]. 2010. Available from: http://earthquake.usgs.gov/earthquakes/eqinthenews/2010/usa00043nx/#summary [2010, December 25].

U.S. Geological Survey (USGS). <u>Magnitude 9.0 - NEAR THE EAST COAST OF HONSHU, JAPAN</u> [Online]. 2011. Available from: http://earthquake.usgs.gov/earthquakes/eqinthenews/2011/usc0001xgp/ [2011, March 30].

U.S. Geological Survey (USGS). <u>Magnitude 9.0 - NEAR THE EAST COAST OF HONSHU, JAPAN</u> [Online]. 2011. Available from: http://earthquake.usgs.gov/earthquakes/recenteqsww/Quakes/usc0004pbm.php#summary [2011, August 20].

World Data Center (WDC) for Geomagnetism. <u>Model field at a point by IGRF (IGRF-11/2010)</u> [Online]. 1995. Available from : http://wdc.kugi.kyoto-u.ac.jp/igrf/point/index.html [2011, November 22].

World Data Center (WDC) for Geomagnetism. <u>Geomagnetic Equatorial Dst Index Home Page</u> [Online]. 1995. Available from : http://wdc.kugi.kyoto-u.ac.jp/dstdir/index.html [2011, November 22].

Yuen, P. C., Weaver, P. F., Suzuki, R. K., and Furumoto, A. S. Continuous, Traveling Coupling between Seismic Waves and the Ionosphere Evident in May 1968 Japan Earthquake Data. <u>J. Geophys. Res.</u> 74, 9 (1969) : 2256-2264.

Zhang, D. H., and Xiao, Z. Study of ionospheric response to the 4B flare on 28 October 2003 using International GPS Service network data. <u>J. Geophys. Res.</u> 110, A3 (2005) : A03307.

APPENDICES

APPENDIX A

The Source Code 2 and 3

The programs

As can be seen from CHAPTER III, the Rinex GPS-TEC program version 2.1 provides the output data which has 10 columns. However, there are only six necessary columns including Time, PRN, Ele, Lat, Lon and Vtec needed for data analysis in this research. The *Source Code 2* plays the role to split the TEC data as PRN 1 to PRN 32. This program saves the data as Excel format which has six columns of necessary data. The final part of *Source Code 2* is the plot function of discontinuous data. However, the program has not been developed completely yet because there is an error occurred while plotting more than two gaps of discontinuous x data. It works well only one gap of discontinuous x data.

Source Code 2

```
%-----------------------------------------by Radchagrit Supakulopas

data = xlsread('nlsn196-2009-07-15.xls');
Jdate = data(:,1);
Time = data(:,2);
PRN  = data(:,3);
Az   = data(:,4);
Ele  = data(:,5);
Lat  = data(:,6);
Lon  = data(:,7);
Stec = data(:,8);
Vtec = data(:,9);
S4   = data(:,10);
File = [Time PRN Ele Lat Lon Vtec];
xlswrite('Data_export', File)

DATA = xlsread('Data_export.xls');
for k=1:32;
find(DATA(:,3) == k);
ak = find(DATA(:,2) == k, 1 );
bk = find(DATA(:,2) == k, 1, 'last' );
Gk = [DATA(ak:bk,1) DATA(ak:bk,2) DATA(ak:bk,3) DATA(ak:bk,4)
DATA(ak:bk,5) DATA(ak:bk,6)];
    if k==1
    xlswrite('G01.xls', Gk)
    elseif k==2
    xlswrite('G02.xls', Gk)
    elseif k==3
    xlswrite('G03.xls', Gk)
    elseif k==4
    xlswrite('G04.xls', Gk)
    elseif k==5
    xlswrite('G05.xls', Gk)
    elseif k==6
```

```matlab
        xlswrite('G06.xls', Gk)
    elseif k==7
        xlswrite('G07.xls', Gk)
    elseif k==8
        xlswrite('G08.xls', Gk)
    elseif k==9
        xlswrite('G09.xls', Gk)
    elseif k==10
        xlswrite('G10.xls', Gk)
    elseif k==11
        xlswrite('G11.xls', Gk)
    elseif k==12
        xlswrite('G12.xls', Gk)
    elseif k==13
        xlswrite('G13.xls', Gk)
    elseif k==14
        xlswrite('G14.xls', Gk)
    elseif k==15
        xlswrite('G15.xls', Gk)
    elseif k==16
        xlswrite('G16.xls', Gk)
    elseif k==17
        xlswrite('G17.xls', Gk)
    elseif k==18
        xlswrite('G18.xls', Gk)
    elseif k==19
        xlswrite('G19.xls', Gk)
    elseif k==20
        xlswrite('G20.xls', Gk)
    elseif k==21
        xlswrite('G21.xls', Gk)
    elseif k==22
        xlswrite('G22.xls', Gk)
    elseif k==23
        xlswrite('G23.xls', Gk)
    elseif k==24
        xlswrite('G24.xls', Gk)
    elseif k==25
        xlswrite('G25.xls', Gk)
    elseif k==26
        xlswrite('G26.xls', Gk)
    elseif k==27
        xlswrite('G27.xls', Gk)
    elseif k==28
        xlswrite('G28.xls', Gk)
    elseif k==29
        xlswrite('G29.xls', Gk)
    elseif k==30
        xlswrite('G30.xls', Gk)
    elseif k==31
        xlswrite('G31.xls', Gk)
    else k==32
        xlswrite('G32.xls', Gk)
    end
end
```

```matlab
%--------------------------------------------------------Plot TEC data
dat1 = xlsread('G01.xls');
T = dat1(:,1);
TEC = dat1(:,6);
  max_step = 1;
  plotstyle = 'k-';
  segends = [find(diff(T) > max_step) length(T)];
  nsegs = length(segends);
  plotargs = cell(3, nsegs);
  segend = 0;
  for segment = 1:nsegs
      segstart = segend+1;
      segend = segends(segment);
      plotargs{1,segment} = T(segstart:segend);
      plotargs{2,segment} = TEC(segstart:segend);
      plotargs{3,segment} = plotstyle;
  end
  plot(plotargs{:});
%--------------------------------------------------------------END
```

The *Source Code 3* is used to plot the maps of study areas in this research. The program can plot earthquake epicenters and GPS stations. It can fix latitude and longitude of interesting areas by indicating "lonlim" and "latlim". It can also indicate latitude and longitude of interesting point in [lat lon]. The code below shows an example of plotting Tohoku earthquake.

Source Code 3

```matlab
%-----------------------------------------by Radchagrit Supakulopas
figure('Color','white')
lonlim = [120 150];
latlim = [30 50];
ax = usamap(latlim,lonlim);
axis off
hold on
geoshow('landareas.shp', 'FaceColor',  [1 1 1])

%%%Tohoku Earthquake%%%
epic = [38.297 142.372];
chan = [43.79071 125.44423];
daej = [36.39943 127.37448];
khaj = [48.52144 135.04617];
mtka = [35.67951 139.56138];
smst = [33.57786 135.93696];
suwn = [37.27552 127.05424];
tskb = [36.10568 140.0875];
usud = [36.13311 138.36204];
yssk = [47.02974 142.71672];
plotm(epic(1), epic(2),'pr','MarkerFaceColor','r','MarkerSize',16);
plotm(chan(1), chan(2),'^b','MarkerFaceColor','b','MarkerSize',9);
plotm(daej(1), daej(2),'^b','MarkerFaceColor','b','MarkerSize',9);
plotm(khaj(1), khaj(2),'^b','MarkerFaceColor','b','MarkerSize',9);
```

```
plotm(mtka(1), mtka(2),'^b','MarkerFaceColor','b','MarkerSize',9);
plotm(smst(1), smst(2),'^b','MarkerFaceColor','b','MarkerSize',9);
plotm(suwn(1), suwn(2),'^b','MarkerFaceColor','b','MarkerSize',9);
plotm(tskb(1), tskb(2),'^b','MarkerFaceColor','b','MarkerSize',9);
plotm(usud(1), usud(2),'^b','MarkerFaceColor','b','MarkerSize',9);
plotm(yssk(1), yssk(2),'^b','MarkerFaceColor','b','MarkerSize',9);
%-------------------------------------------------------------END
```

APPENDIX B

The GPS TEC

The GPS TEC

In the condition of small absorption of radio waves and no effects of geomagnetic field, the dispersion of radio waves or Appleton-Hartree equation is described as

$$n^2 = 1 - \left(\frac{f_p}{f}\right)^2 \qquad (B.1)$$

where n is the refractive index of an ionized medium, f_p is the frequency of the plasma and f is the frequency of radio waves. The formula of plasma frequency is given as B.2.

$$f_p \equiv \frac{\omega_p}{2\pi} = \frac{v_l}{2\pi\lambda_D} \qquad (B.2)$$

where ω_p is angular frequency of plasma, v_l is the longitudinal thermal velocity and λ_D is the Debye length. The formulas of v_l and λ_D are shown below:

$$v_l = \left(\frac{k_B T_e}{m_e}\right)^{1/2} \qquad (B.3)$$

$$\lambda_D = \left(\frac{k_B T_e}{4\pi e^2 N_e}\right)^{1/2} \qquad (B.4)$$

where k_B is Boltzmann's constant, T_e is the absolute temperature of electron, m_e is electron mass ($9.11 \times 10^{-28} g$) and $e = 4.803 \times 10^{-10} esu$. From equations B.3 and B.4, the equation of plasma frequency can be rewritten as:

$$f_p = \sqrt{80.5 N_e} \qquad (B.5)$$

The refractive index of group delay can expressed as B.6

$$n_g = \frac{1}{n} = \left(1 - \left(\frac{f_p}{f}\right)^2\right)^{\frac{1}{2}} \approx 1 + \frac{1}{2}\left(\frac{f_p}{f}\right)^2 \qquad \text{(B.6)}$$

Then, the group delay is determined as follow:

$$d_g = \int (n_g - 1)dl = \int \frac{1}{2}\left(\frac{f_p}{f}\right)^2 dl = \frac{40.3}{f^2}\int N_2 dl \qquad \text{(B.7)}$$

where l the ray path between satellite and receiver. The total electron content is the integration number of electron density along the ray path between satellite and receiver. Then, the equation B.7 can be rewritten as:

$$d_g = \frac{40.3}{f^2}TEC \qquad \text{(B.8)}$$

The pseudorange data from dual-frequency of radio waves are expressed below:

$$P_1 = d_{g1} + b^{r1} + b^{s1} \qquad \text{(B.9)}$$

$$P_2 = d_{g2} + b^{r2} + b^{s2} \qquad \text{(B.10)}$$

From equations B.9 and B.10, the slant TEC is derived below:

$$P_2 - P_1 = 40.3 STEC\left(\frac{1}{f_2^2} - \frac{1}{f_1^2}\right) + b^r + b^s \qquad \text{(B.11)}$$

where b^r is the receiver bias and b^s is the satellite bias. However, the TEC which is derived from pseudorange data alone gives noisy results. The carrier phase provides the precise measure of the TEC. The absolute TEC cannot be obtained if pseudorange is not used. Therefore, pseudorange provides the absolute scale of the TEC, whereas the differential carrier phase increases the measurement accuracy (Tsugawa 2004; Rama Rao *et al*. 2006; Rama Rao *et al*. 2006).

VITAE

Radchagrit SUPAKULOPAS was born on 14 October 1987 in Nakhon Pathom, Thailand. He received the Bachelor of Science Degree in Physics with the 1st Class Honour in 2010 from Department of Physics, Faculty of Science, Silpakorn University. He began his second degree in Earth Sciences at the Department of Geology, Faculty of Science, Chulalongkorn University. He graduated a Master Degree in May 2013.